

# **EXPLORING ATMOSPHERIC EXCHANGE WITH NATURAL TRACERS**

**Inauguraldissertation**

zur

Erlangung der Würde eines Doktors der Philosophie  
vorgelegt der  
Philosophisch-Naturwissenschaftlichen Fakultät  
der Universität Basel

von

Yu Xia  
aus Chongqing  
(V. R. CHINA)

Basel, 2011

Genehmigt von der Philosophisch-Naturwissenschaftlichen Fakultät  
auf Antrag von

Prof. Dr. Christine Alewell  
Fakultätsverantwortliche

Dr. Stefan Reimann  
Korreferent

Basel, den 22.02.2011

Prof. Dr. Martin Spiess  
Dekan

# Abstract

This study is focused on the application of radon ( $^{222}\text{Rn}$ ; half life time of 3.82 days) as an atmospheric tracer for evaluating the exchange of trace compounds between the land surface and the atmosphere and for understanding atmospheric mixing processes. For this purpose established methods for detecting the flux and the atmospheric concentration of  $^{222}\text{Rn}$  were compared. Based on the measurements of the  $^{222}\text{Rn}$  flux and concentration, we explored: (1) the exchange between land surface and the air near surface during nighttime to understand the characteristics of the very stable nocturnal boundary layer, and (2) the exchange between the air near surface and the air at high altitude to estimate the flux density of total bacterial cells from surface to high altitude.

The accuracy of  $^{222}\text{Rn}$  flux measurements is an important issue for the reliability of  $^{222}\text{Rn}$  tracer method. During summer of 2008 the  $^{222}\text{Rn}$  flux from soil was determined with different direct and indirect measurements at four eastern Spanish sites with different geological and soil characteristics. Direct  $^{222}\text{Rn}$  flux measurements with continuous and integrated monitors were in good agreement with the results obtained by indirect methods, which are based on correlations between  $^{222}\text{Rn}$  flux and the terrestrial  $\gamma$  dose rate, or the  $^{226}\text{Ra}$  activity in soil.

Another issue concerning the reliability of the  $^{222}\text{Rn}$  tracer method is the accuracy of atmospheric  $^{222}\text{Rn}$  measurements. For an inter-comparison the atmospheric  $^{222}\text{Rn}$  concentration was measured using either two-filter or one-filter instruments at the Schauinsland station in the Black Forest, Germany. These two types of detectors measured either  $^{222}\text{Rn}$  or its progeny activity concentration in the atmosphere. Generally, the values observed by the two detectors largely show a parallel behavior. However, occasionally meteorological and local conditions lead to differences in the concentrations determined by the two detectors. The  $^{222}\text{Rn}$  progeny, which was attached to aerosols, was negatively influenced by precipitation and forest canopy contact. Hence the disequilibrium between  $^{222}\text{Rn}$  and its progeny became larger during rainy conditions and longer surface contact. Progeny-derived  $^{222}\text{Rn}$  concentration compared to directly measured  $^{222}\text{Rn}$  concentration was reduced by these two factors by about 10 % and 15 %, respectively. Therefore, precipitation and forest canopy contact time should be taken into account when determining atmospheric  $^{222}\text{Rn}$  concentrations through measurements of its short-lived progeny with one-filter detectors.

During a campaign at K-pusztá station in the Carpathian Basin (Hungary) we used the nocturnal inversion trapping of  $^{222}\text{Rn}$ , originating from soil, to verify the stability of the nocturnal boundary layer. The nocturnal  $^{222}\text{Rn}$  concentrations were monitored at two different heights (0.1 m and 6.5 m above the ground) together with

the  $^{222}\text{Rn}$  flux density from the soil. 14 nights were selected that were characterized by strong cooling, light winds and clear skies. Typical nocturnal accumulation of  $^{222}\text{Rn}$  was investigated in a very shallow layer from sunset to sunrise in the following morning. The conservation of on average 72% (s.d. = 20%) of  $^{222}\text{Rn}$  emitted from soil in a shallow boundary layer supported the hypothesis of a two-stratum structure, where the shallow very stable boundary layer is decoupled and isolated from the atmosphere above it. In the large continental basin at K-Puzsta the stable structure was interrupted only intermittently by strong turbulent motions.

Finally the flux of total bacteria up to the high altitude Alpine environment was estimated by parallel observation of  $^{222}\text{Rn}$  concentrations and estimated  $^{222}\text{Rn}$  fluxes. Four campaigns were conducted over a 4-month period from late June to early October 2010 at the High Altitude Research Station Jungfraujoch, Switzerland (3580 m asl). During stable weather conditions, the concentration of total bacteria was fairly constant and no significant flux of total bacteria was observed between the planetary boundary layer and the high altitude. The average background concentration of total bacterial cells at Jungfraujoch was about  $3.4 \cdot 10^4 \text{ cells m}^{-3}$  (s.d. =  $0.8 \cdot 10^4 \text{ cells m}^{-3}$ ). Following windy conditions, both flux and concentration of total bacterial cells increased. This confirms that wind speed is an important factor for the bacterial cells to become airborne. First large-scale estimates of total bacterial flux during fair weather conditions provided values between about 1 to 4 times  $10^2 \text{ cells m}^{-2}\text{s}^{-1}$ .

Our results show that  $^{222}\text{Rn}$  serves well as atmospheric tracer to investigate and quantify the atmospheric mixing and transport processes and to estimate the regional flux density of atmospheric trace compounds and bacteria. These results can be also used to improve regional or global atmospheric transport and climate models.

# Acknowledgements

This dissertation would not have been possible without the guidance and the help of people who in one way or another contributed and extended their valuable assistance in the preparation and completion of this study.

Foremost, I would like to express my sincere gratitude to my supervisor Prof. Christine Alewell for the continuous support of my PhD study and research. Her wide knowledge and her logical way of thinking have been of great value for me. Her understanding and encouraging have provided a good basis for the present thesis.

I wish to express my warm and sincere thanks to my supervisor Dr. Franz Conen for teaching me to be a better scientist. It was a great pleasure for me to work with him and share his enthusiasm in research. He gave me the opportunity to explore new methods and open a wider horizon in the radionuclide applications. My work was always very innovative and interdisciplinary.

My sincere thanks also go to Dr. Wlodek Zahorowski, who supported our field works and helped to prove our hypothesis. His advices were of important values for our work.

Dr. Stefan Riemann deserves special thanks as my thesis committee member and advisor. In particular, thanks for sharing his data to support our observations.

Then thanks a lot to each of our collaborators, Clemen Schlosser, Ulrich Stöhlker, Laszlo Haszpra, and Zita Ferenczi. I thank them for helping manage our setup, sharing their database, spending their valuable time to discuss with me problems concerning the research and helping me during different time of my PhD period. I also thank Claudia Grossi and Prof. Arturo Vargas, who guided me for Spain campaign and explained me different methods to measure radon emission from land surface. Without their efforts chapter 2 would not be published.

Thanks to Xiaomo Wu for teaching me how to operate the bacterial experiments and preparing some solutions for me.

I am indebted to all of my colleagues at the Institute of Environmental Geosciences in the University of Basel to support me in different respect and to comment on my work.

Finally I have enormous gratitude to my husband and my parents for their patience and backup during all these years.

There are some supporting people that I might have forgotten. My humblest apologies go to those who consider having earned for themselves being cited amongst these lines.



# Table of Contents

<b>CHAPTER 1 INTRODUCTION .....</b>	<b>1</b>
<b>CHAPTER 2 INTER-COMPARISON OF DIFFERENT DIRECT AND INDIRECT METHODS TO DETERMINE RADON FLUX FROM SOIL.....</b>	<b>5</b>
2.1 Abstract.....	5
2.2 Introduction .....	6
2.3 Material and methods .....	7
2.3.1 Sites.....	7
2.3.2 Terrestrial $\gamma$ -dose rate .....	9
2.3.3 $^{226}\text{Ra}$ activity .....	9
2.3.4 Radon flux .....	10
2.4 Results and discussion .....	14
2.4.1 Terrestrial $\gamma$ dose rate.....	14
2.4.2 $^{226}\text{Ra}$ soil activity mass .....	15
2.4.3 Radon flux .....	16
2.5 Conclusion .....	17
2.6 Acknowledgement.....	18
<b>CHAPTER 3 COMPARISON OF ONE- AND TWO-FILTER DETECTORS FOR ATMOSPHERIC <math>^{222}\text{Rn}</math> MEASUREMENTS UNDER VARIOUS METEOROLOGICAL CONDITIONS .....</b>	<b>19</b>
3.1 Abstract.....	19
3.2 Introduction .....	19
3.3 Material and Methods .....	20

3.3.1 Sampling site .....	20
3.3.2 Measurement Techniques .....	22
3.3.2.1 Two-filter detector .....	22
3.3.2.2 One-filter detector .....	22
3.4 Results and discussion .....	24
3.4.1 General Description of Data .....	24
3.4.2 Harmonization of instrumental background and calibration.....	26
3.4.3 Effect of precipitation intensity .....	28
3.4.4 Effect of forest canopies .....	29
3.4.5 Effect of precipitation and forest canopy .....	29
3.5 Conclusions .....	31
3.6 Acknowledgements .....	32
<b>CHAPTER 4 EVIDENCE FOR NEARLY COMPLETE DECOUPLING OF VERY STABLE NOCTURNAL BOUNDARY LAYER OVERLAND .....</b>	<b>33</b>
4.1 Abstract.....	33
4.2 Introduction .....	33
4.3 Material and Methods .....	34
4.4 Results and Discussion .....	35
4.5 Suggestions for future studies .....	40
4.6 Conclusions .....	40
4.7 Acknowledgements .....	40
<b>CHAPTER 5 HIGH ALTITUDE OBSERVATIONS OF TOTAL BACTERIAL NUMBER AND COINCIDENT <sup>222</sup>Rn ACTIVITY CONCENTRATION .....</b>	<b>41</b>
5.1 Abstract.....	41
5.2 Introduction .....	41
5.3 Materials and Methods.....	43



5.4 Results and discussions .....	43
5.4.1 June .....	45
5.4.2 July .....	45
5.4.3 September .....	46
5.4.4 October .....	46
5.5 Conclusions .....	47
5.6 Acknowledgements .....	51
<b>CHAPTER 6 OVERALL DISCUSSIONS .....</b>	<b>53</b>
<b>APPENDIX OTHER ASPECTS .....</b>	<b>55</b>
A.1 Further improvement of the <sup>222</sup> Rn flux map .....	55
A.2 Improve the verification of non-CO <sub>2</sub> greenhouse gas emissions by <sup>222</sup> Rn tracer method from Jungfraujoch.....	56
<b>BIBLIOGRAPHY .....</b>	<b>59</b>
<b>CURRICULUM VITAE.....</b>	<b>71</b>



# List of Figures

**Fig. 1.** Map of the location of radiological stations belonging to Spanish surveillance networks. The selected Spanish sites in the inter comparison campaign are labeled in the map by circular points: Madrid (10i), Quintanar de la Orden (16i) and Teruel (25i) are included in the Spanish Automatic Surveillance Network (REA). Los Pedrones station (26i) belongs to the radiological network of the Autonomous Valencia region..... 8

**Fig. 2.** Scheme of the ionization chamber type H (E-PERM) used for radon flux measurement. The ionization chamber (EIC) is located on the ground (black space) and the exhaled radon can enter through the Tyvek window (T). The radon concentration is proportional to the potential drop due to radon decay on the positively charged electret (E) located on the chamber top in the air chamber. .... 10

**Fig. 3.** The dose rate measured at each site by RS-112 (INTE), LB-1236 (UHU) and GammaTracer (BASEL) monitors are shown. The dose rate for each REA station and their corrected values are reported in according to Saez-Vergara et al. (2002). Furthermore, values obtained from the MARNA map are also included. .... 14

**Fig. 4.** Radium activity concentration measured by the INTE-UPC laboratory (pointed bar), UHU laboratory (vertical line bar) and that obtained by using the MARNA equation ,  $D_{Ra} = 0.24 \cdot D_{tot}^{1.01}$  (diagonal line bar) are shown..... 16

**Fig. 5.** Radon flux levels measured at each site by direct and indirect methods are presented. Values measured by the continuous Sun Nuclear (HUH) and AlphaGUARD (BASEL) monitors, and by the integrated detectors E-PERM (INTE) and charcoal (UHU), are compared. Radon flux (y) estimated in order to apply the equation proposed in Szevagry et al. (2007),  $y = 0.89x - 11.01$  , which dose rate (x) data from measurements by RS-112 (INTE) and by Gamma-Tracer (BASEL) are also reported. Furthermore, radon flux is also estimated by using the equation  $F = C_{Ra} \lambda f \rho [D_c / (\lambda \varepsilon)]^{1/2}$  at each site. .... 17

**Fig. 6.** (left) Sketch of topography and forest cover (solid line indicates forest edge) around the measurement station (asterisk in the exact centre) in the Black Forest. (right) Frequency distribution of wind directions for 30° sectors during the observation period. Wind from the sector 120° - 180° is considered to have been least influenced by vegetation. .... 21

**Fig. 7.** The One-filter detector system contains a membrane filter and a stack of three independent, methane-filled, proportional counters having the same length and width as the active filter area. The middle counter detects the high energy  $\alpha$ -activity of  $^{212}\text{Po}$  ( $^{220}\text{Rn}$  progeny). Activity of  $^{212}\text{Po}$ , together with the change in  $^{212}\text{Po}$  activity over time, are used to determine total  $^{220}\text{Rn}$  progeny contribution to total counts in the lower counter. By difference, the  $^{222}\text{Rn}$  progeny activity is derived from the lower counter. The upper counter counts  $\beta$  particles only (redrawn from Stockburger & Sittkus, 1966). ..... 24

**Fig. 8.** Time series of hourly means of  $^{222}\text{Rn}$  activity concentration (measured with a two-filter detector) and short-lived  $^{222}\text{Rn}$  progeny, expressed in  $^{222}\text{Rn}$  equivalent (measured with a one-filter detector) before harmonizing background and calibration between instruments, hourly precipitation, mean wind speed, wind direction, air temperature and relative humidity at Schauinsland station from Oct. 2007 to April 2008. .... 25

<b>Fig. 9.</b> Average altitude of air masses (ensemble means of single particle trajectories) during the 24 hours before arrival at the station for the lowest (0-25 <sup>th</sup> ) to the highest (75 <sup>th</sup> -100 <sup>th</sup> ) quartile of observed <sup>222</sup> Rn activity concentrations. ....	26
<b>Fig. 10.</b> Correlation between activity concentrations of <sup>222</sup> Rn (measured by two-filter detector) and short-lived <sup>222</sup> Rn progeny (expressed in <sup>222</sup> Rn equivalent; measured by one-filter detector) as determined by the two independently calibrated instruments for events with no surface wet deposition and wind from the reference sector (values in brackets are standard errors of regression parameters). The Spearman rank correlation coefficient <i>r</i> equals 0.946. ....	27
<b>Fig. 11.</b> Ratio of the activity concentrations of progeny-derived <sup>222</sup> Rn and <sup>222</sup> Rn summarized for different ranges of precipitation intensity (instrumental background and calibration have been harmonized between detectors). Boxes indicate median, upper and lower quartile, whiskers 10 <sup>th</sup> and 90 <sup>th</sup> percentile, crosses are outliers. Each range includes between about 120 and 180 hourly values, except for precipitation intensities >3.2 mm h <sup>-1</sup> ( <i>n</i> =29). The lowest precipitation intensities are near the detection limit of the instrument and therefore only approximate. ....	28
<b>Fig. 12.</b> Correlation between activity concentration of progeny-derived <sup>222</sup> Rn and <sup>222</sup> Rn for the reference sector (a, b) and the two sectors influenced by forest cover (c, d, e, f), for without precipitation (a, c, e) and with precipitation (b, d, f) (values in brackets are standard errors of regression parameters). Instrumental background and calibration have been harmonised between detectors. ....	30
<b>Fig. 13.</b> Diurnal cycles (time progresses clockwise in 1-hr steps between symbols): mean values for same hour of day during clear sky conditions of atmospheric <sup>222</sup> Rn concentrations at 6.5 m height versus (left) air temperature at 2.0 m height, and (right) wind speed at 9.4 m height (open symbols for daytime and closed symbols for nighttime). Sunset and sunrise are indicated by grey dots. Error bars show ± 1 standard deviation. ....	36
<b>Fig. 14.</b> Changes in (top) temperature at 2.0 m height, and (bottom) wind speed at 9.4 m height during the selected 14 nights. Thick lines indicate the two nights when <sup>222</sup> Rn at 0.1 m height around sunrise was not significantly different from that around the preceding sunset (dashed line: 28 August; continuous line: 1 September). Increase in temperature and wind speed on 19 August (thin continuous line) did not seem to have resulted in a loss of <sup>222</sup> Rn from the very stable boundary layer. ....	39
<b>Fig. 15.</b> Variations of bacterial number concentration (error bars indicate ± 1 s.e.) and <sup>222</sup> Rn activity concentration (error bars smaller than symbol) (upper panels), and atmospheric pressure and wind speed prior and during the four campaigns (lower panels). ....	50
<b>Fig. 16.</b> Empirical relation between <sup>222</sup> Rn flux and γ-dose rate. The green points show the values we measured in Spain. The white line and red line represent the fitted linear slope before and after adding the Spanish points, respectively. ....	56
<b>Fig. 17.</b> Measurements of <sup>222</sup> Rn and HFC at Jungfraujoch during late July to early August 2008 (HFC data from Stefan Reimann, Empa). ....	57

# List of Tables

<b>Tab. 1.</b> Overview of the site characteristics. Latitude and longitude are reported in decimal degree together with site height. Present average humidity and temperature conditions during the measurement campaign were also recorded.....	8
<b>Tab. 2.</b> Overview on characteristics of direct and indirect measurements methods to determine $^{222}\text{Rn}$ flux from soil.....	13
<b>Tab. 3.</b> Means and standard deviation (s.d.) of meteorological parameters for the three main wind sectors during dry (no precipitation) and wet (precipitation > 0) conditions.....	31
<b>Tab. 4.</b> Observed changes between sunset (1800 UTC) and sunrise (0500 UTC) during nights with strong cooling, light winds and clear-sky conditions: temperature at 2.0 m above ground ( $\Delta T$ ), atmospheric $^{222}\text{Rn}$ concentrations at 0.1 m ( $\Delta^{222}\text{Rn}_{0.1\text{m}}$ ) and 6.5 m ( $\Delta^{222}\text{Rn}_{6.5\text{m}}$ ) above ground. Estimated amounts of $^{222}\text{Rn}$ accumulated during this period are based on the assumption of exponential $^{222}\text{Rn}$ concentration profiles around sunset and sunrise. ....	38
<b>Tab. 5.</b> Results of four campaigns to measure total bacterial cell number and $^{222}\text{Rn}$ activity concentrations at the High Altitude Research Station Jungfraujoch (3450 m above sea level). Bacterial flux density estimates were derived by mass balance with $^{222}\text{Rn}$ and related to duration of entire campaigns, except for the campaign in July, where only the first two measurement points were used because of changed weather conditions later. Time stamps are at the end of 3 h measurement intervals and are in local time (UTC +2). Values in brackets indicate 1 standard error .....	48
<b>Tab. 6.</b> Results of $^{222}\text{Rn}$ flux measurement using AlphaGUARD.....	55
<b>Tab. 7.</b> Comparison of flux estimates for HFC-134a based on the current assumption of a spatially homogenous $^{222}\text{Rn}$ flux of $76 \text{ Bqm}^{-2}\text{h}^{-1}$ and based on our improved $^{222}\text{Rn}$ estimates.....	56



# Chapter 1

## Introduction

Of all the naturally occurring radioactive elements, radon ( $^{222}\text{Rn}$ ) has been one of the mostly widely used atmospheric tracers.  $^{222}\text{Rn}$  is a naturally occurring radioactive inert gas. It originates from the decay of  $^{226}\text{Ra}$  in the decay series of  $^{238}\text{U}$ , which is ubiquitous in all soils (Fig. 1). The only sink of  $^{222}\text{Rn}$  in air is its radioactive decay. Since  $^{222}\text{Rn}$  is relatively insoluble in water and does not attach to aerosols, dry or wet atmospheric removal processes do not influence its atmospheric concentration variations (Jacob and Prather, 1990; Li and Chang, 1996).  $^{222}\text{Rn}$  has a half-life of 3.82 days, which is comparable with the chemical lifetimes of short-lived air pollutants such as  $\text{NO}_x$ ,  $\text{SO}_2$ , and with the time scale of many important boundary layer processes. In several studies,  $^{222}\text{Rn}$  has been applied as an inert tracer of near-surface turbulent transport and gas flux estimates (Morrizumi et al., 1996; Wilson et al., 1997; Lehmann et al., 2001; Schmidt et al., 2003).

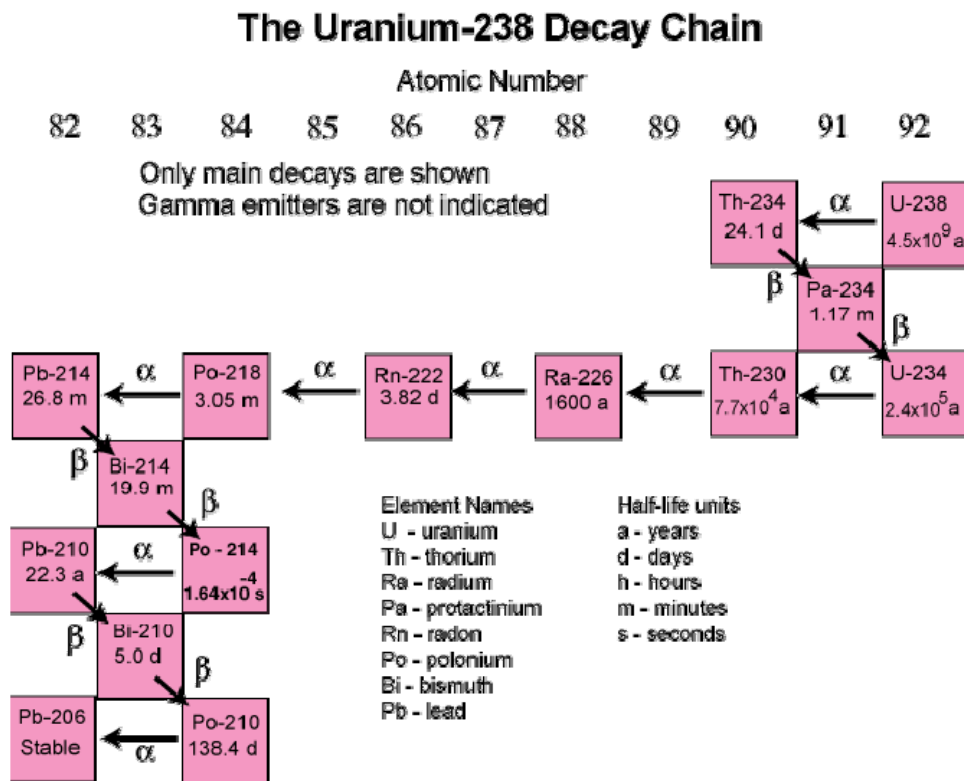


Fig.1: The radioactive decay chain of Uranium-238 with half-life time and decay mode (<http://pubs.usgs.gov>).

Interactions between the land surface and the atmosphere and associated boundary layer processes are of key importance to the variability in the climate system. They determine how much energy and mass are exchanged between the land surface and the atmospheric boundary layer (ABL), and between the ABL and the free troposphere. In turn, climate change affects the variations of the land surface structure and land-atmosphere interactions. For instance, temperature and soil moisture affect the emission of gases and aerosol from surface into the atmosphere.

The ABL is defined as “...*the part of the troposphere that is directly influenced by the presence of the earth’s surface, and responds to surface forcing with a time scale of about an hour or less.*” (Stull, 1988). After sunrise the solar radiation starts to rapidly warm the surface, initiating thermal instability or convection. Because of the following strong mixing, atmospheric compounds like trace gases and aerosols are well mixed and homogenized. After sunset the surface is rapidly cooled due to radiative heat loss. The lowest part of the ABL, which is closest to the surface, cools fastest and forms a stable nocturnal boundary layer. Above it, the remnants of the daytime ABL form a residual layer. In the stable near surface layer, the nocturnal boundary layer, turbulent vertical mixing is strongly suppressed, even though intermittent turbulence (e.g. when cold air advects over a warm surface) may cause the interruption of this stability. Most atmospheric gases and pollutants, originating at or near the surface, are retained in this stable layer and cannot be released into the free troposphere. Better understanding of the stable nocturnal boundary layer helps to improve atmospheric transport models, to forecast the night climate and to determine pollutant dispersion and build-up of greenhouse gas concentrations at night over land. However, using purely meteorological variables and traditional turbulence measurements, it is very difficult to demonstrate the vertical decoupling between a stable nocturnal boundary layer and the atmosphere above it because of intermittency issues. The observations of near-surface behavior of a passive tracer can provide more convincing information on the performance of the stable nocturnal boundary layer and meteorological effects associated with it.

Aerosols have been well recognized to play an important role in affecting the climate system. Aerosols both absorb and scatter the solar radiation, so they change the way radiation is transmitted through the atmosphere, which is the so-called direct effect (Coakley et al., 1983; Charlson et al., 1992; Penner et al., 1992). In addition aerosols can indirectly modify cloud microphysical and optical properties by acting as cloud condensation nuclei or as ice nuclei (Twomey, 1977; Albrecht, 1989). Bacteria are one of the many types of biogenic aerosol particles that are ubiquitous in the atmosphere (Jaenicke et al., 2007). Because some bacteria are highly effective in acting as cloud condensation nuclei and as ice nuclei, airborne bacteria deserve particular attention for their potentially significant influence on cloud processes. Due to their small size, bacteria have a long atmospheric residence time of about 1 ~ 2 weeks and can be transported over a long distance. Location and environmental conditions such as humidity, source density and temperature have a great effect on the amount of bacterial cells in the air. Some of the major sources of airborne bacteria are plants, soil and water surfaces (Jones and Harrison, 2004). Bacteria can become



airborne through active mechanisms, including ejection from surface into the atmosphere, or passive mechanisms of meteorological processes such as wind gusts (Burrows et al., 2009b). Once entering into the atmosphere, bacteria experience the same transport and mixing as other air constituents. Typical concentrations of bacterial cells near the surface over land are on the order of 1000 - 10000 cells m<sup>-3</sup> (Burrows et al., 2009a). Existing flux estimates are few and strictly focused on the culturable bacteria (Lindemann et al., 1982; Lindemann and Upper, 1985; Lighthart and Shaffer, 1994). Flux measurements of total bacteria have not been made so far. However, the total bacterial flux density is a crucial factor for cloud processes, since dead cells and even cell fragments may still act as condensation and ice nuclei (Möhler et al., 2008). The mass balance with <sup>222</sup>Rn as an atmospheric tracer gas may provide a reliable way to estimate the flux density of total bacterial cells from surface to free troposphere. The principle is based on the hypothesis that bacteria are transported and mixed in air with the same efficiency as the tracer gas <sup>222</sup>Rn to a remote site and that bacteria and <sup>222</sup>Rn from different sources within a footprint are well mixed upon arrival at a remote site. According to a mass balance approach, we may estimate the flux density of total bacterial cells by measuring flux and concentration of a tracer gas and the number concentration of total bacterial cells.

The research reported in this dissertation shows how the naturally occurring isotope <sup>222</sup>Rn can be utilized successfully as an atmospheric tracer for studying the land-atmospheric interactions and boundary layer processes. Accuracy of measuring <sup>222</sup>Rn flux and concentrations is an important issue. Hence inter-comparisons of different techniques for measuring <sup>222</sup>Rn emission and concentration were part of this study. Then, based on measurements of <sup>222</sup>Rn flux and concentrations, we evaluate the evolution of stable nocturnal boundary layer and estimate the flux density of total bacterial cells between boundary layer and free troposphere. This dissertation mainly consists of four chapters:

**Chapter 2** of the dissertation presents a comparison of <sup>222</sup>Rn flux measurements with direct and indirect methods. The campaign was carried out in the summer of 2008 in four selected Spanish sites. We contributed as co-authors to determine the <sup>222</sup>Rn flux from soil surface by (a) accumulation method and (b) measurements of gamma dose rate, which was suggested to have a correlation with <sup>222</sup>Rn flux (Szegvary, 2007). Measurements of <sup>222</sup>Rn flux from soil obtained by different methods agreed well. This paper has been published in the journal *Radiation Measurements* (Grossi et al., 2011).

**Chapter 3** presents measurements of atmospheric <sup>222</sup>Rn concentration by two different types of detectors, a two-filter and one-filter type of detector, which measure <sup>222</sup>Rn and its short-lived progeny, respectively. This campaign was conducted at Schauinsland station in the black forest in South-West Germany. Results from the two different types of detectors showed some agreement. However, precipitation and forest canopy in the fetch had a negative influence on measurements made with the one-filter detector, which estimated <sup>222</sup>Rn concentration via its short-lived aerosol-attached progeny. This paper has been published in *Atmospheric Measurement Techniques* (Xia et al., 2010).

**Chapter 4** reports on flux and vertical mixing profiles of  $^{222}\text{Rn}$  during night applied to explore the characteristics of the nocturnal stable boundary layer structure. Nights with light wind, clear skies and strong cooling were selected in the summer of 2009 at K-puszta station in the Hungarian part of the Carpathian Basin. Vertical profiles of  $^{222}\text{Rn}$  concentration and  $^{222}\text{Rn}$  flux were simultaneously monitored. We observed that  $^{222}\text{Rn}$  concentration increased during the nights and reach a maximum at dawn. Most  $^{222}\text{Rn}$  emitted from the surface was trapped in a shallow layer near the surface. These observations support the theory of a two-stratum structure of the nocturnal boundary layer (Banta et al., 2007). This paper has been published in the journal *Boundary-Layer Meteorology* (Xia et al., 2011).

**Chapter 5** is related to evaluating the characteristics of emission and transport of bacteria in the atmosphere using  $^{222}\text{Rn}$  as a tracer gas. Once airborne, both bacteria and  $^{222}\text{Rn}$  are transported with the same efficiency. At the High Altitude Research Station Jungfraujoch, we simultaneously measured the  $^{222}\text{Rn}$  and total bacterial cell number concentration in the air. The fact that the variation in both concentrations behaved in different ways indicated that the source / sink processes of total bacteria are not as homogeneous or stable as those of  $^{222}\text{Rn}$ . The meteorological conditions have an important effect on both flux density and concentration of total bacteria in air. This paper has been submitted to *Atmospheric Environment*.

## Chapter 2

# Inter-comparison of different direct and indirect methods to determine radon flux from soil

This paper in press by Radioation Measurements as: Grossi, C., Vargas, A., Camacho, A., López-Coto, I., Bolívar, J.P., Xia, Y., Conen, F. (2011) Inter-comparison of different direct and indirect methods to determine radon flux from soil, Radiation Measurements, 46 (1), 112-118.

### 2.1 Abstract

The physical and chemical characteristics of radon gas make it a good tracer for use in the application of atmospheric transport models. For this purpose the radon source needs to be known on a global scale and this is difficult to achieve by only direct experimental methods. However, indirect methods can provide radon flux maps on larger scales, but their reliability has to be carefully checked. It is the aim of this work to compare radon flux values obtained by direct and indirect methods in a measurement campaign performed in the summer of 2008. Different systems to directly measure radon flux from the soil surface and to measure the related parameters terrestrial  $\gamma$  dose and  $^{226}\text{Ra}$  activity in soil, for indirect estimation of radon flux, were tested. Four eastern Spanish sites with different geological and soil characteristics were selected: Teruel, Los Pedrones, Quintanar de la Orden and Madrid. The study shows the usefulness of both direct and indirect methods for obtaining radon flux data. Direct radon flux measurements by continuous and integrated monitors showed a coefficient of variation between 10 % and 23 %. At the same time, indirect methods based on correlations between  $^{222}\text{Rn}$  and terrestrial  $\gamma$  dose rate, or  $^{226}\text{Ra}$  activity in soil, provided results similar to the direct measurements, when these proxies were directly measured at the site. Larger discrepancies were found when proxy values were extracted from existing data bases. The participating members involved in the campaign study were the Institute of Energy Technology (INTE) of the Technical University of Catalonia (UPC), Huelva University (UHU), and Basel University (BASEL).

## 2.2 Introduction

Radon characterization from the soil surface allows estimating the external contribution to indoor  $^{222}\text{Rn}$  concentrations and provides a necessary input term to the study of atmospheric transport processes. In the first case, generating radon flux maps can be useful for regulatory national organizations in order to classify radon prone areas (Bohicchio, 2008; Kreuzer et al., 2003). In the second case, the  $^{222}\text{Rn}$  source term, in combination with observations of atmospheric  $^{222}\text{Rn}$  concentration, facilitates the evaluation and calibration of atmospheric transport models (Zahorowski et al., 2004, Arnold et al., 2010). The  $^{222}\text{Rn}$  source is mainly located on the land surfaces. Its only sink in the atmosphere is by radioactive decay with a half-life of 3.8 days. The large contrast between terrestrial and oceanic radon flux makes  $^{222}\text{Rn}$  an ideal atmospheric tracer at a regional scale (Lupu and Cuculeanu, 2001; Whittlestone et al., 1992). Development of atmospheric dispersion models has progressed to a point where improved knowledge of the  $^{222}\text{Rn}$  source term becomes necessary for more accurate validation (WMO, 2004). The  $^{222}\text{Rn}$  concentration in soil and its emission rate depend on the geology of an area, the porosity and permeability of the soil, the terrain structure and the associated  $^{238}\text{U}$  mineralization. Diffusion is the process which allows  $^{222}\text{Rn}$  to escape from soil pores to the atmosphere after its formation by  $^{226}\text{Ra}$  decay. In spite of sufficient understanding of the theoretical processes controlling release of  $^{222}\text{Rn}$  from soil to the atmosphere (Nazaroff and Nero, 1988; Porstendörfer, 1994), comprehension of the radon flux and its distribution over the earth is still under question because of a lack of direct radon flux measurements in many regions. Direct measurements of radon flux are ideally made using the accumulation method (Keller et al., 1982; Keller and Schutz, 1988) which allows  $^{222}\text{Rn}$  gas to accumulate and to be measured in a chamber placed over the soil. Nevertheless, this approach is not practical on a worldwide scale. A more realistic alternative might be to obtain at least a modest number of accumulator measurements, but at carefully chosen locations, representative of different geological regions and to extrapolate these measurements to similar regions.

Nowadays, other approaches are also used to overcome the need for labor-intensive direct observations. Indirect mapping of radon flux is possible thanks to existing knowledge about parameters related to radon flux and for which more large-scale information is available than for radon flux itself. Different approaches have been applied in order to indirectly map the radon flux. The simplest assumption is that of a radon flux value from the land surface of  $1 \text{ atom cm}^{-2} \text{ s}^{-1}$  between  $60^\circ\text{S}$  and  $60^\circ\text{N}$ , of  $0.5 \text{ atom cm}^{-2} \text{ s}^{-1}$  between  $60^\circ\text{N}$  and  $70^\circ\text{N}$  and of  $0 \text{ atom cm}^{-2} \text{ s}^{-1}$  for the sea (Rash et al., 2000). A modification with a linear decrease from  $1 \text{ atom cm}^{-2} \text{ s}^{-1}$  at  $30^\circ\text{N}$  to  $0.2 \text{ atom cm}^{-2} \text{ s}^{-1}$  at  $70^\circ\text{N}$  was proposed (Conen and Robertson, 2002). These estimates are based on atmospheric  $^{222}\text{Rn}$  inventories. Another approach has been recently developed within the Swiss project "European radon flux map for atmospheric tracer applications" by Basel University. It is based on the determination of an empirical linear relation between the radon flux and the terrestrial  $\gamma$  dose on a European scale. These last values were extracted during the project from routinely

reported emergency monitoring data. These data are available in quasi real time at the Joint Research Centre of the European Commission of ISPRA (Italy) from each of the 3,600 stations of the national emergency monitoring network in Europe, EURDEP (Szegvary et al., 2007).

Knowledge about the used detectors from each contributing country, the detector elevation above sea level and the possible contribution from artificial radionuclides, mainly  $^{137}\text{Cs}$ , enables the extraction and the spatial modeling of the terrestrial  $\gamma$  dose (Szegvary et al., 2007). The dose-rate values for the EURDEP network regarding Spain are provided by the REA, the Spanish Automatic Surveillance Network of the Spanish Nuclear Safety Council (CSN). Another option to obtain the terrestrial  $\gamma$  dose rates is by radiometric data generated through the Spanish National Uranium Exploration and Investigation Plan. This work has developed into the Spanish MARNA project (Quindós et al., 2004).

The present study aims to compare different methods for direct and indirect radon flux estimation in specific Spanish areas and under their most typical climatologic conditions. An inter-comparison campaign was carried out at four selected Spanish sites in the summer of 2008. Direct radon flux measurement systems required to be compared and previous indirect methods (Szegvary et al., 2007; Quindós et al., 2004) wanted to be validated. Continuous and integrated techniques were applied for direct measurements of radon flux from soil. Terrestrial  $\gamma$  dose-rate and  $^{226}\text{Ra}$  activity soil measurements were done and used to indirectly estimate radon flux. The members involved in the campaign were Huelva University (UHU), Basel University and the Institute of Energy Technology (INTE) of the Technical University of Catalonia (UPC).

## 2.3 Material and methods

The measurement campaign across Eastern Spain was performed during the summer of 2008, in the middle of July. In order to avoid rainy episodes that may influence soil humidity, terrestrial  $\gamma$  dose rate or radon flux, the campaign was carried out during the most typical eastern Spanish climatologic conditions. The radon flux ( $\text{Bq m}^{-2} \text{ h}^{-1}$ ) and  $\gamma$  dose rates ( $\text{nSv h}^{-1}$ ) were measured at each site by several monitors and in different points in order to get an average values. The  $^{226}\text{Ra}$  activity ( $\text{Bq kg}^{-1}$ ) was determined in the laboratory on soil samples collected during this time. Each parameter was determined with different equipment by the campaign members with the aim of comparing the results.

### 2.3.1 Sites

Four Eastern Spanish sites were selected in this measurement campaign. The chosen locations were Teruel, Los Pedrones, Quintanar de la Orden and Madrid shown in Fig.1. The location characteristics, the average humidity and the temperature conditions during the measurement campaign are reported in Table 1. These locations are included within the Spanish Automatic Surveillance Network (REA) which allows an evaluation between our measurements of terrestrial  $\gamma$  dose rates with the routine

REA data. Furthermore, this selection of sites promised a wide range of radon flux values to be obtained as suggested by the European radon map (Szegvary et al., 2009). Finally, the direct measurements were considered a validation of the anomalously high radon flux values indicated by this map in comparison to the rest of Europe.

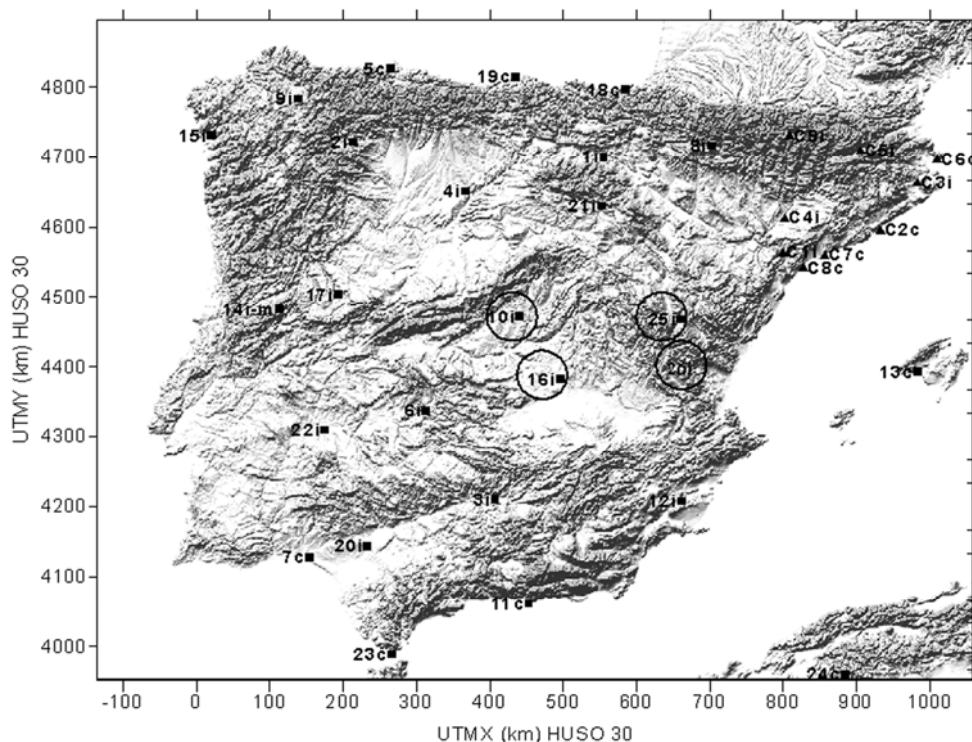


**Fig. 1.** Map of the location of radiological stations belonging to Spanish surveillance networks. The selected Spanish sites in the inter comparison campaign are labeled in the map by circular points: Madrid (10i), Quintanar de la Orden (16i) and Teruel (25i) are included in the Spanish Automatic Surveillance Network (REA). Los Pedrones station (26i) belongs to the radiological network of the Autonomous Valencia region.

**Tab. 1.** Overview of the site characteristics. Latitude and longitude are reported in decimal degree together with site height. Present average humidity and temperature conditions during the measurement campaign were also recorded.

Site	Latitude	Longitude	Height (m)	R.H. (%) min-max	T (°C) min-max
Teruel	40.4505	-1.0587	1082	33-36	30-33
Los Pedrones	39.4714	-0.9705	678	50-60	22-25
Q. de la Orden	39.7870	-3.5377	693	48-53	22-26
Madrid	40.5799	-3.6232	682	37-50	25-31

### 2.3.2 Terrestrial $\gamma$ -dose rate

Total  $\gamma$  dose measurements were performed at each station at 1 m above the ground with the following portable monitors. A High Pressure Ionization Chamber RS-112 (HPIC, GE Reuter-Stockes, Inc.) was used by the INTE-UPC. This model has a volume of 4.2 liters. It is filled with Argon gas at a pressure of 25 atm. Its measurement range is between  $10 \text{ nGy h}^{-1}$  and  $5 \text{ } \mu\text{Gy h}^{-1}$  with a precision of 5 %. A GammaTRACER (Genitron Instruments GmbH, Frankfurt, Germany) with a dual Geiger-Müller-tube was used by Basel University. This device has one tube with 110 pulses per min at  $100 \text{ nSv h}^{-1}$  and another tube with 0.2 pulses per min at  $100 \text{ nSv h}^{-1}$ . The measurement range is between  $10 \text{ nSv h}^{-1}$  and  $10 \text{ Sv h}^{-1}$ . A proportional counter probe LB 123D by the Berthold company was used by the UHU. Its sensitivity is  $0.20 \text{ } \mu\text{Sv h}^{-1}$  per 1 cps. The energy range is from 30 KeV to 2 MeV. The dose rate range covers 6 decades from  $50 \text{ nSv h}^{-1}$  to  $10 \text{ mSv h}^{-1}$ . All devices were located within 5 m from each other. The measurements represent the total  $\gamma$  dose rate. They include a terrestrial component, mainly from  $^{40}\text{K}$ ,  $^{238}\text{U}$ ,  $^{232}\text{Th}$  and their progeny, a cosmic component, principally muons, an anthropogenic component, largely from  $^{137}\text{Cs}$ , and an inherent background of the measurement devices. The terrestrial natural  $\gamma$  dose rate was obtained by subtraction of all the other components.

Terrestrial dose-rate data have also been reported from the REA monitoring network, the MARNA map (Quindós et al., 2004), which has a spatial resolution of 1 km, and the European radon map (Szegvary et al., 2007). The REA Network has an automatic radiological station (ERA) at each site which consists of dual Geiger-Müller tubes, model BAI9305 from the Berthold Company, to observe both low and high  $\gamma$  doses. Two data series were extracted from the REA Network. One is directly provided by the Spanish Nuclear Safety Council (CSN) and the other has been corrected according to a past optimization quality study carried out by Saéz-Vergara et al. (2002). This last correction was effectively realized by a comparison between the reference CIEMAT dose-rate monitors, located at standard height of 1 m above the ground, and the REA dose-rate monitors.

### 2.3.3 $^{226}\text{Ra}$ activity

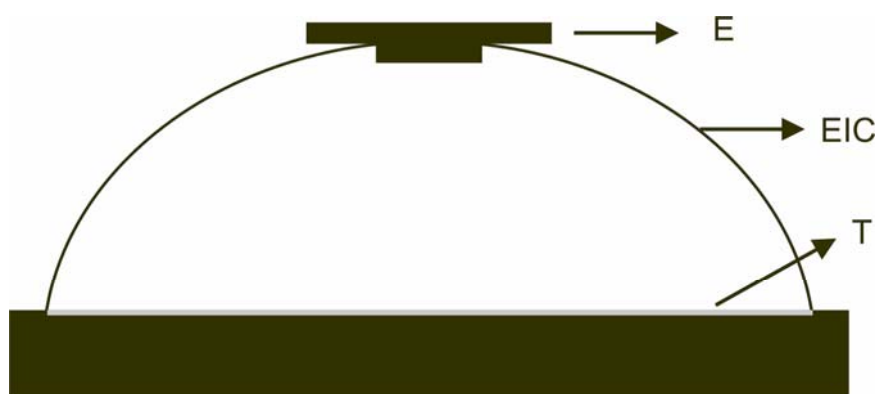
Soil samples were collected at each campaign station at different depths between 0 and 70 cm by rock sampling technique. The soil samples of 100 g in weight were then put into air-tight Petri dishes of 100 ml in volume. The Petri dishes were kept for 30 days to allow the  $^{226}\text{Ra}$  to reach secular equilibrium with its short-lived progeny. The soil samples were then analyzed at the INTE-UPC and at the UHU laboratories by  $^{214}\text{Pb}$  and  $^{214}\text{Bi}$  radium progeny  $\gamma$ -spectrometry. The  $^{226}\text{Ra}$  activity was also reported from the MARNA map. This method, as opposed to spectrometry, uses acquired terrestrial  $\gamma$  dose from all the natural radio nuclides ( $D_{\text{tot}}$ ) to obtain the  $^{226}\text{Ra}$  contribution to the dose ( $D_{\text{Ra}}$ ) by the empirical equation,  $D_{\text{Ra}} = 0.24 \cdot D_{\text{tot}}^{1.01}$ . This result is then employed to derive the radium activity in the soil using the hypothesis that  $^{226}\text{Ra}$  activity is closely related to  $^{238}\text{U}$  activity (Quindós et al., 2004).

### 2.3.4 Radon flux

The radon flux at the selected Spanish locations was measured during this campaign by four different systems; two integrating systems and two continuous monitors. The first were the electret radon flux monitor and the activated charcoal method. The continuous devices were an AlphaGUARD (Genitron Instruments GmbH, Frankfurt, Germany) and a Sun Nuclear model 1027. All these integrated and continuous systems are based on the well known accumulation method (Morawska and Phillips, 1980). The evolution  $^{222}\text{Rn}$  concentration in the chamber can be measured by continuous monitoring or estimated after a given time period by the integrated systems.

A commercial version of a radon flux monitor (E-PERM) has been used in this study with short-term, ST, electret and H chamber of 960 ml volume. This is a hemispherical dome with a 15 cm diameter Tyvek window (Kotrappa, 1993). It works as an integrating ionization chamber with an electrically charged electret on its internal top. The Tyvek window allows the radon gas exhaled from the soil to enter the electret ion chamber over a time period  $T$ . The electret voltage drops in relation to the total ionized air due to the radon decay inside the chamber. The electret system response is not influenced by the environmental temperature and humidity conditions as has been tested in different works such as in Vargas and Ortega, 2006).

The single device scheme is illustrated in Fig. 2 as representative of all accumulation methods. A number of 8 H chambers were used in this campaign at each site, integrating over 6 h measurement time. Three of them were used to subtract the radioactive background. The chambers were located at 50 cm distance from each other, covering a total area of  $1 \text{ m}^2$ .



E : Electret  
T : Tyvek window  
EIC : Electret Ion Chamber

**Fig. 2.** Scheme of the ionization chamber type H (E-PERM) used for radon flux measurement. The ionization chamber (EIC) is located on the ground (black space) and the exhaled radon can enter through the Tyvek window (T). The radon concentration is proportional to the potential drop due to radon decay on the positively charged electret (E) located on the chamber top in the air chamber.



The other integrating system used to determine the radon flux, involved  $^{222}\text{Rn}$  adsorption on activated charcoal, has been explained in detail elsewhere (Countess, 1976; Fremman and Hartley, 1986; Dueñas, 2007). The charcoal response is influenced by the environmental conditions as previous studies have shown (Ronca-Battista, 1988; Vargas and Ortega, 2006). The  $^{222}\text{Rn}$  collector is placed on the soil surface to be accumulate  $^{222}\text{Rn}$  over a time period  $T$ .  $^{222}\text{Rn}$  is then determined through its progeny  $^{214}\text{Pb}$  (295 KeV and 352 KeV) and  $^{214}\text{Bi}$  (609 KeV) in secular equilibrium conditions by gamma spectrometry (Kaplan, 1963). A number of 3 charcoal canisters were exposed at each site during 6 hours and covering a total surface area of around  $0.5 \text{ m}^2$ . Each charcoal canister was made of a cylindrical box with a circular surface approximately of 10 cm diameter and 1.3 cm high. The canisters were located directly on soil surface, avoiding void volume between this and absorbent material. The  $^{222}\text{Rn}$  activity concentration accumulates inside a closed volume which is placed on the soil surface. The  $^{222}\text{Rn}$  gas, in the chamber volume was measured continuously by the AlphaGUARD monitor (Genitron) and the Sun Nuclear model 1027 monitors. The Sun Nuclear monitor is a patented electronic detecting device using a diffused-junction photodiode sensor to measure  $^{222}\text{Rn}$  gas concentration by radon progeny electrodeposition (López-Coto et al., 2009). The monitor was located directly inside the accumulation volume and the radon flux was measured by  $^{218}\text{Po}$  (6 MeV) alpha spectrometry during 6 h at one point in each measurement location. The AlphaGUARD monitor was placed near the accumulation volume chamber. The sampling air was pumped inside the monitor at a flow rate of 0.3 l/min and concentration values were provided for each 10 min interval. A small 1-l plastic bottle was used to prevent aerosols and  $^{220}\text{Rn}$  from entering into the AlphaGUARD (Lehmann et al., 2003). The AlphaGUARD have been acquiring during 2 h at 3 different points at each measurement location.

The four different systems were located close to each others, covering a circular surface area with a radius of about 5 m. Table 2 summarises the device characteristics and their geometrical position during the campaign measurements.

The  $^{222}\text{Rn}$  emitted from the soil surface is accumulated during a time period ( $T$ ) in each integrated and continuous known volume monitor (De Martino and Sabbarese, 1997). The temporal variation of the  $^{222}\text{Rn}$  concentration in the chamber is expressed by the follow equation:

$$\frac{dC(t)}{dt} = \frac{E_{\text{Rn}}}{V_{\mu}} - \lambda^0 C(t) \quad (1)$$

where  $C(t=0) = 0$  is the initial concentration ( $\text{Bq m}^{-3}$ );  $E_{\text{Rn}}$  is the exhalation velocity which is defined as the  $^{222}\text{Rn}$  gas quantity leaving the soil in the time unit ( $\text{Bq h}^{-1}$ );  $V_{\mu}$  is the available chamber volume ( $\text{m}^3$ ) and the constant  $\lambda^0 = \lambda + \lambda^*$  ( $\text{h}^{-1}$ ) is given by the sum between the  $^{222}\text{Rn}$  decay ( $\lambda$ ) and the ventilation constants ( $\lambda^*$ ). The  $\lambda^*$  quantifies the possible changes of  $^{222}\text{Rn}$  with external air because of leaks in the chamber. Another physical factor which may be taken into account in the  $^{222}\text{Rn}$  accumulation is called back-diffusion and it means the possibility of  $^{222}\text{Rn}$  being

adsorbed back from the soil surface. This last factor is not significant for short time measurements (Morawska, 1989) as applied in our analysis. The solution of the Eq. 1 is:

$$C(t) = \frac{E_{Rn}}{\lambda^0 V_{\mu}} (1 - e^{-\lambda^0 t}) \quad (2)$$

where value  $E_{Rn} \lambda^{0-1} V_{\mu}^{-1}$  (Bq m<sup>-3</sup>) is the saturation concentration value exhaled in the air-tight chamber after almost 30 days. In the case of short-time measurements and negligible leakages in the chamber,  $\lambda^0 t \ll 1$  can be assumed.

The previous Eq. 2 can be simplified by developing the exponential into Eq. 3:

$$C(t) = \frac{E_{Rn}}{V_{\mu}} t = \frac{F \cdot A}{V_{\mu}} t \quad (3)$$

Equation 3 describes a linear relation between the <sup>222</sup>Rn concentration in the chamber and time. F (Bq m<sup>-2</sup> s<sup>-1</sup>) is the radon flux and A is the surface area covered by the accumulation chamber. The linear method (Eq. 3) was used for both continuous methods in the present study.

The radon fluxes by integrated systems have been measured using the average <sup>222</sup>Rn concentration inside the chamber above a given time T calculated by equation:

$$\overline{C(Rn)} = \frac{1}{T} \int_0^T C(t) dt = \frac{E_{Rn}}{\lambda^0 V_{\mu}} \left[ 1 - \left( \frac{1 - e^{-\lambda^0 T}}{\lambda^0 T} \right) \right] = \frac{F \cdot A}{\lambda^0 V_{\mu}} \left[ 1 - \left( \frac{1 - e^{-\lambda^0 T}}{\lambda^0 T} \right) \right] \quad (4)$$

From Eq. 3 and Eq. 4 the radon flux F can be easily derived, for the continuous and the integrated methods, respectively.

Radon fluxes have also been estimated using two indirect methods. The first method (GDR in Table 2) consists of the empirical equation  $y = 0.89x - 11.01$ , derived by Szgevary<sup>a</sup> et al. 2007. The previous relationship has been extrapolated using local  $\gamma$ -dose rate data that have a resolution depending on European Radiological Data Exchange Platform, EURDEP (<http://eurdep.jrc.ec.europa.eu/>) data (Szgevary, 2007). The y, in the empirical equation, represents the estimated radon flux (Bq m<sup>-2</sup> h<sup>-1</sup>) and x is the available terrestrial  $\gamma$ -dose in nSv h<sup>-1</sup>. The  $\gamma$  dose-rates measured by RS-112 (GDR-1) and by the GammaTRACER (GDR-2) have been used as input data. Furthermore, the reference Radon map method, GDR, was analyzed.

**Tab. 2.** Overview on characteristics of direct and indirect measurements methods to determine  $^{222}\text{Rn}$  flux from soil.

Method	Principle	Technique	N. of device/ measurement replicates	N. of location for each measurement site	Single measurement period (h)	Reference
<b>Direct Methods</b>						
Charcoal	Accumulation of $^{222}\text{Rn}$ in charcoal canister;	$\gamma$ spectrometry	3/1	1 on ground surface	6	Dueñas, 2007
E-Perm	Accumulation of $^{222}\text{Rn}$ in chamber	Voltage discharge in Teflon	8/1	1 on ground surface	6	Kotrappa, 1993
AlphaGUARD	Accumulation of $^{222}\text{Rn}$ close volume	$\alpha$ spectrometry	1/3	1 on ground surface	1	Lehmann et al. 2003
Sun Nuclear	Accumulation of $^{222}\text{Rn}$ in closed volume	$\alpha$ spectrometry	1/1	1 on ground surface	4	-
<b>Indirect Methods</b>						
GDR-1 Szegvary-RS112	Empirical relation with measured $\gamma$ dose rate	dual Geiger-Müller	1/1	1 at 1m above ground	5	Szegvary et al., 2009
GDR-2 Szegvary-GammaTRACE R	Empirical relation with measured $\gamma$ dose rate	Ionization chamber	1/2	2 at 1m above ground	2	Szegvary et al., 2007
$^{226}\text{Ra}$ (INTE/UHU)	Empirical relation with $^{226}\text{Ra}$ concentration in soil	Laboratory $\gamma$ spectrometry	1/1	1 at depth of 0-30 cm	1	Quindos, 2004; Nazaroff et al, 1988
<b>Indirect Reference Methods</b>						
GDR Radon Map	Empirical relation with $\gamma$ dose rate extracted from EURDEP database	-	-	-	-	Szegvary et al., 2007
$^{226}\text{Ra}$ MARNA map	Empirical relation with $^{226}\text{Ra}$ concentration in soil derived from MARNA project	-	-	-	-	Quindos, 2004; Nazaroff et al, 1988

The other indirect method ( $^{226}\text{Ra}$  in Table 2) is based on the diffusion equation  $F = C_{\text{Ra}} \lambda f \rho [D_c / (\lambda \varepsilon)]^{1/2}$  (Nazaroff and Nero, 1988), where  $C_{\text{Ra}}$  is the  $^{226}\text{Ra}$  activity ( $\text{Bq kg}^{-1}$ ),  $F$  is the radon flux,  $f$  is the emanation material coefficient,  $\rho$  is the soil density,  $D_c$  is the bulk material diffusion coefficient, which is influenced by soil characteristic and conditions (T and HR), and  $\varepsilon$  is the material porosity. Typical geological parameters, for soil characteristics similar to the soil sites campaign, have been chosen for  $f$  (0.23),  $\rho$  ( $1.5 \cdot 10^3 \text{ kg m}^{-3}$ ),  $D_c$  ( $2.0 \cdot 10^{-7} \text{ m}^2 \text{ s}^{-1}$ ) and  $\varepsilon$  (0.25) (Nazaroff and Nero, 1988).  $^{226}\text{Ra}$  activity was obtained from the MARNA dose rate data and its conversion to activity concentration using the equation described in section 2.3.3. The indirect methods and their comparative applications within this study are summarized in Table 2.

## 2.4 Results and discussion

In the following section the obtained results for the terrestrial  $\gamma$  dose rate,  $^{226}\text{Ra}$  activity and the radon flux are presented and discussed.

### 2.4.1 Terrestrial $\gamma$ dose rate

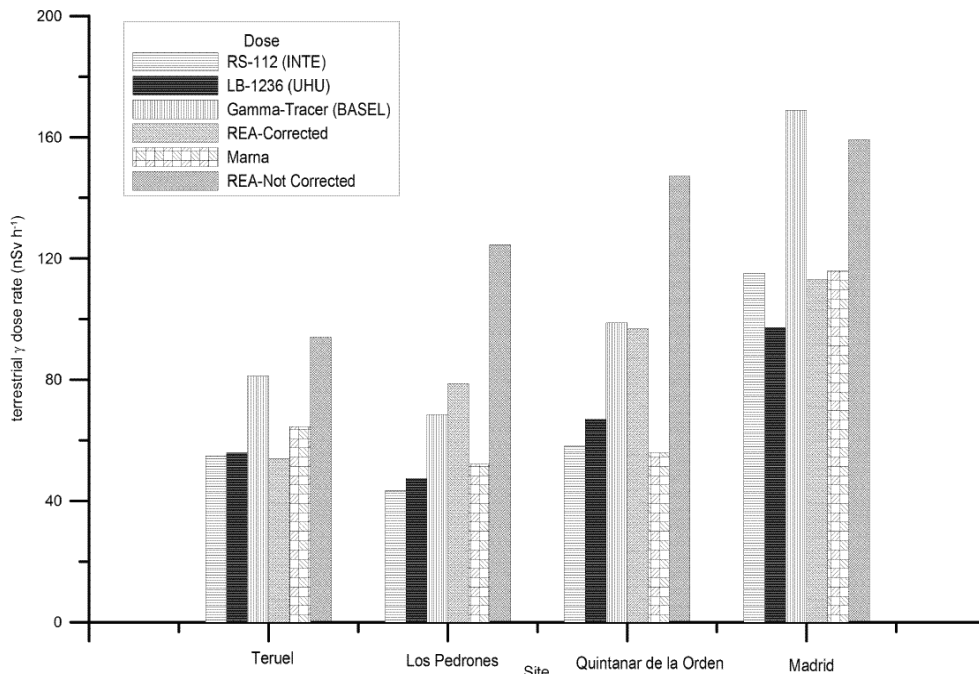


**Fig. 3.** The dose rate measured at each site by RS-112 (INTE), LB-1236 (UHU) and GammaTracer (BASEL) monitors are shown. The dose rate for each REA station and their corrected values are reported in according to Saez-Vergara et al. (2002). Furthermore, values obtained from the MARNA map are also included.

Fig. 3 shows the terrestrial dose rate results obtained by the different equipment and methods. The measured data from the RS-112 (INTE-UPC) and the LB-1236 (UHU) monitoring were in good agreement with the MARNA map for each campaign site. The measured value from the uncorrected REA is too high in comparison with the other measured values. However, the same REA are significantly closer to the other measured values after the correction developed by Saéz-Vergara et al., 2002. The values measured by GammaTRACER tended to be higher than the other data.

#### **2.4.2 $^{226}\text{Ra}$ soil activity mass**

$^{226}\text{Ra}$  soil activity mass in soil samples from each campaign site was analyzed at the INTE-UPC and the UHU laboratories. The  $^{226}\text{Ra}$  activity results in the soil samples from the first terrain layer, which ranges between 0 and 30 cm, were compared as shown in Fig. 4.  $^{226}\text{Ra}$  activities were also measured for deeper soil sampled, until 70 cm, showing a quite homogeneous distribution. The radioactivity concentrations measured at aforementioned laboratories are in agreement within a confidence level of 95 %. An evaluation was also done between previous data and the  $^{226}\text{Ra}$  activity calculated by the MARNA empirical equation (Quindos et al., 2004). These last values were within a range of +/- 5% of the directly measured  $^{226}\text{Ra}$  activity average for Teruel, Q. de la Orden and Los Pedrones soil samples. The results show less agreement for the Madrid soil sample, where the MARNA  $^{226}\text{Ra}$  activity was within a range of +/- 15% of the directly measured average concentration. In order to explain this difference, the gamma spectrum obtained from the soil samples in Madrid was analyzed. The analysis showed a high activity concentration of  $^{40}\text{K}$  (1200 Bq kg<sup>-1</sup>) and of  $^{228}\text{Ra}$  (50 Bq kg<sup>-1</sup>) at the Madrid site, which could influence the reliability of the empirical equation presented in section 2.3.3. The  $^{40}\text{K}$  and the  $^{226}\text{Ra}$  activity at the other sites have a mean value, respectively, of 300 Bq kg<sup>-1</sup> and 23 Bq kg<sup>-1</sup>, which are on average expected in Spain (UNSCEAR, 2000). Therefore, the high activity found in Madrid undermines the hypothesis to obtain at least 65 % of contribution from  $^{226}\text{Ra}$ . It could explain the difference between MARNA derived values and campaign results observed in Madrid.

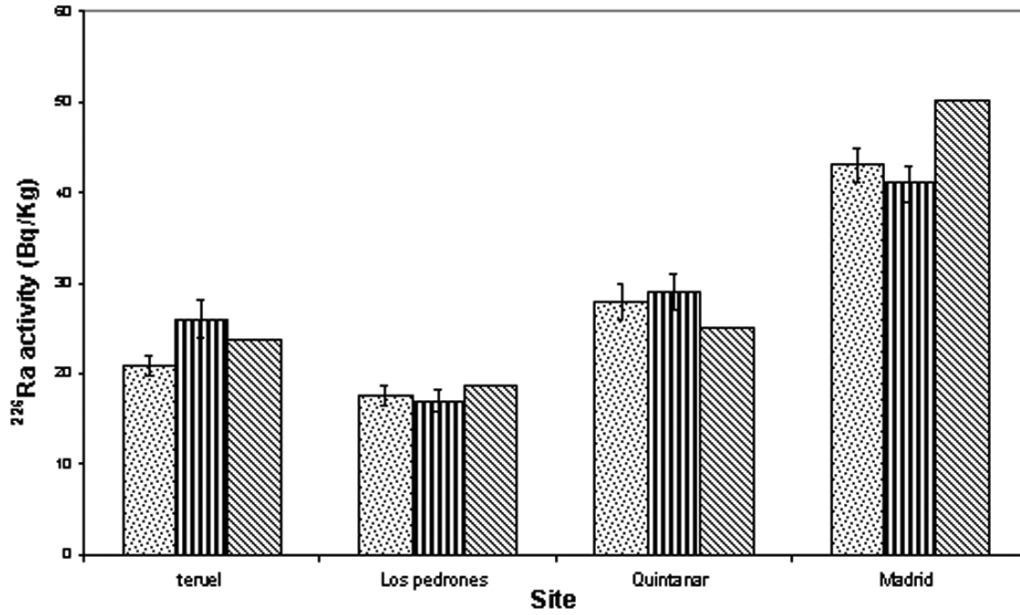


**Fig. 4.** Radium activity concentration measured by the INTE-UPC laboratory (pointed bar), UHU laboratory (vertical line bar) and that obtained by using the MARNA equation,  $D_{\text{Ra}} = 0.24 \cdot D_{\text{tot}}^{1.01}$  (diagonal line bar) are shown.

### 2.4.3 Radon flux

The results of radon flux data by direct measurements and indirect methods are shown in Fig. 5. The plot shows the observations by different campaign partners. Radon flux data calculated by the equation obtained from Szegvary et al. (2007), and by the diffusion equation methods, both described in section 2.3.4, are also reported. The data measured by continuous monitors, AlphaGUARD and Sun Nuclear, and by integrated methods, EPERM and charcoal, show that the agreement among the participants was about 10 % (SD/mean) in Los Pedrones and Q. de la Orden sites, and about 23 % in Teruel and Madrid sites. The activated charcoal gives some differences, compared to the other systems, in Madrid and in Teruel sites. Nevertheless, these values fall within  $2\sigma$  and they have not been rejected. Indirect radon flux estimation, obtained by applying the empirical equation by Szegvary et al. (2007) in section 2.3.4, were within a range of +/- 30% of the directly measured radon flux average when they were based on the terrestrial dose directly measured by RS-112 (GDR-1). These indirect radon flux estimates were larger than the direct radon flux measurements when we used dose-rates from the EURDEP (GDR) data base or from GammaTRACER (GDR-2) measurements. This is due to the high dose-rate values

shown in Fig. 3. Indirect radon flux values, obtained by applying the MARNA equation in section 2.3.4 were within 20 % and 40 % of the directly measured radon flux averages when  $^{226}\text{Ra}$  activity in the soils were obtained from literature ( $^{226}\text{Ra}$  MARNA map) and by laboratories measurements ( $^{226}\text{Ra}$  INTE/UHU), respectively.

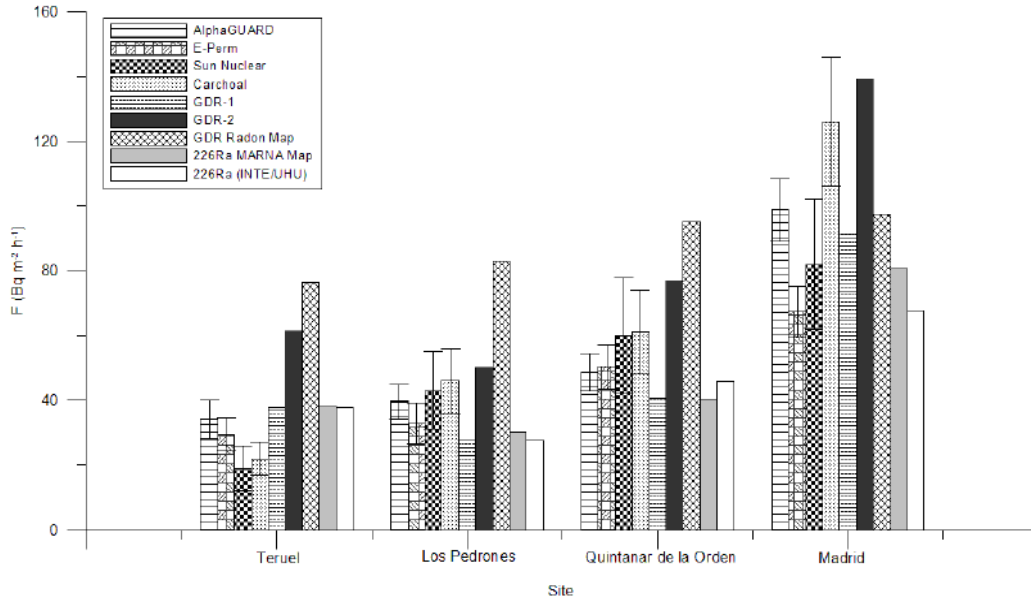


**Fig. 5.** Radon flux levels measured at each site by direct and indirect methods are presented. Values measured by the continuous Sun Nuclear (HUH) and AlphaGUARD (BASEL) monitors, and by the integrated detectors E-PERM (INTE) and charcoal (UHU), are compared. Radon flux ( $y$ ) estimated in order to apply the equation proposed in Szevagy et al. (2007),  $y = 0.89x - 11.01$ , which dose rate ( $x$ ) data from measurements by RS-112 (INTE) and by Gamma-Tracer (BASEL) are also reported. Furthermore, radon flux is also estimated by using the equation  $F = C_{\text{Ra}} \lambda f \rho [D_c / (\lambda \varepsilon)]^{1/2}$  at each site.

## 2.5 Conclusion

Direct and indirect methods, for the determination of radon flux from soil have been used in an intercomparison campaign carried out at four selected Spanish sites in summer 2008 under the most typical climatologic conditions for the eastern Spain. The geological characteristics of the object sites allowed observing a wide range of radon flux values ranging from  $40 \text{ Bq m}^{-2} \text{ h}^{-1}$  and  $90 \text{ Bq m}^{-2} \text{ h}^{-1}$ . Direct methods to determine radon flux, including both continuous and integrated systems, showed a

good agreement with a coefficient of variation between 10 and 23 %. This value is in accordance with the 34 % found out in the study by Hutter and Knutson (1998). Indirect methods based on the measurement of terrestrial  $\gamma$  dose-rate, or  $^{226}\text{Ra}$  soil activity, and their empirical correlation with radon flux, have been applied and evaluated. Results show that these correlations give radon flux values within +/- 20 - 40 % of the directly measured radon flux average when the  $^{226}\text{Ra}$  activity and the terrestrial dose-rate measurements are accurately measured. This was observed for  $^{226}\text{Ra}$  activity obtained either by MARNA map or by direct measurement at INTE and at UHU laboratories and when terrestrial dose rate was measured by RS-112 and by LB-1236 monitors. However, it was found that the terrestrial  $\gamma$  dose-rate values from the Automatic Spanish Surveillance network (REA) and those obtained by GammaTRACER resulted in an overestimation of radon flux. Finally, the influence of seasonal and daily environmental conditions fluctuations on radon flux values are going to be studied in a new campaign which will be carried out during 2010.

## **2.6 Acknowledgement**

This study was supported by the Swiss National Science Foundation (grant no. 200020-117622/1) to FC. Thank to Cristina Parages and José Carlos Saez-Vergara, from the CSN and from the CIEMAT respectively, who helped us to enter into the REA stations during the measurements campaign.



## Chapter 3

# Comparison of one- and two-filter detectors for atmospheric $^{222}\text{Rn}$ measurements under various meteorological conditions

This chapter is published as: Xia, Y., Sartorius, H., Schlosser, C., Stöhlker, U., Conen, F., and Zahorowski, W. (2010) Comparison of one- and two-filter detectors for atmospheric  $^{222}\text{Rn}$  measurements under various meteorological conditions. *Atmos. Meas. Tech.*, 3, 723-731.

### 3.1 Abstract

Parallel monitoring of  $^{222}\text{Rn}$  and its short-lived progeny ( $^{218}\text{Po}$  and  $^{214}\text{Pb}$ ) were carried out from November 2007 to April 2008 close to the top of the Schauinsland Mountain, partly covered with forest, in South-West Germany. Samples were aspired from the same location at 2.5 m above ground level. We measured  $^{222}\text{Rn}$  with a dual flow loop, two-filter detector and its short-lived progeny with a one-filter detector. A reference sector for events, facing a steep valley and dominated by pasture, was used to minimize differences between  $^{222}\text{Rn}$  and progeny-derived  $^{222}\text{Rn}$  activity concentrations. In the two major wind sectors covered by forest to a distance between 60 m and 80 m towards the station progeny-derived  $^{222}\text{Rn}$  activity concentration was on average equal to 87 % (without precipitation) and 74 % (with precipitation) of  $^{222}\text{Rn}$  activity concentration. The observations show that most of the time both detector types follow the same pattern. Still, there is no single disequilibrium factor that could be used to exactly transform short-lived progeny to  $^{222}\text{Rn}$  activity concentration under all meteorological conditions.

### 3.2 Introduction

$^{222}\text{Rn}$  in the lower atmosphere originates from the decay of  $^{226}\text{Ra}$ , a member in the decay series of  $^{238}\text{U}$ , which is present in trace amounts in all soils. Emission rates of  $^{222}\text{Rn}$  vary in space and time (Szegvary et al., 2009). Its only sink in the atmosphere is radioactive decay with a half-life of 3.8 days. This time scale is comparable to the

lifetimes of short-lived atmospheric pollutants and the atmospheric residence time of water and aerosols. It is also comparable to important aspects of atmospheric dynamics, making it a useful tracer at local, regional or global scales for testing and validating atmospheric transport models (Israel, 1951; Jacob et al., 1997; Dentener et al., 1999; Taguchi et al., 2002) and for estimating the emission of greenhouse gases by mass balance approach (Dörr et al., 1983; Gaudry et al., 1992; Schmidt et al., 1996, 2001, 2003; Wilson et al., 1997; Biraud et al., 2000; Conen et al., 2002; Hirsch et al., 2006). Decay products of  $^{222}\text{Rn}$ , such as  $^{218}\text{Po}$  and  $^{214}\text{Pb}$  cluster within less than one second forming small particles with diameters from 0.5 to 5 nm. Besides the cluster formation, these radionuclides attach to the existing aerosol particles in the atmosphere within 1 - 100 s, forming the radioactive aerosol (Porstendörfer, 1994). Either way, they are subject to dry or wet surface deposition (Wyers and Veltkamp, 1997; Yamamoto et al., 1998; Akata et al., 2008; Petroff et al., 2008).

$^{222}\text{Rn}$  activity concentration in air is measured using either two-filter or one-filter detectors. Two-filter detectors involve a first filter removing all air-borne progeny from the air sample, a delay volume where air has a constant mean residence time and where new progeny is produced under controlled conditions, and a second filter to collect the newly produced progeny to be counted (e.g. Whittlestone and Zahorowski, 1998). Measuring  $^{222}\text{Rn}$  with a one-filter detector involves accumulation of its short-lived aerosol-bound progeny directly from the atmosphere onto one filter, its counting, and an assumption about the disequilibrium factor (activity of short-lived progeny/activity of  $^{222}\text{Rn}$ ) between counted progeny and its precursor  $^{222}\text{Rn}$  (Haxel, 1953; Levin et al., 2002). Worldwide, a total of 23 stations forming part of the Global Atmosphere Watch program of the World Meteorological Organization (GAW/WMO) are measuring atmospheric  $^{222}\text{Rn}$  activity concentrations (WMO, 2004). Nine of these stations are equipped with two-filter detectors and 14 use one-filter detectors. The principle difference between one- and two-filter detectors is that two-filter detectors sample from the atmosphere  $^{222}\text{Rn}$  gas while one-filter detectors sample aerosol-bound  $^{222}\text{Rn}$  progeny, which is subject to deposition depending on meteorological conditions. Our objective was to investigate what difference changing meteorological conditions may cause between  $^{222}\text{Rn}$  measurements with one- and two-filter detectors. After the inter-comparison of four different detectors, Collé et al. (1996) draw the following conclusion that stimulated our study: *“Without question, continuous inter-comparison measurements over longer time intervals, two or more uninterrupted weeks or even months, would have been much better. Equally, it would have been more useful to conduct correlations with meteorological data and with  $^{222}\text{Rn}$  progeny measurements and equilibrium ratios.”*

## 3.3 Material and Methods

### 3.3.1 Sampling site

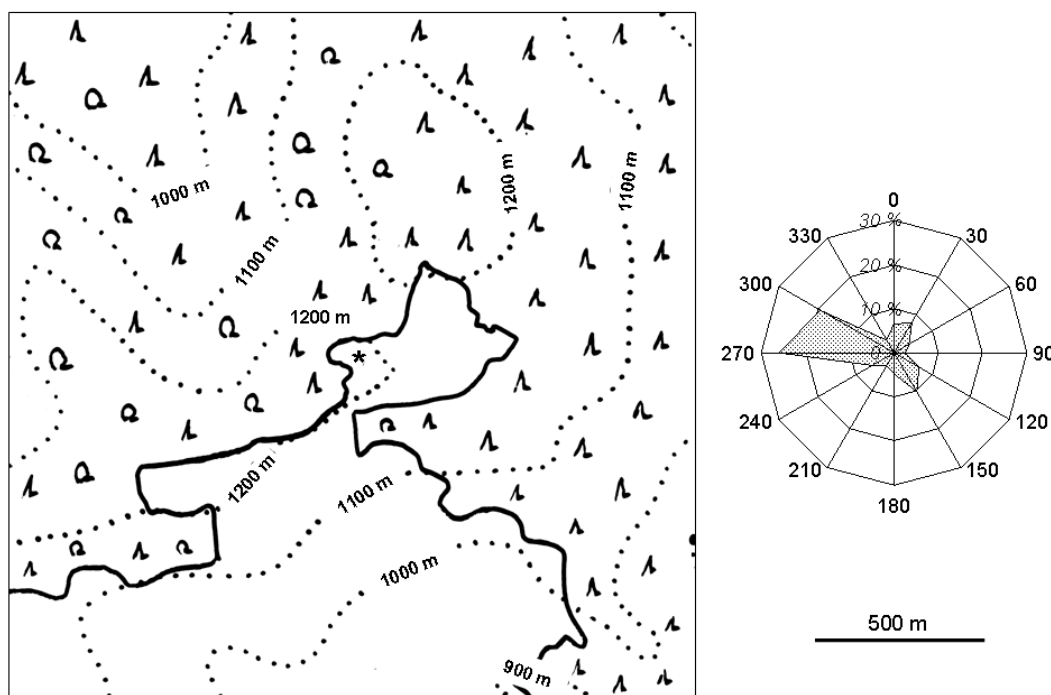


**Fig. 6.** Left: Sketch of topography and forest cover (solid line indicates forest edge) around the measurement station (asterisk in the exact centre) in the Black Forest. Right: Frequency distribution of wind directions for 30° sectors during the observation period. Wind from the sector 120° - 180° is considered to have been least influenced by vegetation.

The sampling site (Fig. 6) is located in the Black Forest in South-West Germany (47°54'15" N, 7°54'33" E, 1200 m a.s.l.) about 750 m North-East of the Schauinsland mountain top (1284 m a.s.l.). Air inlets of both measurement systems were next to each other at 2.5 m above ground. The Schauinsland is a westerly advanced mountain top of the Black Forest mountain range with steep slopes to neighbouring valleys to the North, South and West (Rhine Valley). The orography and local meteorological transport conditions were described in detail by Volz-Thomas et al. (1999) and Seibert et al. (2008). The station is an intensive monitoring station equipped with a number of different sensors and belongs to the Federal Office for Radiation Protection of Germany (Bundesamt für Strahlenschutz, BfS). It is situated approximately 1000 m above the Rhine valley and is surrounded by meadows and woods. Dominating tree species around the station are *Picea abies* and *Fagus sylvatica*, with tree heights between 10 m and 20 m. In winter, the area around the station is usually covered with snow. During night, the Schauinsland is usually above the boundary layer inversion of the Rhine Valley. During day time, and particularly in summer, it mostly lies within the boundary layer (Schmidt et al., 1996). Meteorological parameters are continuously measured about 120 m South-South-East (SSE) of the station by the Federal Environment Agency (Umweltbundesamt), which is at the same time a regional Global Atmosphere Watch (GAW) station. During the

measurement period from 12 October 2007 to 28 April 2008, the dominant wind sector was West-North-West (WNW) (Fig. 6), passing along the forested ridge and traversing only about 60 m grassland before reaching the air inlet at the station. Another frequent wind sector was North-North-East (NNE), along the rather flat, forested mountain top with grassland covering around 80 m between forest edge and station. A third wind sector is to the South-South-East (SSE). Flat grassland extends from the station in this direction for 160 m before the terrain falls off into a steep valley, the upper edge of which is in this direction covered by a narrow strip of mixed forest. We use the last sector as a reference sector while comparing effects of forest cover and precipitation on differences between one- and two-filter detectors in the two other sectors.

### **3.3.2 Measurement Techniques**

#### **3.3.2.1 Two-filter detector**

The two-filter detector we used in this study has been described in detail by Whittlestone and Zahorowski (1998) and Brunke et al. (2002). Air is continuously drawn at a rate of  $0.70 \cdot 10^{-3} \text{ m}^3 \text{ s}^{-1}$  through an inlet tube (diameter 5 cm diameter; length 10 m) and a first delay volume (two  $0.200 \text{ m}^3$  barrels in series) to remove the short-lived  $^{220}\text{Rn}$  ( $t_{1/2} = 56 \text{ s}$ ), then through a first membrane filter to remove all ambient progenies of  $^{222}\text{Rn}$  and  $^{220}\text{Rn}$ . The cleaned air, containing  $^{222}\text{Rn}$  but no progeny, then enters a second delay volume ( $0.75 \text{ m}^3$ ), where  $^{222}\text{Rn}$  decay produces new progenies under controlled conditions. Air inside the second delay volume circulates at a rate of  $0.013 \text{ m}^3 \text{ s}^{-1}$  in an internal loop, where it passes through a second filter (mesh wire,  $20 \text{ }\mu\text{m}$ ). Here, newly formed progenies deposit by Brownian diffusion. Light pulses on a nearby ZnS surface are counted by a photomultiplier. Internal background during the measurement period was around 1 cps and sensitivity  $3.3 \text{ Bq m}^{-3} \text{ cps}^{-1}$ . Three background measurements were carried out during the observation period. The instrument was calibrated monthly with a passive  $^{222}\text{Rn}$  source (21.887 kBq; calibrated against NIST standards; Pylon Electronics Inc., Ottawa, Canada).

#### **3.3.2.2 One-filter detector**

The one-filter detector used in this study is the BfS system ( $\alpha/\beta$  Monitor P3), which is described in more detail in Stockburger and Sittkus (1966). Beside the continuous measurement of natural atmospheric radioactivity the detector system was mainly developed to monitor the artificial atmospheric  $\beta$ -activity from nuclear weapons fall-out and from releases of nuclear power plants, like during the incident in Chernobyl in spring 1986. The electronics for counting and data recording as well as the pumping system was modernized several times since 1966 but the detector system is still unchanged. Ambient air is continuously drawn through an aerosol filter (membrane filters, mixed cellulose ester)  $1.2 \text{ }\mu\text{m}$ ,  $150 \times 250 \text{ mm}$  ME 28 Schleicher and Schuell). The effective filter area is  $300 \text{ cm}^2$ . At a distance of 14 mm above the filter is a stack of three independent, methane-filled, proportional counters having the same length and width as the active filter area (Fig. 7). The proportional counters

operate in the proportional range such that the lower counter measures  $\alpha$ -activity from progeny of  $^{222}\text{Rn}$  and  $^{220}\text{Rn}$ . The middle counter detects the high energy  $\alpha$ -activity of  $^{212}\text{Po}$  ( $^{220}\text{Rn}$  progeny). The half life of  $^{212}\text{Pb}$  (10.6 h) is relevant for the time required to reach an equilibrium on the filter. Therefore, we cannot always assume equilibrium between activity in air and activity on the filter. Changes in atmospheric concentrations can occur before equilibrium is reached on the filter. However, a determination of actual  $^{212}\text{Po}$  activity in air is possible, if not only the activity on the filter but also its change over time is taken into account. By difference, the  $^{222}\text{Rn}$  progeny activity is derived from the lower counter. The upper counter counts  $\beta$  particles only. Air is continuously pumped at  $0.014 \text{ m}^3 \text{ s}^{-1}$  through an air duct (cross section  $35 \text{ cm} \times 45 \text{ cm}$ ; length  $5 \text{ m}$ ) over the filter for one week. After one week the pump is switched off, the filter is replaced, a one hour check calibration using a  $^{241}\text{Am}/^{90}\text{Sr}$  source is performed, followed by a background check with a new filter for an additional hour and then the air flow is started again. The sensitivity for short-lived  $^{222}\text{Rn}$  progeny, expressed in  $^{222}\text{Rn}$  equivalent, is  $3.367 \text{ Bq cps}^{-1}$  or  $0.0673 \text{ Bq m}^{-3} \text{ cps}^{-1}$  for an air flow rate of about  $0.014 \text{ m}^3 \text{ s}^{-1}$ . The background count rate used for data evaluation is  $0.043 \text{ cps}$  and was determined during a period of several days without an air flow. The  $^{222}\text{Rn}$  equivalent activity concentration is calculated based on the assumption of equilibrium between  $^{222}\text{Rn}$  activity and  $^{218}\text{Po}$  and  $^{214}\text{Po}$  activity in the atmosphere. The activity of  $^{218}\text{Po}$  and  $^{214}\text{Po}$  measured on the filter is only in equilibrium with the atmospheric  $^{222}\text{Rn}$ , if the atmospheric activity is constant. If the latter changes, it is taken into account during the calculations by a correction factor which is a function of the half-life.

The one-filter detector on Schauinsland represents one commonly applied principle to estimate atmospheric  $^{222}\text{Rn}$  concentrations based on the collection and  $\alpha$ -counting of both short-lived  $^{222}\text{Rn}$  progeny ( $^{218}\text{Po}$  and  $^{214}\text{Po}$ ) from atmospheric air. For example, all one-filter detectors mentioned as operating at GAW stations in the WMO/GAW report No. 155 (2004) derive estimates of atmospheric  $^{222}\text{Rn}$  from the combined detection of  $^{218}\text{Po}$  and  $^{214}\text{Po}$ . We are aware of other one-filter detectors that derive  $^{222}\text{Rn}$  estimates exclusively from atmospheric  $^{218}\text{Po}$  concentration such as the ‘Radgrabber’ (e.g. Lee and Larsen, 1997) or some commercial instruments. Also the two-filter detector we used, is not the only instrument measuring atmospheric  $^{222}\text{Rn}$  instead of atmospheric  $^{222}\text{Rn}$  progeny. Other instruments include those based on the design by Iida et al. (1996) and widely used in East Asia (e.g. Moriizumi et al., 2008), and the two filter detector developed by the Environmental Measurements Laboratory (EML) as described in Collé et al. (1996). Hence, the instruments in our study represent the two measurement principles of a majority of detectors currently in use.

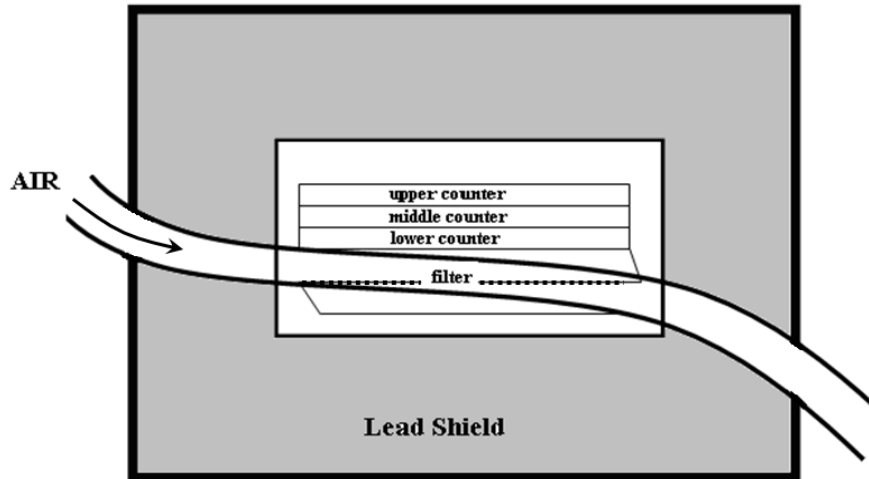


**Fig. 7.** The One-filter detector system contains a membrane filter and a stack of three independent, methane-filled, proportional counters having the same length and width as the active filter area. The middle counter detects the high energy  $\alpha$ -activity of  $^{212}\text{Po}$  ( $^{220}\text{Rn}$  progeny). Activity of  $^{212}\text{Po}$ , together with the change in  $^{212}\text{Po}$  activity over time, is used to determine total  $^{220}\text{Rn}$  progeny contribution to total counts in the lower counter. By difference, the  $^{222}\text{Rn}$  progeny activity is derived from the lower counter. The upper counter counts  $\beta$  particles only (redrawn from Stockburger and Sittkus, 1966).

## 3.4 Results and discussion

### 3.4.1 General Description of Data

The time series of hourly values of atmospheric activity concentration of  $^{222}\text{Rn}$  (measured with the two-filter detector), short-lived  $^{222}\text{Rn}$  progeny, expressed in  $^{222}\text{Rn}$  equivalent (measured with the one-filter detector), and meteorological parameters observed at Schauinsland station from October 2007 to April 2008 shows structures on the synoptical time scale (Fig. 8). Precipitation occurred from time to time with intensities ranging from 0.1 to 10.5 mm h<sup>-1</sup> in form of snow, rain or drizzle. Air temperature fluctuated between -10 °C to 10 °C with a mean of 1 °C. The relative humidity (RH) remained most of the time above 90 % with some short periods of substantially smaller values, usually associated with southerly winds. Wind directions were already described above. Mean hourly wind speed ranged from 0.2 to 22.5 m s<sup>-1</sup>. We note that atmospheric activity concentration of  $^{222}\text{Rn}$  and short-lived  $^{222}\text{Rn}$  progeny obtained by the different detector types follow a very similar pattern, even before harmonization of instrumental background and calibration. Activity concentrations of  $^{222}\text{Rn}$  and short-lived  $^{222}\text{Rn}$  progeny ranged from 0.5 to 10.8 Bq m<sup>-3</sup> with a mean value of 2.8 (s.d. = 1.5) Bq m<sup>-3</sup> for activity concentration of  $^{222}\text{Rn}$ , and from 0.1 to 10.7 Bq m<sup>-3</sup> with a mean value of 1.8 (s.d. = 1.3) Bq m<sup>-3</sup> for short-lived  $^{222}\text{Rn}$  progeny expressed in  $^{222}\text{Rn}$  equivalent, respectively. Of all hourly values, 84 %

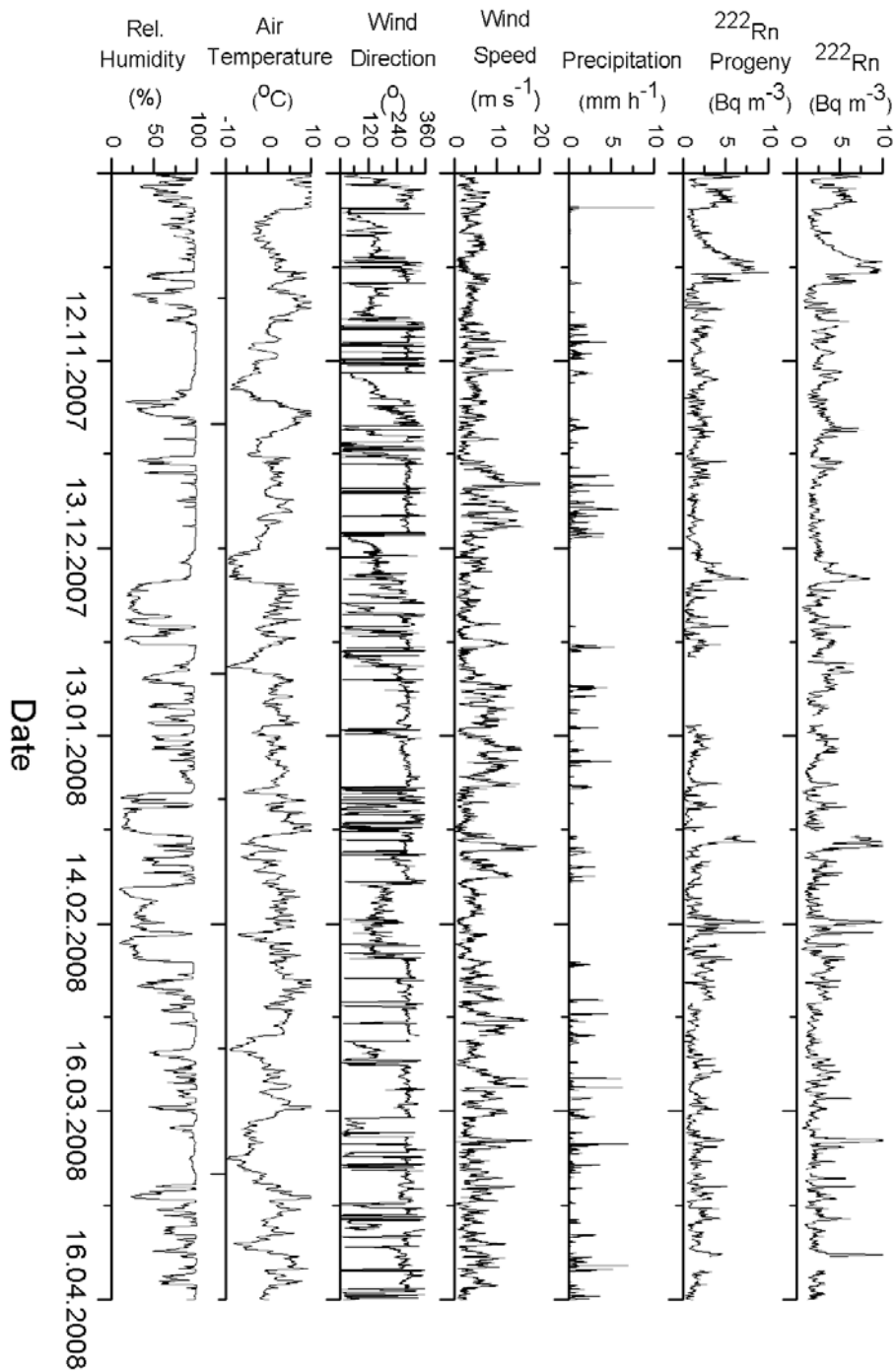


**Fig. 8.** Time series of hourly means of <sup>222</sup>Rn activity concentration (measured with a two-filter detector) and short-lived <sup>222</sup>Rn progeny, expressed in <sup>222</sup>Rn equivalent (measured with a one-filter detector) before harmonizing background and calibration between instruments, hourly precipitation, mean wind speed, wind direction, air temperature and relative humidity at Schauinsland station from October 2007 to April 2008.

were below  $4 \text{ Bq m}^{-3}$ . Close to the mountain top, changes in the origin of advected air, be it from the boundary layer or from the free troposphere, drive fluctuations in  $^{222}\text{Rn}$  activity concentrations. This assumption is supported by the analysis of back-trajectories calculated using version 4.6 of NOAA Air Resources Laboratory's (ARL) Hybrid Single-Particle Lagrangian Integrated Trajectory (HYSPPLIT) model for all hourly  $^{222}\text{Rn}$  values (Draxler and Rolph, 2003). The upper quartile of observed  $^{222}\text{Rn}$  activity concentrations was clearly associated with air masses that have reached the station from a lowest altitude, suggesting advection of boundary layer air masses (Fig. 9). In contrast, the lowest  $^{222}\text{Rn}$  activity concentrations were found in air that has reached the station from a greater height and has most likely not been in contact with land surfaces for some time before arrival.

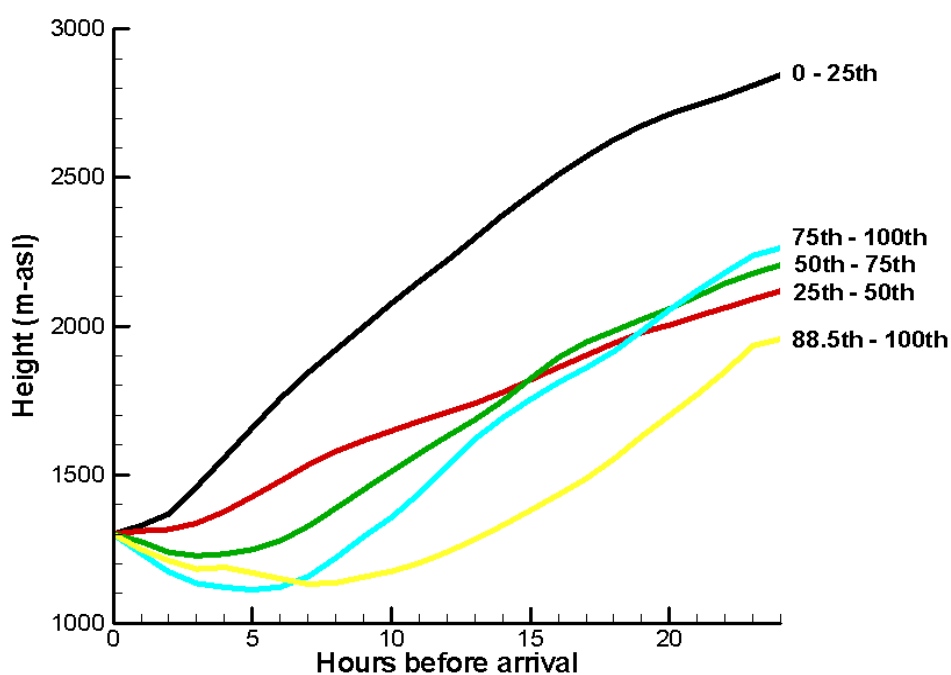


**Fig. 9.** Average altitude of air masses (ensemble means of single particle trajectories) during the 24 hours before arrival at the station for the lowest (0 - 25<sup>th</sup>) to the highest (75<sup>th</sup> - 100<sup>th</sup>) quartile of observed  $^{222}\text{Rn}$  activity concentrations.

### 3.4.2 Harmonization of instrumental background and calibration

Differences between measured activity concentration of  $^{222}\text{Rn}$  and short-lived  $^{222}\text{Rn}$  progeny are caused by differences in instrumental background and calibration in addition to changes of the progeny/ $^{222}\text{Rn}$  disequilibrium in air with meteorological conditions. As we are interested in the effect of meteorological conditions on  $^{222}\text{Rn}$  estimates made by one- and two-filter detectors, we have to minimize differences caused by instrumental background and calibration, including the selection of an



appropriate disequilibrium factor to transform short-lived  $^{222}\text{Rn}$  progeny activity to  $^{222}\text{Rn}$  activity concentration. To this end we selected conditions when progeny removal was considered minimal. Since forest canopies and precipitation increase the deposition rate (Petroff et al., 2008), we choose those data, when there was no precipitation and air arrived from the reference wind sector ( $120^\circ - 180^\circ$ ). This air has travelled above a steep valley where only the upper slope is covered by a narrow strip of forest that does not extend onto the grassland plateau forming the last 160 m to the station. The correlation between measured activity concentrations for this selection (Fig. 10) is strong (Spearman rank correlation coefficient = 0.946). There is an off-set of  $0.382 \text{ Bq m}^{-3}$  between detectors and values of short-lived  $^{222}\text{Rn}$  progeny tend to be smaller than those of  $^{222}\text{Rn}$  by a factor of 0.898. This is very close to the disequilibrium factor (0.85) estimated for this station by Schmidt (1999, as cited in Schmidt et al., 2003). Much larger differences between detectors have been reported (Collé et al., 1996). Because of physical plausibility we assume in our further analysis that the observed off-set is entirely due to internal instrumental effects and not explained by environmental factors. An instrumental effect leading to this off-set, for example, could be an over-estimate of the  $^{220}\text{Rn}$  progeny activity ( $^{212}\text{Po}$ ) by the one-filter detector. This would lead to a lower estimate of short-lived  $^{222}\text{Rn}$

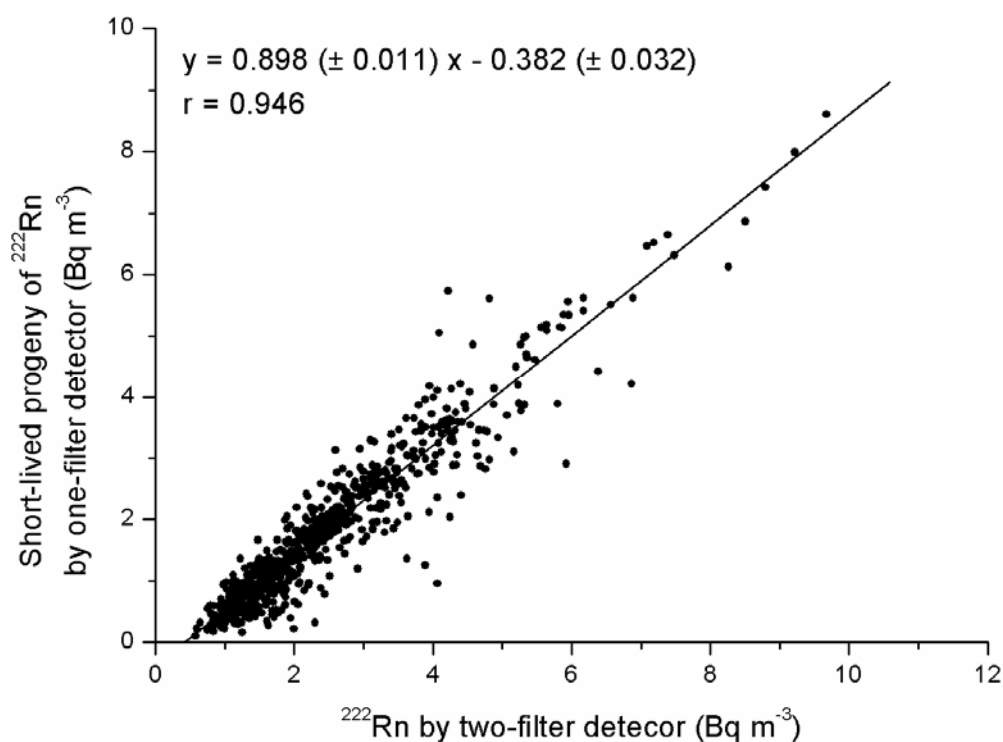


**Fig. 10.** Correlation between activity concentrations of  $^{222}\text{Rn}$  (measured by two-filter detector) and short-lived  $^{222}\text{Rn}$  progeny (expressed in  $^{222}\text{Rn}$  equivalent; measured by one-filter detector) as determined by the two independently calibrated instruments for events with no surface wet deposition and wind from the reference sector (values in brackets are standard errors of regression parameters). The Spearman rank correlation coefficient  $r$  equals 0.946.

progeny activity. For the purpose of this study it is irrelevant to know which instrument is more accurate. We are interested in relative differences between  $^{222}\text{Rn}$  and progeny-derived  $^{222}\text{Rn}$  caused by meteorological conditions. For further analysis, we add  $0.382 \text{ Bq m}^{-3}$  to the short-lived  $^{222}\text{Rn}$  progeny activity concentration measured with the one-filter detector and divide it by 0.898, thereby transforming short-lived  $^{222}\text{Rn}$  progeny activity concentration into progeny-derived  $^{222}\text{Rn}$  activity concentration. However, this way to harmonize background and calibration should not suggest that we think the two-filter detector is better background corrected or calibrated than the one-filter detector.

### 3.4.3 Effect of precipitation intensity

To investigate the effect of precipitation intensity, we selected all hourly values with precipitation larger than zero from the harmonized data set and sorted them into ranges with a similar number of observations in each range (Fig. 11). Within each range, there is a large variation in the ratio of progeny-derived  $^{222}\text{Rn}$  to  $^{222}\text{Rn}$ . We only can give plausible arguments for the reason of this behavior. Uncertainty in the measurements is certainly one cause. If this would be negligible, the ratio should always be  $\leq 1$ . Another reason may be associated with the process of wet deposition itself. A precipitation event, for example of  $1 \text{ mm h}^{-1}$ , may be caused by a short spell

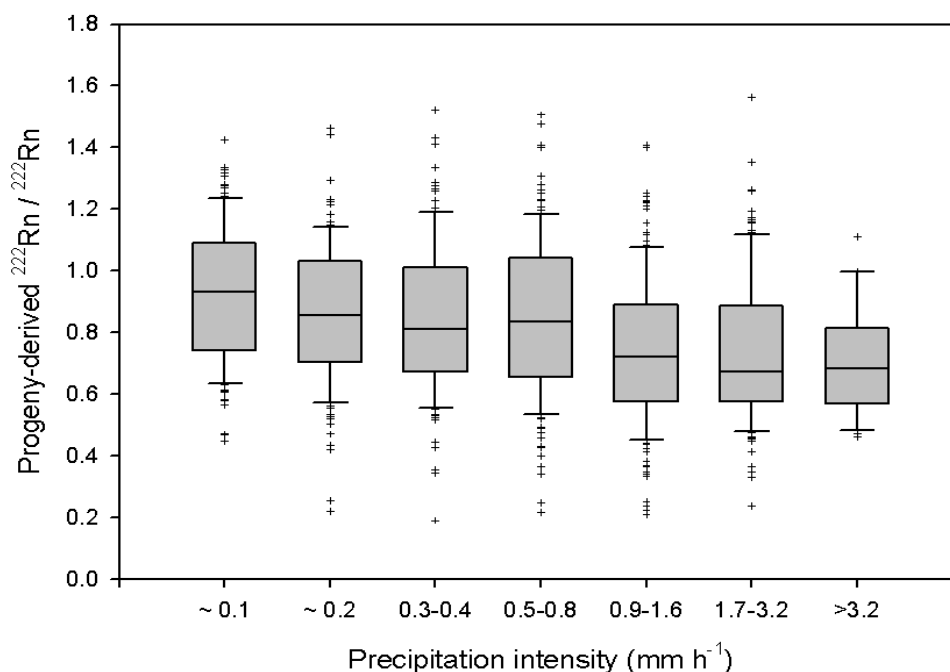


**Fig. 11.** Ratio of the activity concentrations of progeny-derived  $^{222}\text{Rn}$  and  $^{222}\text{Rn}$  summarized for different ranges of precipitation intensity (instrumental background and calibration have been harmonized between detectors). Boxes indicate median, upper and lower quartile, whiskers 10<sup>th</sup> and 90<sup>th</sup> percentile, crosses are outliers. Each range includes between about 120 and 180 hourly values, except for precipitation intensities  $>3.2 \text{ mm h}^{-1}$  ( $n = 29$ ). The lowest precipitation intensities are near the detection limit of the instrument and therefore only approximate.

of large rain drops with small specific surface areas for interaction with aerosol. If so, its effect on wash-out of progeny is short and small. Alternatively, the same amount of rain may fall in a drizzle where the same amount of precipitation has an orders of magnitudes larger specific surface area and where interaction with short-lived progeny lasts the entire integration interval of the measurement. Despite the scatter of values within each range, our data suggests a weak tendency towards larger disequilibria with increasing precipitation intensity. Yet, it is impossible to provide precipitation-dependent factors to reliably convert progeny signal to  $^{222}\text{Rn}$  concentration.

### 3.4.4 Effect of forest canopies

Aerosols, such as short-lived progeny of  $^{222}\text{Rn}$ , can be collected by vegetation due to the interaction of aerosols with every vegetation surface (leaves, trunks, twigs, heads and fruits). Different mechanical processes generate the deposition. From smaller to larger particle sizes these are mainly Brownian diffusion, interception, inertial impaction and sedimentation. Compared to other types of land surfaces, research in the field of acid deposition to forest has shown largely increased deposition velocities above forest (Petroff et al., 2008). Smaller activity concentration of  $^{214}\text{Pb}$  below canopy compared to above canopy have been reported (Wyers and Veltkamp, 1997). As indicated in Fig. 6, the Schauinsland station is partly surrounded by forest. To estimate the effect of forest canopy on differences between progeny-derived  $^{222}\text{Rn}$  and  $^{222}\text{Rn}$ , we plotted values from the three major wind directions for conditions when there was no precipitation. By default (section 3.4.2), the slope of the regression in the reference sector ( $120^\circ - 180^\circ$ ) is 1 (Fig. 12a). Deviations from 1 in the two other sectors can be ascribed to the effect of forest canopy on progeny removal. On average, values of progeny-derived  $^{222}\text{Rn}$  were 0.86 and 0.87 times those of  $^{222}\text{Rn}$  in the forest covered sectors  $240^\circ - 300^\circ$  and  $0^\circ - 60^\circ$ , respectively (Fig. 12c, e).

### 3.4.5 Effect of precipitation and forest canopy

Ideally, we would have liked to compare progeny-derived  $^{222}\text{Rn}$  and  $^{222}\text{Rn}$  for the open wind sector, with and without precipitation, to get an estimate for the mean effect of precipitation only. Unfortunately, there were only 10 one-hourly intervals with precipitation from the open sector during the observation period. This is obviously not enough. For completeness, we nevertheless added the data to Fig. 12b. Consequently, the effect of precipitation, irrespective of intensity, can only be investigated in combination with the effect of forest canopy. Compared to forest canopies under dry conditions, precipitation reduced progeny-derived  $^{222}\text{Rn}$  in the analyzed air by 9 % and 21 % for the wind sector  $240^\circ - 300^\circ$  and  $0^\circ - 60^\circ$ , respectively (Fig. 12d, f). Thus, the effect of precipitation seems to be of similar magnitude as the effect of forest canopy. Yet both influences cannot be clearly separated because of a possible interaction between precipitation and forest canopy. It may well be that a forest canopy is more efficient in progeny removal when wet than when dry. During precipitation, average wind speed and air temperatures were similar,

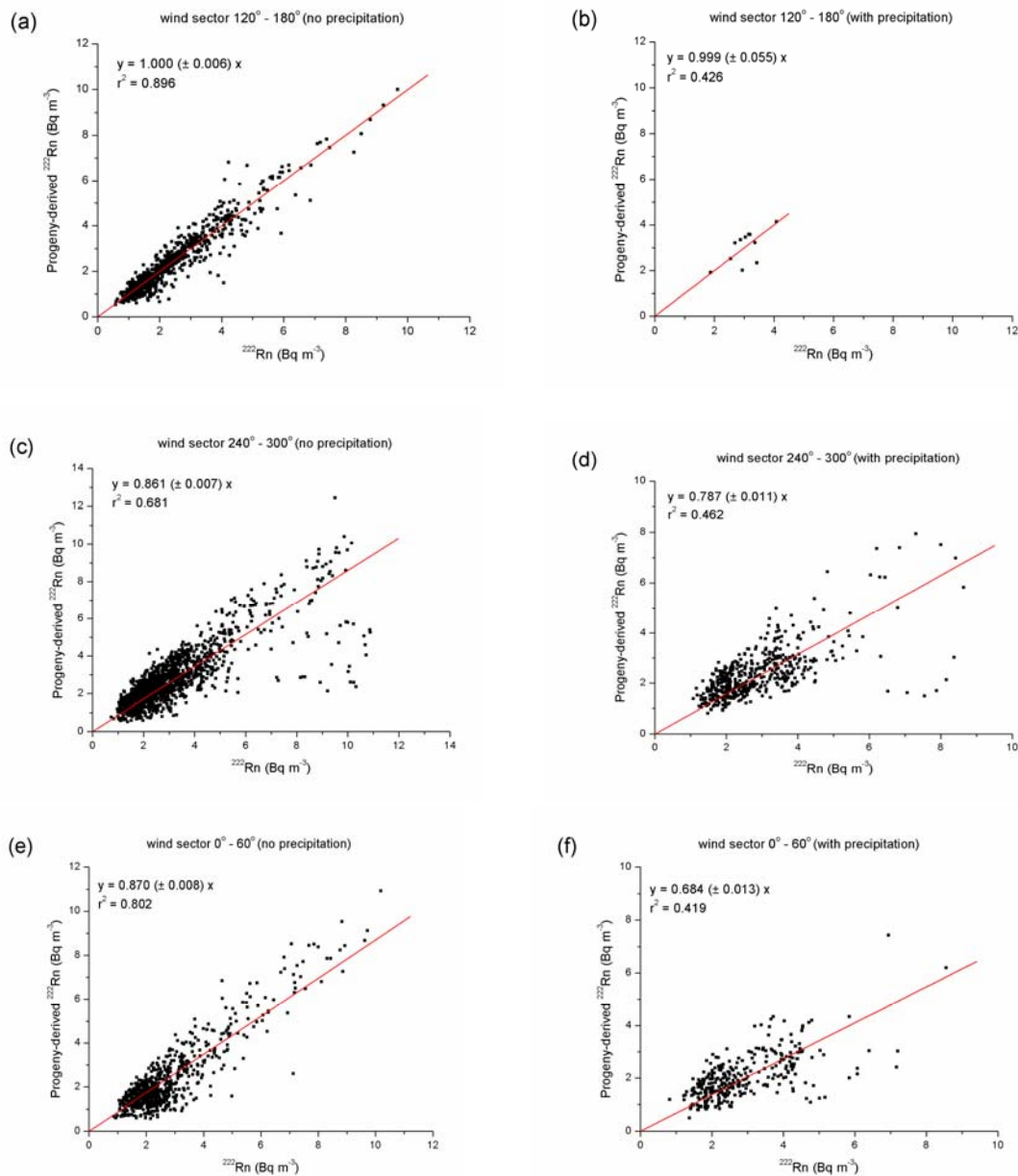


**Fig. 12.** Correlation between activity concentration of progeny-derived  $^{222}\text{Rn}$  and  $^{222}\text{Rn}$  for the reference sector (a, b) and the two sectors influenced by forest cover (c, d, e, f), for without precipitation (a, c, e) and with precipitation (b, d, f) (values in brackets are standard errors of regression parameters). Instrumental background and calibration have been harmonised between detectors.

while relative humidity was larger, compared to conditions without precipitation (Tab. 3). The degree to which deposition of  $^{222}\text{Rn}$  progeny is affected by forest canopies in various wind sectors would be different at other stations, which may be closer or further away from a forest edge, or where forest canopies are not similar to those on Schauinsland. The effect of precipitation is probably less site-specific. However, more generally, our results show that changing meteorological conditions affect the relative difference between one- and two-filter detectors. Consequently, there is not one single

**Tab. 3.** Means and standard deviation (s.d.) of meteorological parameters for the three main wind sectors during dry (no precipitation) and wet (precipitation > 0) conditions.

Wind sector		Wind speed (m s <sup>-1</sup> )		Temperature (°C)		Relative humidity (%)	
		mean	s.d.	mean	s.d.	mean	s.d.
120°-180°	dry	4.0	1.6	0.0	5.0	70.0	27.0
	wet	3.0	1.2	0.7	4.4	95.2	2.4
240°-300°	dry	6.1	3.4	2.5	4.1	75.4	24.4
	wet	8.2	3.8	0.9	3.0	96.5	4.7
0°-60°	dry	2.6	1.2	0.2	4.0	81.2	25.9
	wet	3.2	1.5	-0.7	3.2	97.7	2.1

disequilibrium factor for a specific site that could be used to directly transform short-lived progeny to <sup>222</sup>Rn activity concentration. Site-specific disequilibrium factors cover a range of values depending on meteorological conditions. This more general outcome of our study applies to probably most other stations.

### 3.5 Conclusions

The observations show that one- and two-filter systems are suitable to continuously monitor <sup>222</sup>Rn in ground level air. Most of the time both systems follow the same pattern and produce very similar results, except under special meteorological conditions, when precipitation or forest canopy remove short-lived progeny from the air mass to be measured. Such effects are generally much smaller than the large fluctuations in activity concentrations of <sup>222</sup>Rn and progeny-derived <sup>222</sup>Rn on diurnal and synoptical time scales. The average altitude of air masses a few hours prior to arrival at a mountain station is expected to largely influence activity concentrations.

There is no clear relationship between precipitation intensity and the magnitude of the difference between progeny-derived <sup>222</sup>Rn and <sup>222</sup>Rn activity concentration. Thus, there is no precipitation-dependent factor to reliably convert progeny signal to <sup>222</sup>Rn concentration. Disequilibrium between <sup>222</sup>Rn and its short-lived progeny near the surface of a mountain top may be affected to a similar magnitude by the interaction between air and forest canopy and by wet deposition. Each factor may, cumulatively, reduce progeny-derived <sup>222</sup>Rn activity concentration between about 10 % and 15 % compared to <sup>222</sup>Rn activity concentration. These two effects and their influence on the <sup>222</sup>Rn data were studied in this work and should be known for the interpretation and intercomparison of <sup>222</sup>Rn data measured with different systems and at different sites. Deviation of progeny-derived <sup>222</sup>Rn from directly measured <sup>222</sup>Rn activity concentration will be smaller where one-filter detectors specifically count <sup>218</sup>Po only, instead of the combined activity concentration of <sup>218</sup>Po and <sup>214</sup>Po.

### **3.6 Acknowledgements**

This project was funded by the Swiss National Science Foundation (project no. 200020-117622/1). We would like to thank Frank Meinhardt from the German Environment Agency for providing the meteorological data for the site. The presented data would not be available without the conscientiousness of the local station operators at the BfS station Schauinsland in operating and maintain the systems. One of us (WZ) would like to acknowledge help of Jagoda Crawford and Sylvester Werczynski of ANSTO in back trajectory analysis. We thank two anonymous reviewers for their constructive and helpful comments.

## Chapter 4

# Evidence for nearly complete decoupling of very stable nocturnal boundary layer overland

This chapter is in press by *Boundary-Layer Meteorology* as: Xia, Y., Conen, F., Haszpra, L., Ferenczi, Z., and Zahorowski, W. (2010) Evidence for nearly complete decoupling of very stable nocturnal boundary layer overland. *Boundary-layer Meteo.* 138 (1), 163-170.

### 4.1 Abstract

Concentrations of  $^{222}\text{Rn}$  at 0.1 m and 6.5 m height above ground level and  $^{222}\text{Rn}$  flux density were measured during nights characterized by strong cooling, light winds and clear sky conditions in the Carpathian Basin in Hungary. A very stable boundary layer (vSBL) formed on 14 nights between 15 August and 3 September 2009. On 12 nights, an estimated 72 % (s.d. 20 %) of  $^{222}\text{Rn}$  emitted from the surface since sunset was retained within the lowest 6.5 m above the ground until sunrise the following morning. On two nights an intermittent increase in wind speed at 9.4 m height was followed by a rise in temperature at 2.0 m height, indicating a larger atmospheric motion that resulted in  $^{222}\text{Rn}$  at 0.1 m around sunrise being the same as around the preceding sunset. It does not seem to be rare in a large continental basin for a vSBL to be nearly completely decoupled from the atmosphere above for the entire period from sunset to sunrise.

### 4.2 Introduction

Shortly before sunset, thermals in the convectively mixed boundary layer fade away. Radiative heat loss from the surface stabilizes a shallow layer of cooling air that is in direct contact with the ground (Malhi, 1995; Oyha et al., 1997; Mahrt, 1998), and in light wind, clear-sky conditions, large temperature gradients develop that severely suppress turbulent mixing and lead to the formation of a very stable boundary layer (vSBL). Mahrt (1998) demonstrated the breakdown of existing turbulence formulations under such conditions, where meandering and other mesoscale motions add to the elusiveness of the situation. Structure and dynamics of a stable nocturnal boundary layer are determined by complex interactions between the static stability of

the atmosphere and such mesoscale motions that intermittently generate mechanical turbulence (Stull, 1988; Sun et al., 2004). Variations in these processes in time and space at different heights and scales make it very difficult to predict transport pathways and diffusion of pollutants (Beyrich, 1994; Bowen et al., 2000; Salmond et al., 2005).

Banta et al. (2007) found the vSBL to be isolated and decoupled from the atmosphere above for several hours by the presence of what they termed a quiescent layer. This implies that pollutants, or any other gaseous or particulate emissions from near the surface, may be quantitatively conserved in the vSBL for prolonged periods at night. It seems to us that only a tracer experiment is able to convincingly demonstrate a prolonged decoupling of near-surface air from the atmosphere above. Serendipitously, we identified a number of such decoupling events while estimating non-CO<sub>2</sub> greenhouse gas emissions in the Carpathian Basin by a mass balance approach with <sup>222</sup>Rn, such as was done before in Japan (Moriizumi et al., 1996), Australia (Wilson et al., 1997), Switzerland (Conen et al., 2002) and many other parts of the world. All land surfaces naturally emit the radioactive noble gas <sup>222</sup>Rn to the atmosphere where it is lost by decay (half time life of 3.82 days). Measurements of <sup>222</sup>Rn concentrations are usually made at a single height above the ground.

Our experimental set-up included two measurement heights that were both well within the vSBL, since at both levels we saw substantial increases in <sup>222</sup>Rn concentration during the whole night. Since we also measured <sup>222</sup>Rn flux density, we were able to determine with some confidence the proportion of emitted <sup>222</sup>Rn that accumulated between sunset and sunrise in the vSBL. A shortcoming associated with the unexpectedness of our observations is the lack of high frequency three-dimensional wind data, and temperature measurements performed at only one height. This does not compromise our <sup>222</sup>Rn budget of the vSBL or its testimony of prolonged decoupling, but limits meteorological analysis of the 14 nights that we present.

### 4.3 Material and Methods

Observations were made at K-puszta, a regional background air pollution monitoring station (46°58' N, 19°33' E, 125 m above sea level), located in a sparsely grass covered clearing of about 10<sup>4</sup> m<sup>2</sup> in a mixed forest reserve, about 45 km east of the Danube river, on the Hungarian Great Plain in the middle of the Carpathian Basin. The maximum difference in elevation between the 10 geodesic points within a radius of 5 km is 11.3 m. The larger elevations are in the north-east, the smaller in the south-west part of this circle. Immediately surrounding the clearance are plots dominated by pine (*Pinus sp.*), mostly between 3 and 5 m tall. Soils are sandy and poor and so is plant growth. Intermediate surroundings include large plots that have been cleared for re-planting. Land use outside a radius of about 2 to 3 km is dominated by row crops and grazing. The region is climatologically calm and characterised by intensive solar radiation during summer (Haszpra, 1998). Prevailing winds are from the north-west and the annual average scalar wind speed for the past



decade is  $2.3 \text{ m s}^{-1}$  at 9.4 m above the ground according to the database of the Hungarian Meteorological Service. The station is part of the Global Atmospheric Watch (GAW) network and the European Monitoring and Evaluation Programme (EMEP). Meteorological parameters measured at the station include, among others, hourly air temperature at 2.0 m height, scalar averaged wind speed at 9.4 m height and global radiation. The site characteristics are conducive to the development of the vSBL. If a vSBL was isolated from the atmosphere by what Banta et al (2007) call a quiescent layer, which may numerically be represented by a free-slip layer preventing the exchange of trace species between the vSBL and the atmosphere above, then all  $^{222}\text{Rn}$  emitted should accumulate within the vSBL so long as stability is not disturbed.

Atmospheric  $^{222}\text{Rn}$  concentrations were measured continuously at a height of 6.5 m with a  $0.700 \text{ m}^3$  dual-flow loop, two-filter detector as described in Whittlestone and Zahorowski (1998); the detector was built at the Australian Nuclear Science and Technology Organisation (ANSTO). At a height of 0.1 m above the surface, and 15 m north-north-west of the measurements at 6.5 m height,  $^{222}\text{Rn}$  concentrations were determined by a small ionisation chamber (AlphaGUARD PQ 2000Pro, Genitron Instruments, Frankfurt, Germany). This instrument is less sensitive than the ANSTO detector but useful for near-surface concentration measurements and for determining  $^{222}\text{Rn}$  flux density with accumulation chambers (Lehmann et al., 2001; 2004). Both detectors measure  $^{222}\text{Rn}$ , not the progeny, and both have been calibrated to standards traceable to the National Institute of Standards and Technology (NIST). Parallel measurements at the same height have yielded similar results. The small ionisation chamber was continuously flushed with air ( $1.4 \cdot 10^{-5} \text{ m}^3 \text{ s}^{-1}$ ) aspirated through an inlet at 0.10 m above the soil surface and located within a 0.23-m diameter open-top plastic collar, which extended 0.17 m above and 0.10 m below the soil surface. The few shoots of grass growing inside the collar were regularly removed. Aspirated air was continuously returned via an outlet tube into the same collar. The collar was opened each day during six time intervals of 2.5 h duration. During these intervals ambient air was flushed through the ionization chamber and  $^{222}\text{Rn}$  decay was counted. The top of the collar was closed in between these intervals by a rotating shutter for 1.5 h intervals to determine the  $^{222}\text{Rn}$  flux density.

The time reference for all reported measurements is UTC, and all measured quantities are one-hourly means. Time stamps are at the end of an integration period. Instruments operated, with some interruptions, from the end of March to the end of September 2009; the period from 15 August to 2 September has been selected for analysis. Nights are referred to by the date marking their end.

## 4.4 Results and Discussion

From 15 August to 2 September 2009, sunset was between 1853 and 1724 UTC and sunrise between 0439 and 0539 UTC.  $^{222}\text{Rn}$  concentration measurements at 0.1 m height are available for the hours terminating at 1800 UTC and at 0500 UTC. So during this period they are close to sunset and sunrise. The daily global radiation maxima ranged from  $250 \text{ W m}^{-2}$  to  $300 \text{ W m}^{-2}$ , increasing and decreasing smoothly

from dawn to dusk, indicating clear sky conditions. Exceptions are the 23, 24 and 30 August, when global radiation in midday showed substantial variations with intermittent abrupt falls to 100 - 150 W m<sup>-2</sup>. On 23 and 30 August total precipitation was 9.3 mm and 4.1 mm, respectively; there was no precipitation during other days or nights. We assume that nights bracketed by clear-sky days (0500 – 1800 UTC) also had clear-sky conditions, an assumption supported by cloudiness data from the nearest (15 km) station. In our further analysis we will analyse the 14 nights (1800 - 0500 UTC) fulfilling this criterion. Nocturnal air temperature at 2.0 m height ranged from 27.9 °C to 9.0 °C with an average value of 16.0 °C, while nocturnal wind speed at 9.4 m height ranged from zero to 2.8 m s<sup>-1</sup> with an average value of 0.8 m s<sup>-1</sup>. Values pooled by the same hour of day illustrate that <sup>222</sup>Rn accumulation begins around sunset and terminates with sunrise. Although air temperature and wind speed decrease already before sunset, <sup>222</sup>Rn concentrations at 6.5 m height only start to substantially increase after sunset (Fig. 13). Strong cooling, light winds, a substantial increase in atmospheric <sup>222</sup>Rn concentrations, and presumably clear-sky conditions, point to the formation of a very stable boundary layer (vSBL) during the 14 selected nights.

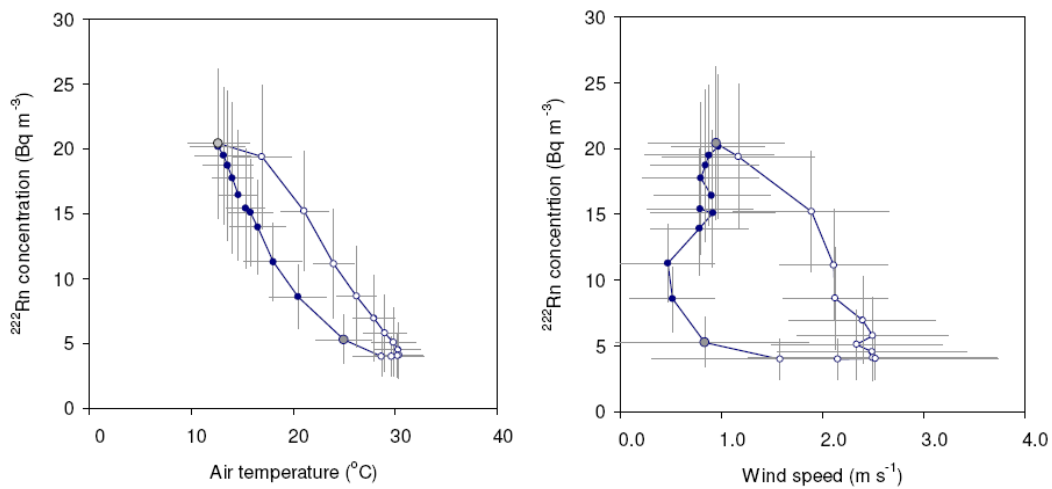


**Fig. 13.** Diurnal cycles (time progresses clockwise in 1-hr steps between symbols): mean values for same hour of day during clear sky conditions of atmospheric <sup>222</sup>Rn concentrations at 6.5 m height versus (left) air temperature at 2.0 m height, and (right) wind speed at 9.4 m height (open symbols for daytime and closed symbols for nighttime). Sunset and sunrise are indicated by grey dots. Error bars show  $\pm 1$  standard deviation.

We now postulate that stability lasts the entire period from sunset to sunrise, and verify this postulate by comparing accumulated <sup>222</sup>Rn with emitted <sup>222</sup>Rn. Accumulated <sup>222</sup>Rn is estimated from the concentration increase between sunset and sunrise at 0.1 m height ( $\Delta^{222}Rn_{0.1m}$ ) and 6.5 m height ( $\Delta^{222}Rn_{6.5m}$ ), and the assumption of the vertical profile of accumulated <sup>222</sup>Rn to fit an exponential function ( $Rn_z = a/e^{bz}$ , where  $Rn_z$  is the <sup>222</sup>Rn concentration at height  $z$ , and  $a$  and  $b$  are fitted parameters). This is the case if <sup>222</sup>Rn concentration profiles at sunset and at sunrise follow exponential functions, which is likely to be true (Stull, 1988; Keller et al., 2010). The

median  $\Delta^{222}\text{Rn}_{0.1\text{m}}$  was 62.1 Bq m<sup>-3</sup> and the median  $\Delta^{222}\text{Rn}_{6.5\text{m}}$  was 14.8 Bq m<sup>-3</sup> (Table 4). Average statistical counting errors associated with  $\Delta^{222}\text{Rn}_{0.1\text{m}}$  are  $\pm 7.4$  Bq m<sup>-3</sup>, and  $\Delta^{222}\text{Rn}_{6.5\text{m}} \pm 0.2$  Bq m<sup>-3</sup>. During the nights ending on 28 August and 1 September, the <sup>222</sup>Rn concentration did not change significantly at 0.1 m height but increased at 6.5 m by 9.0 and 10.0 Bq m<sup>-3</sup>, which is at the lower end of the observed  $\Delta^{222}\text{Rn}_{6.5\text{m}}$ . We will look at these two nights in more detail below. For the remaining 12 nights we fit an exponential function to  $\Delta^{222}\text{Rn}$  over height and integrate between the surface and infinite height. This generates values for the accumulated <sup>222</sup>Rn between 410 Bq m<sup>-2</sup> and 181 Bq m<sup>-2</sup> with a mean of 312 Bq m<sup>-2</sup> (s.d. 84 Bq m<sup>-2</sup>). Flux density of <sup>222</sup>Rn did not differ significantly between nights, and on average it was 8.6 mBq m<sup>-2</sup> s<sup>-1</sup>. The standard deviation between nights was 0.8 mBq m<sup>-2</sup> s<sup>-1</sup> and was largely due to errors associated with the <sup>222</sup>Rn counting statistics of the small ionization chamber. Hence, we can assume it remained the same during all 14 nights. A potentially larger uncertainty arises from the possibility that our <sup>222</sup>Rn flux measurement may not have been in a location that is representative of the larger source area. We believe that this is unlikely. The European <sup>222</sup>Rn flux map with 1°x1° resolution generated by Szegvary et al. (2009) indicates a mean annual flux density in the source area of 7.8 mBq m<sup>-2</sup> s<sup>-1</sup>. Our measured value is 10 % larger, which may be explained by the seasonally enhanced flux during summer because of relatively dry soil conditions (Szegvary et al., 2009). Accounting for the natural decay, no more than 328 Bq m<sup>-2</sup> would be expected to have accumulated between sunset and sunrise. Thus, an average of 95% (s.d. 26 %) of <sup>222</sup>Rn emitted from the ground during the night appears to have remained in the vSBL. This is an upper bound estimate because it is based on the integration from the ground to infinite height, which is obviously beyond the height of the vSBL. A lower bound estimate is the amount of <sup>222</sup>Rn accumulated between the surface and upper measurement height (6.5 m). Within this layer, 236 Bq m<sup>-2</sup> (s.d. 64 Bq m<sup>-2</sup>) had accumulated, which is equal to 72 % (s.d. 20 %) of <sup>222</sup>Rn emitted (Table 4). Consequently, the vSBL must have been very shallow and there was little loss of <sup>222</sup>Rn from it to the atmosphere above.

We are aware of only one other detailed observation in the vSBL where the data lend themselves to a similar interpretation. Lehmann et al. (2001) measured <sup>222</sup>Rn concentrations at four levels between the surface and 4.45 m height above a grassland in the Swiss plateau. During a ‘...very calm night in summer 2000 (Aug 19 to Aug 20) when the meteorological and the soil conditions were stable (no wind, no rain)...’, values in Lehmann et al. (2001) for  $\Delta^{222}\text{Rn}_{0.08\text{m}}$  and  $\Delta^{222}\text{Rn}_{4.45\text{m}}$  between 1800 and 0400 LT (local time) were around 85 and 30 Bq m<sup>-3</sup>, respectively. If we fit an exponential function and integrate between the surface and 6.5 m height we see that 286 Bq m<sup>-2</sup> probably accumulated in this layer. Accounting for decay, this is 64 % of the <sup>222</sup>Rn emitted during that night (<sup>222</sup>Rn flux density = 13.0 mBq m<sup>-2</sup> s<sup>-1</sup>), so well within the range of our observations in the Carpathian Basin. Lehmann et al. (1999) have analysed their data in a different way. They used the <sup>222</sup>Rn data together with data of the short-lived (half time of life 56 s) <sup>220</sup>Rn isotope to estimate the near-surface turbulent diffusion coefficients ( $K$ ). Their estimate for  $K$  at 0.2 m above ground ( $K_{0.2\text{m}}$ ) was  $5.9 \cdot 10^{-4}$  m<sup>2</sup> s<sup>-1</sup>, assuming  $K$  is constant with height, and  $4.1 \cdot 10^{-4}$

**Tab. 4.** Observed changes between sunset (1800 UTC) and sunrise (0500 UTC) during nights with strong cooling, light winds and clear-sky conditions: temperature at 2.0 m above ground ( $\Delta T$ ), atmospheric  $^{222}\text{Rn}$  concentrations at 0.1 m ( $\Delta^{222}\text{Rn}_{0.1\text{m}}$ ) and 6.5 m ( $\Delta^{222}\text{Rn}_{6.5\text{m}}$ ) above ground. Estimated amounts of  $^{222}\text{Rn}$  accumulated during this period are based on the assumption of exponential  $^{222}\text{Rn}$  concentration profiles around sunset and sunrise.

Date	$\Delta T$ ( $^{\circ}\text{C}$ )	$\Delta^{222}\text{Rn}$ ( $\text{Bq m}^{-3}$ )		Accumulated $^{222}\text{Rn}$ ( $\text{Bq m}^{-2}$ )	
		0.1 m	6.5 m	total	below 6.5 m
16 Aug 2009	-12.3	81.8	18.4	360	281
17 Aug 2009	-12.1	93.0	21.1	410	319
18 Aug 2009	-11.5	66.2	15.6	299	231
19 Aug 2009	-15.7	73.0	10.4	248	213
20 Aug 2009	-11.8	55.2	7.4	181	157
21 Aug 2009	-13.2	44.8	13.2	241	171
22 Aug 2009	-13.9	91.0	15.0	332	279
26 Aug 2009	-8.4	58.0	11.8	239	191
27 Aug 2009	-13.2	73.0	21.1	384	275
28 Aug 2009	-8.1	-2.3	9.0	-	-
29 Aug 2009	-10.1	34.8	14.5	260	152
1 Sep 2009	-8.6	-4.2	10.0	-	-
2 Sep 2009	-11.3	55.0	17.7	316	216
3 Sep 2009	-11.1	95.3	25.5	472	349

$\text{m}^2 \text{s}^{-1}$ , if  $K$  was height-dependent. We can make a rough estimate for  $K_{0.2\text{m}}$  in our study by assuming that the flux ( $j$ ) at 0.2 m height approximately equals the  $^{222}\text{Rn}$  flux density at the surface measured with the accumulation chamber. From the exponential  $^{222}\text{Rn}$  concentration profile fitted to our measurements at 0.1 m and 6.5 m height, we derive the  $^{222}\text{Rn}$  concentration gradient at 0.2 m ( $dc/dz$ ). Values for  $K_{0.2\text{m}}$ , calculated as  $j / (dc/dz)$  ranged from  $3.5 \cdot 10^{-4}$  to  $1.9 \cdot 10^{-3} \text{ m}^2 \text{ s}^{-1}$  with a median value of  $5.6 \cdot 10^{-4} \text{ m}^2 \text{ s}^{-1}$ . This is very close to the much more sophisticatedly derived estimate by Lehmann et al. (1999).

We now come back to the two nights when  $\Delta^{222}\text{Rn}_{0.1\text{m}}$  was not significantly different from zero (28 August and 1 September). A closer look at the meteorological conditions shows the temperature at 2.0 m above the ground suddenly increased by about  $5^{\circ}\text{C}$  within two hours during the night (Fig. 14). An increase in wind speed at 9.4 m height preceded the temperature surge in both cases and lasted throughout the temperature disturbance. The disturbance is visible in the atmospheric  $^{222}\text{Rn}$  decrease at 6.5 m level. Available meteorological information does not lend itself to a detailed analysis of the situation. However, we presume that larger atmospheric motions caused local thermal and shear instabilities resulting in wind gusts that reached to the

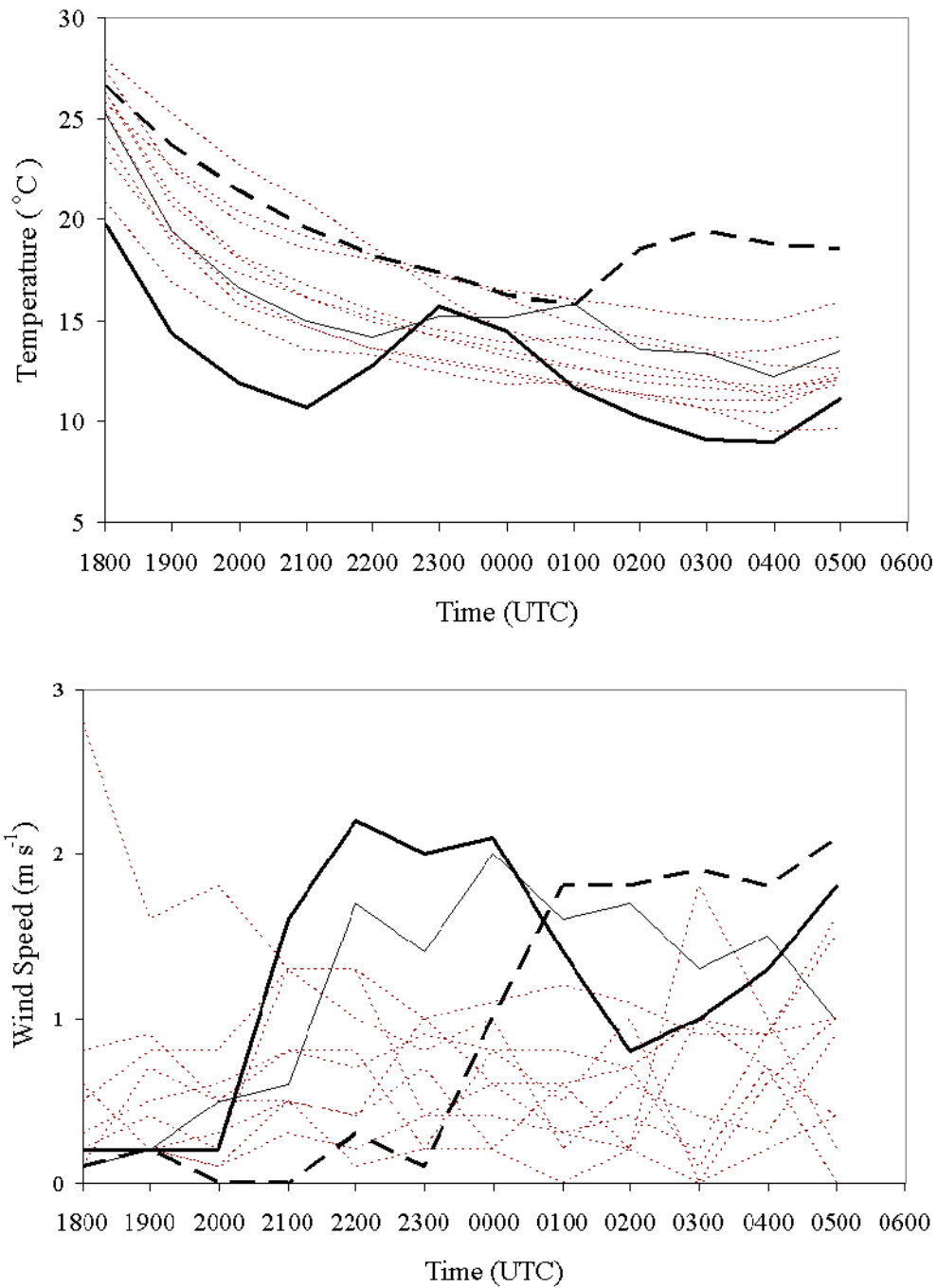


**Fig. 14.** Changes in (top) temperature at 2.0 m height, and (bottom) wind speed at 9.4 m height during the selected 14 nights. Thick lines indicate the two nights when  $^{222}\text{Rn}$  at 0.1 m height around sunrise was not significantly different from that around the preceding sunset (dashed line: 28 August; continuous line: 1 September). Increase in temperature and wind speed on 19 August (thin continuous line) did not seem to have resulted in a loss of  $^{222}\text{Rn}$  from the very stable boundary layer.

ground and transported cold  $^{222}\text{Rn}$ -rich air above warm  $^{222}\text{Rn}$ -poor air, thereby inverting the  $^{222}\text{Rn}$  concentration profile. Examples of large-scale motions that may lead to such a situation in the nocturnal boundary layer are density currents, solitary and internal waves (Sun et al., 2004). A similar but smaller such disturbance occurred on the night of 19 August (Fig. 14), but did not seem to have resulted in a loss of  $^{222}\text{Rn}$  from the vSBL.

## 4.5 Suggestions for future studies

A more comprehensive future field campaign should include the following changes and additional measurements. Manual soil chamber measurements for at least one night at several locations around the site would decrease the uncertainty associated with the large-scale  $^{222}\text{Rn}$  flux density. Also with little effort, the timing of atmospheric  $^{222}\text{Rn}$  measurements at the lower level could be set closer to the times of sunset and sunrise. With more instrumentation available, wind speed and temperature should be measured at the same levels as atmospheric  $^{222}\text{Rn}$  concentrations. Extending the measurement of meteorological parameters to a height likely to be above the vSBL, say to 40 m, would be a next step. If instrumentation is available, measurements of vertical velocity variance and relative humidity at several levels would add significant information, to determine the Richardson number,  $z/L$  and others. This would help quantify the impact of turbulent events.

## 4.6 Conclusions

$^{222}\text{Rn}$  measurements at the K-pusztá station in the Carpathian Basin during nights with strong cooling, light winds and clear skies provide evidence for a nearly complete decoupling of the very stable boundary layer (vSBL) from the atmosphere, lasting the entire period from sunset to sunrise. The shallow vSBL can be decoupled and isolated from the atmosphere above it. In a continental basin, interruption of this structure by what are probably larger scale atmospheric motions seems to be rare.

## 4.7 Acknowledgements

This project was funded by the Swiss National Science Foundation (project no. 200020-117622/1). We would like to thank the support from K-pusztá station in Hungary for providing the meteorological data for the site and also cordially thank Endre Lowinger, Maria Kiss and Szilard Szoke for maintaining the installations at the station, for downloading data and for responding to our numerous little queries. A big thank you to Lukas Zimmermann for helping with transfer, set-up, de-installation and return of equipment brought from Basel to K-Pusztá.

## Chapter 5

# High altitude observations of total bacterial number and coincident $^{222}\text{Rn}$ activity concentration

This chapter has been submitted to Atmospheric Environment.

### 5.1 Abstract

Bacteria in the atmosphere can act as ice nuclei, thus potentially affecting cloud development and precipitation. Currently, little is known about their concentration and variability at cloud altitudes, or their source density at landscape scale. Over a period from June to October 2010, we carried out four short campaigns at the High Altitude Research Station Jungfrauoch (3450 m above sea level) to determine bacterial number concentrations by collecting aerosol with liquid impingers, followed by filtration, fluorescent staining and counting with a microscope. Parallel measurements of  $^{222}\text{Rn}$  enabled us to distinguish between free troposphere and boundary layer air, and to estimate net flux densities of bacterial cells from surface to free troposphere. When  $^{222}\text{Rn}$  in air was  $< 0.5 \text{ Bq m}^{-3}$ , which we assume to be representative of free tropospheric air, concentration of total bacteria was on average  $3.4 \times 10^4 \text{ cells m}^{-3}$  (s.d. =  $0.8 \times 10^4 \text{ cells m}^{-3}$ ). When wind conditions preceding sampling were calm, or when the station was in clouds during sampling, there was little difference observed in bacterial number concentrations between free tropospheric and boundary layer air ( $^{222}\text{Rn} \sim 1 \text{ to } 4 \text{ Bq m}^{-3}$ ). One campaign was preceded by a storm. Here, boundary layer air reaching the station was enriched in bacterial cells (up to  $7.5 \times 10^4 \text{ cells m}^{-3}$ ). The estimated flux density during this campaign was 455 (s.e. = 125)  $\text{cells m}^{-2} \text{ s}^{-1}$ . Our results suggest a highly variable flux density of bacterial cells to cloud altitude, concurrently driven by mechanisms turning bacteria airborne and by the vertical mixing of air masses.

### 5.2 Introduction

Bacteria are omnipresent in the atmosphere (Jaenicke et al., 2007). In a recent study, it was indicated that “...with the growing awareness of climate changes on our planet, interest in atmospheric processes that define climate has heightened and diversified thereby bringing new attention to the possible roles of micro-organisms in

*these processes*” (Morris et al., 2008). Among the roles, the ice-nucleating activity of some bacteria catches particular attention because of a potential impact on cloud formation and development of precipitation (Yankofsky et al., 1981; Morris et al., 2005; Moehler et al., 2007; Christner et al., 2008). Plant canopies provide large surfaces for bacterial growth and are major sources of airborne bacteria, while bare soils are supposed to play a minor one (Lindemann et al., 1982). Growth of bacterial communities on surfaces depends on moisture, temperature, substrate availability and other environmental factors (Harrison et al. 2005). Release into the atmosphere is largely driven by wind speed (Jones and Harrison, 2004). Among those released, biological particles of 0.2-10  $\mu\text{m}$  size have long atmospheric residence times. Particles in this range may remain airborne for several days to a few weeks (Raes et al., 2000). Thus, they can be transported with air currents over long distances (Prospero et al., 2005). They are removed from the atmosphere slowly by dry deposition or, much faster, by wet deposition.

Historically, most studies have focused on the concentration of cultivable bacteria, sometimes misleadingly referred to as viable bacteria. However, concentrations of cultivable bacteria are two or three orders of magnitude smaller in comparison to concentrations of total bacteria (Chi and Li, 2007). Estimating total from cultivable cell numbers is impossible because the cultivable proportion depends on meteorological factors, such as temperature and UV radiation (Chi and Li, 2007). However, the sum of all investigations to date show that mean concentrations of total bacteria in ambient air are likely to be generally larger than  $1 \cdot 10^4$  cells  $\text{m}^{-3}$  over land. Over sea they tend to be 2 to 3 orders of magnitude lower than over land (Burrows et al., 2009). The few existing flux estimates relate only to culturable bacteria (Lindemann et al., 1982; Lindemann and Upper, 1985; Lighthart and Shaffer, 1994). Flux measurements of total bacteria have not been made so far, although the flux of total bacteria to cloud altitudes is of primary importance from a meteorological point of view (DeMott and Prenni, 2010), since dead cells and even cell fragments may still act as condensation and ice nuclei (Möhler et al., 2008). Concentrations of bacteria at cloud altitude depend on their flux into near surface air, so on their dissociation from the surfaces they grow on and on getting airborne, the mixing of near surface air to cloud altitudes, and on wet or dry deposition rates. Mixing of near surface air to cloud altitudes can be traced with  $^{222}\text{Rn}$ , which is naturally emitted from land surfaces at well known rates (Szegvary et al., 2009). Its only sink in the atmosphere is by radioactive decay with a half-life time of 3.82 days. Simultaneous observations of total bacterial number and atmospheric  $^{222}\text{Rn}$  activity concentrations at cloud-relevant heights during fair weather conditions, with little or no wet deposition, may tell us something about the flux of bacteria under such conditions to cloud altitudes.

We did a first step into this direction by measuring total bacterial number concentrations in free tropospheric and in boundary layer air. Both atmospheric compartments were accessed at the High Altitude Research Station Jungfrauoch (3450 m a.s.l.) in the Swiss Alps and distinguished by their  $^{222}\text{Rn}$  activity concentration. The station is known to be mostly influenced by free tropospheric air (Collaud Coen et al., 2011). However, especially during fine summer days, the station



is also under the influence of boundary layer air from early afternoon until late at night (Gäggeler et al., 1995; Collaud Coen et al., 2011). Results of four short campaigns between June and October 2010, during which the first author stayed on Jungfraujoch to collect the samples, are presented and discussed.

### 5.3 Materials and Methods

Sampling was carried out at the High Altitude Research Station Jungfraujoch (7° 59' E, 46° 33' N; 3450 m a.s.l) in the Swiss Alps. The station is part of the Global Atmosphere Watch Program of the World Meteorological Organization (GAW/WMO). Due to its elevated position, the station is an ideal site to investigate the exchange between surface and free troposphere above a continental region (Lugauer et al., 2000). We continuously operated a 700 litre volume, dual-loop, two-filter <sup>222</sup>Rn detector (Whittlestone and Zahorowski, 1998) at the station. One 4-day, two 3-day and one 1-day campaign were carried out between June and October 2010, including the measurement of weather conditions (Tab. 5).

For total bacterial number concentrations, a single sampling event consisted of collecting aerosol during a 3 h period with a liquid impinger (BioSampler; SKC, Inc.). In previous tests at the station we found no measurable change in sampling efficiency over such a prolonged period, as long as we added sterile H<sub>2</sub>O to the collectors at 30-min intervals to maintain a constant volume of liquid. Air was aspirated through a 4 cm diameter, 50 cm length, glass tube from outside the station. A mesh (1 mm) at the tube inlet prevented entry of insects or other larger particles. Prior to sampling, the liquid impinger was washed with ethanol and sterilised in dry heat (1 h at 220 °C). It was then filled with 20 ml of 0.1 M tetrasodium PP<sub>i</sub> dispersant (Kepner and Pratt, 1994). The flow rate during sampling was maintained at 0.75 m<sup>3</sup> h<sup>-1</sup>. After collection, the sample was fixed with formalin (2% (vol/vol) final concentration). All liquids were filtered through a 0.2-µm-pore-size filter prior to use. Blank samples were prepared with the same equipment and procedures, except that no air was passed through the dispersant liquid. Bacteria fixed with formalin were captured within 1 h after sampling by microfiltration through a 0.2-µm-pore-size, 25-mm, black polycarbonate membrane filter (Millipore, Isopore) placed in a glass vacuum filter funnel unit (Sartorius Stedim Biotech GmbH) equipped with a custom built inlay to reduce the effective filter area to a diameter of 6 mm. Pressure difference across the filter during sampling was maintained at 100 mbar. Glass funnel and filter holder were sterilised prior to use by the same procedure as the liquid impinger. Until analysis within less than a week, the filter was kept at -20 °C. For analysis, it was stained for 10 min with 4',6-diamidino-2-phenylindole (DAPI), a DNA binding dye at a final concentration of 0.01% (wt/vol). The filter was mounted on a glass slide and bacterial cells, identified by size and shape, were counted with a fluorescence microscope (Leica DM2500) equipped with a 100 W high-pressure mercury lamp, a 100 x ocular lens, a 460-nm filter and an objective with 10 x 10 10-µm grids. Total cell numbers were determined since no distinction can be made between live and dead cells with

the stain we used. Ten microscope fields were selected on the filter by turning the microscope stage randomly without watching the microscope. The counting for one filter was finished within 30 min before the fluorescence started fading. The total number of bacterial cells  $\text{m}^{-3}$  (N) was calculated as:

$$N = \frac{M \times A_f}{V} \quad (5)$$

Where M represents the average number of bacteria per field count (typically between 20 and 50),  $A_f$  the ratio of effective area of the filter to the area of the counting grid, V the volume of sampled air ( $\text{m}^3$  at local pressure and temperature). Blank counts were about one order of magnitude smaller than sample counts. The standard error of N was determined by the standard deviation of numbers counted in the ten fields on each slide divided by the square root of ten. In addition to bacteria, it would have been interesting to also determine the abundance of spores or pollen, as was done by Wiedinmyer et al. (2009) for samples from Storm Peak Laboratory in Colorado (3200 m above sea level). However, the number of large particles on our slides was too small to provide reliable values. In addition, the few large particles we occasionally saw under the microscope were not clearly identifiable by their morphology.

Concentrations of  $^{222}\text{Rn}$  activity were determined with the detector mentioned above over the same 3-h periods as the liquid impingers were operated. Statistical counting error over a 3-h period with this instrument at  $0.5 \text{ Bq m}^{-3}$  is 3 %. Average  $^{222}\text{Rn}$  flux density within a circle of 300 km around the station is  $12.6 \text{ mBq m}^{-2} \text{ s}^{-1}$  (Szegvary et al., 2009). We used this value in a  $^{222}\text{Rn}$  calibrated mass balance (Moriizumi et al., 1996; Wilson et al., 1997; Schmidt et al., 2003; Obrist et al., 2006) to estimate the regional flux of total bacterial cells from the land surface to station altitude (3450 m a.s.l.). The  $^{222}\text{Rn}$  mass balance approach is based on the principle that the flux of a target species X ( $F_x$ ) is derived from the flux of  $^{222}\text{Rn}$  ( $F_{\text{Rn}}$ ) and concentration differences in both, X ( $\Delta x$ ) and  $^{222}\text{Rn}$  ( $\Delta \text{Rn}$ ) as measured at different times:

$$F_x = \frac{F_{\text{Rn}} \times \Delta x}{\Delta \text{Rn}} \quad (6)$$

Variations in atmospheric transport efficiency between surface and measurement height drive differences in  $^{222}\text{Rn}$  activity ( $\Delta \text{Rn}$ ) and total bacterial number ( $\Delta x$ ) concentrations at measurement height. These differences ( $\Delta$ ) were not quantified individually but in combination. Values for the term  $\Delta x / \Delta \text{Rn}$  were derived from the slope of linear regressions fitted to plots of x versus Rn for parallel measurements of both parameters (Fig. 15), such as in Moriizumi et al. (1996) and Obrist et al. (2006). Atmospheric constituents reaching the height of our measurement point have been shown to remain at that height during further horizontal transport and can be

considered as injected into the free troposphere (Henne et al., 2005). Consequently, our estimates are for net flux densities of total bacterial cells from surface to free troposphere.

## 5.4 Results and discussions

### 5.4.1 June

The days before the first campaign the station was at times clear, at times in clouds, intermittently affected by frost and experiencing snowfall. At the beginning of the campaign, atmospheric pressure had increased and wind speeds had decreased. Free tropospheric air ( $^{222}\text{Rn} = 0.44 - 0.50 \text{ Bq m}^{-3}$ ) surrounded the station during the first day, bacterial number concentrations were  $\leq 3 \cdot 10^4 \text{ cells m}^{-3}$  (Tab. 5). Days 2 to 4 of the campaign saw  $^{222}\text{Rn}$  concentrations increase several-fold during afternoons and return to values around  $0.5 \text{ Bq m}^{-3}$  the following mornings. So, air arriving in the afternoon clearly was mixed with boundary layer air and can be assumed to have had recent contact with the land surface, hence its enrichment in  $^{222}\text{Rn}$ . However, this air from the boundary layer was not enriched with bacterial cells compared to the free troposphere sampled in the mornings. Still, average cell concentrations were somewhat larger during days 2 to 4 ( $3.3 - 3.9 \cdot 10^4 \text{ m}^{-3}$ ) than during day 1. The slope of a linear regression through bacterial number concentrations plotted against coincident  $^{222}\text{Rn}$  concentrations ( $\Delta x / \Delta \text{Rn}$ ) (Fig.15 A) yields a value of  $0.60$  (s.e. =  $0.71$ )  $\cdot 10^4 \text{ cells Bq}^{-1}$ . There was no significant correlation between both parameters ( $p = 0.45$ ). Consequently, no statistically significant amount of bacteria were injected into the free troposphere during this campaign, although there was air mass transport from surface to the station as reflected in an increase of  $^{222}\text{Rn}$  concentrations during afternoons. Fitting a linear regression to estimate a slope and its standard error still makes sense insofar, as it tells us something about the precision of our measurement. Multiplied by an average  $^{222}\text{Rn}$  flux density of  $12.6 \text{ mBq m}^{-2} \text{ s}^{-1}$ , slope and standard error of the linear regression yield estimates for the net bacterial cell flux density from land surface to the free troposphere of  $75$  (s.e. =  $90$ )  $\text{cells m}^{-2} \text{ s}^{-1}$ . Bacterial flux density would have needed to be much larger than  $90 \text{ cells m}^{-2} \text{ s}^{-1}$  to be reliably quantified under these conditions and with the limited number of samples available from this campaign. Here, the standard error (s.e.) of the flux estimate only takes into account the error in the slope ( $\Delta x / \Delta \text{Rn}$ ) of the linear regression, which is the most uncertain factor in our flux estimate. In none of the four campaigns this error was smaller than 27 % of the flux estimate itself. Using a fixed value for the average  $^{222}\text{Rn}$  flux density incurs an additional error, which is difficult to estimate but certainly smaller. Even, if it was 20 %, an error of 27 % in a flux estimate would only increase to 34 %, according to the rules for error propagation. The small value for bacterial flux density estimated for the campaign in June could result from rainfall events during the five days preceding the campaign across all of Switzerland, which may have washed out bacteria from the boundary layer. Flux of bacteria during rain events

is clearly downward (Constantinidou et al., 1990; Lindemann and Upper, 1985). Wet surfaces combined with low wind speeds during our campaign the following days may have prevented larger numbers of cells from becoming airborne.

### 5.4.2 July

The weather situation was variable during the second campaign. Initially clear skies were clouding in the first evening of our sample collection on 20. June. Average relative humidity increased from 30 % to 81 % the first day. Heavy fog enclosed the whole Jungfrauoch region with low visibility until the end of this campaign. Relative humidity remained high between 71 and 100 %. High pressure dominated the station site. Free tropospheric air ( $0.30 \text{ Bq m}^{-3}$ ) influenced the station during the morning of the first day. Coincident total bacterial number concentration was  $2.5 \cdot 10^4 \text{ m}^{-3}$ . In the afternoon of the same day, boundary layer air moved up to the station ( $1.22 \text{ Bq m}^{-3}$ ) with increased bacterial number concentrations ( $4.0 \cdot 10^4 \text{ m}^{-3}$ ). When heavy fogs enclosed the station in the evening, the changes in  $^{222}\text{Rn}$  and bacterial number concentrations did no longer follow the same pattern.  $^{222}\text{Rn}$  concentration more than doubled while bacterial number concentrations were reduced almost to half the value in the afternoon. Although  $^{222}\text{Rn}$  concentrations remained 2 to 3 times higher during days 2 and 3, bacterial number concentrations were on average smaller ( $3.2 \cdot 10^4 \text{ m}^{-3}$ ) during the same period compared to the clear afternoon of the first day (20. June, 18:00). During foggy conditions, upward moving bacterial cells may have been intercepted and removed by wet deposition before reaching station altitude. What we see under such conditions are net fluxes that may be much different from the gross flux of bacteria into the near surface atmosphere. However, deposition during the first two sampling events under clear sky conditions was probably small. For these first two samples, taken under clear conditions, we estimated an upward net flux of bacterial cells from surface to free troposphere of  $198 \text{ m}^{-2} \text{ s}^{-1}$ . A standard error for this flux estimate cannot be derived because this estimate is based on only two data points. A higher sampling frequency to obtain more data points during the short clear period would have been desirable and would have allowed such an error estimate.

### 5.4.3 September

The air was cold and moist during this short campaign where free tropospheric background conditions prevailed.  $^{222}\text{Rn}$  concentrations remained low ( $\leq 0.4 \text{ Bq m}^{-3}$ ). Bacterial number concentrations were around  $4.0 \cdot 10^4 \text{ m}^{-3}$ . Combined with the samples from free tropospheric air during the other campaigns, we estimate that the background number concentration of total bacteria in free tropospheric air ( $^{222}\text{Rn} < 0.5 \text{ Bq m}^{-3}$ ) above the Alpine region during summer and early autumn was around  $3.4 \cdot 10^4 \text{ cells m}^{-3}$  (s.d. =  $0.8 \cdot 10^4 \text{ cells m}^{-3}$ ). This is larger than the total bacterial number concentrations reported for out-of-cloud samples at Mt. Rax (1644 m a.s.l.) in the Austrian Alps. These were in a range from  $6.7 \cdot 10^3$  to  $1.9 \cdot 10^4 \text{ cells m}^{-3}$  (Bauer et al., 2002). This small concentration of bacterial cells at Mt. Rax may be due to the snow cover during the campaign effectively suppressing emission of bacterial cells into the atmosphere. A recent atmospheric simulation study estimates a zonal average

of  $10^3$  to  $10^4$  cells  $m^{-3}$  for the latitude and pressure where Jungfraujoch station is located (Hoose et al. 2010). This estimate is likely to be a lower limit for comparison with our values because it includes air at these altitudes above land and sea, and concentrations above sea is much lower than above most land surfaces (Burrows et al., 2009). Furthermore, we conducted our campaigns during the growing period for vegetation, when concentrations are expected to be larger than during winter (Burrows et al., 2009).

#### **5.4.4 October**

There was a storm in the lowlands surrounding the station as well as at the station itself the days before our fourth campaign. Mean hourly wind speeds at the station exceeded  $20 \text{ m s}^{-1}$  two days prior this campaign. Wind direction alternated between NW and SE. At the beginning of the campaign, atmospheric pressure increased and wind speed had decreased. During the entire campaign period, the station experienced clear skies. Free tropospheric air in the morning and afternoon of the first day ( $0.35 - 0.37 \text{ Bq m}^{-3}$ ) became slightly enriched with boundary layer air towards later the evening ( $0.58 \text{ Bq m}^{-3}$ ). Bacterial number concentrations also increased slightly during the first evening. The following morning, bacterial number and  $^{222}\text{Rn}$  concentrations were both back to smaller values. From there on, both parameters continued to increase and decrease in synchrony until the end of the campaign. This demonstrates a clear enrichment of boundary layer air in bacterial cells compared to the free tropospheric background. Bacterial cell flux density was estimated to be  $455$  (s.e. =  $125$ )  $\text{m}^{-2} \text{ s}^{-1}$ , which is clearly larger than during the other campaigns. This estimate is above the upper limit of simulated values for land surfaces ( $140 - 380 \text{ m}^{-2} \text{ s}^{-1}$ ) (Burrows et al., 2009). We may see this largest flux of all four campaigns as a result of the preceding storm. It probably had led to an increased release of bacteria from the surfaces they grew on and enriched boundary layer air with bacterial cells, which were then transported up to the station in the afternoon and evenings when boundary layer air was injected into the free troposphere. Wind speed has been found to have a significant positive influence on bacterial number concentrations in air in previous studies. Lindemann and Upper (1985), making measurements over a plot of snap beans, found that bacterial number concentrations, and upward flux correlated positively with wind speed and that there was no upward bacterial cell flux when wind speed was less than  $1 \text{ m s}^{-1}$ . Di Giorgio et al. (1995) also found that bacterial number concentrations increased with wind speed. Turnbull et al. (1998) observed airborne bacteria downwind from point sources only in strong wind conditions.

**Tab. 5.** Results of four campaigns to measure total bacterial cell number and  $^{222}\text{Rn}$  activity concentrations at the High Altitude Research Station Jungfrauoch (3450 m above sea level). Bacterial flux density estimates were derived by mass balance with  $^{222}\text{Rn}$  and relate to the duration of entire campaigns, except for the campaign in July, where only the first two measurement points were used because of changed weather conditions later. Time stamps are at the end of 3 hour measurement intervals and are in local time (UTC + 2). Values in brackets indicate 1 standard error.

Campaign	Date	Time	Relative humidity (%)	Air temperature (°C)	Wind speed (m/s)	Sky	Wind direction	$^{222}\text{Rn}$ (Bq m <sup>-3</sup> )	Bacteria (in 10 <sup>4</sup> m <sup>-3</sup> )	Bacterial flux (m <sup>-2</sup> s <sup>-1</sup> )
A	22.06.2010	11:00	11 - 13	-2.8	2.8	Clear		0.50	2.1 (± 0.2)	
		18:00	9 - 13	1.3	4.2	Clear		0.44	3.0 (± 0.5)	
	23.06.2010	11:00	16 - 29	0.4	3.3	Clear		0.68	-	
		18:00	17 - 24	3.9	2.5	Clear		1.05	3.3 (± 0.4)	
	24.06.2010	11:00	20 - 21	-0.5	3.3	Clear	NW	0.41	3.9 (± 0.3)	
		18:00	42 - 98	0.2	3.8	Clear		1.22	-	
	25.06.2010	11:00	31 - 32	-0.7	1.8	Clear		0.52	3.5 (± 0.4)	
		18:00	42 - 95	2.2	1.1	Clear		1.43	3.9 (± 0.3)	75 (±90)
B	20.07.2010	11:00	30 - 37	3.9	4.5	Clear		0.30	2.5 (± 0.2)	
		18:00	46 - 75	6.9	0.7	Clear		1.22	4.0 (± 0.3)	198 (-)
		21:00	75 - 81	5.7	0.3	Heavy fog		2.70	2.3 (± 0.2)	
	21.07.2010	11:00	79 - 86	3.5	4.6	Heavy fog		3.23	3.1 (± 0.6)	
		18:00	71 - 92	5.7	3.4	Heavy fog		3.68	3.9 (± 0.4)	
		21:00	76 - 92	4.2	2.3	Heavy fog	SE	3.71	3.0 (± 0.4)	
	22.07.2010	11:00	94 - 100	2.0	9.2	Heavy fog		2.46	4.3 (± 0.3)	
		18:00	96 - 100	3.1	8.3	Heavy fog		2.63	3.9 (± 0.2)	
		21:00	99 - 100	2.3	6.0	Heavy fog	2.69	2.2 (± 0.4)	-	

C	01.09.2010	11:00	57- 60	-5.0	7.1	Clear	NW	0.40	3.7 ( $\pm$ 0.4)	-
		18:00	58 - 64	-1.4	4.8	Clear		0.34	3.8 ( $\pm$ 0.5)	
		21:00	64 - 67	-1.7	4.9	Clear		0.38	4.6 ( $\pm$ 0.5)	
D	06.10.2010	11:00	9 - 67	1.4	1.7	Clear	NW & SE	0.35	3.7 ( $\pm$ 0.3)	455 ( $\pm$ 125)
		18:00	54 - 63	3.6	0.8	Clear		0.37	3.7 ( $\pm$ 0.5)	
		21:00	50 - 65	1.9	3.3	Clear		0.58	4.0 ( $\pm$ 0.5)	
	07.10.2010	11:00	41 - 46	1.2	4.0	Clear		0.31	3.1 ( $\pm$ 0.2)	
		18:00	40 - 68	3.1	2.3	Clear		0.64	3.9 ( $\pm$ 0.2)	
		21:00	48 - 75	1.2	4.7	Clear		1.04	7.5 ( $\pm$ 0.9)	
	08.10.2010	11:00	69 - 77	0.6	2.9	Clear		0.69	3.5 ( $\pm$ 0.3)	
		18:00	57 - 87	2.0	1.3	Clear		0.94	4.6 ( $\pm$ 0.4)	
		21:00	78 - 91	0.1	2.7	Clear		1.16	5.8 ( $\pm$ 0.4)	

---

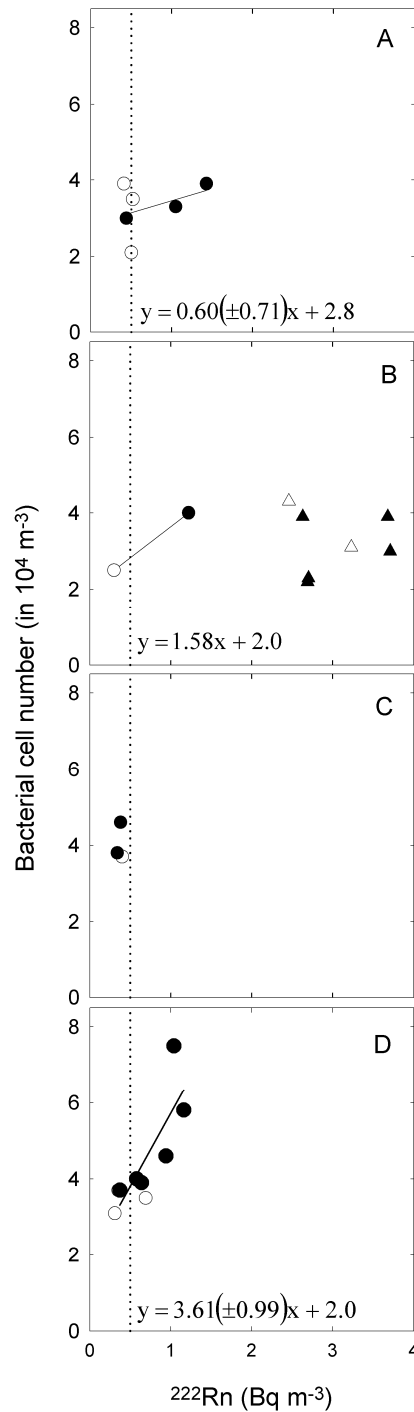


**Fig. 15.** Estimates of the term  $\Delta x / \Delta \text{Rn}$  in Eq. 1 made by fitting linear regressions to plots of concurrently measured values of total bacterial cell number and  $^{222}\text{Rn}$  activity concentrations at the High Altitude Research Station Jungfrauoch (3450 m above sea level) in (A) June, (B) July, (C) September, and (D) October 2010. Circles indicate data obtained under clear sky conditions. Linear regressions were fitted to these data. Triangles show data collected when heavy fog enclosed the station. Open symbols are for measurements before noon (local time), closed symbols for measurements in the afternoons and evenings. Values in brackets indicate, where appropriate, 1 standard error. The dotted vertical line points out the upper limit ( $0.5 \text{ Bq m}^{-3}$ ) of  $^{222}\text{Rn}$  concentrations when the station can be expected not to be influenced by boundary layer air.



## 5.5 Conclusions

Four campaigns to measure total bacterial number concentrations were carried out at the High Altitude Research Station Jungfrauoch between June and October 2010. Timing of the campaigns concentrated on fair weather conditions. Consequently, our results only cover a narrow range of weather situations occurring throughout a year. Parallel measurements of  $^{222}\text{Rn}$  activity concentration allowed us to distinguish between conditions when the station was in free tropospheric air, and when air with recent surface contact (boundary layer air) was transported to the station. Concentrations of total bacteria in free tropospheric air were fairly constant, on average around  $3.4 \times 10^4$  cells  $\text{m}^{-3}$  (s.d. =  $0.8 \times 10^4$  cells  $\text{m}^{-3}$ ). Our measurements indicate that flux density of bacterial cells to cloud altitude is highly variable. First large-scale estimates of total bacterial flux during fair weather conditions provided values between about  $1$  to  $5 \cdot 10^2$  cells  $\text{m}^{-2} \text{s}^{-1}$ . Variability in flux seems to be driven concurrently by mechanisms causing the release of bacteria into the atmosphere (e.g. high wind speed) and by the vertical mixing of air masses. Both mechanisms can be strong at times immediately preceding heavy thunderstorms. Future campaigns to reveal more about the injection of bacteria to cloud altitude should include such weather situation.

## 5.6 Acknowledgements

This project was funded by the Swiss National Science Foundation (project no. 200020-117622/1). Further financial support was provided by the Freiwillige Akademische Gesellschaft Basel. We thank the International Foundation High Altitude Research Stations Jungfrauoch and Gornergrat (HFSJG), 3012 Bern, Switzerland, for providing the infrastructure and making it possible for us to work at the High Altitude Research Station at Jungfrauoch. In particular, we like to thank the custodians of the High Altitude Research Station Jungfrauoch for hospitality and support.



## Chapter 6

# Overall Conclusions and Implications

Our study evaluated the use of radon ( $^{222}\text{Rn}$ ) in exploring atmospheric exchange between land surface and boundary layer, and between boundary layer and free troposphere. Specifically, the long term monitoring techniques and vertical profile surveys provide helpful information to locate the characteristics of boundary layer evolution, to quantify the amount and flux of aerosols and air pollutants and to monitor the progress of atmospheric transport.

Radon is a useful tracer as it does not undergo chemical reactions and now can be measured with enough accuracy. The existing approaches to determine flux and concentration of  $^{222}\text{Rn}$  were inter-compared. In the campaign of  $^{222}\text{Rn}$  flux measurements, the indirect method to determine  $^{222}\text{Rn}$  flux through the relationship between  $^{222}\text{Rn}$  and gamma dose rate was demonstrated to be as useful as direct measurements of  $^{222}\text{Rn}$  flux. Temporal monitoring of  $^{222}\text{Rn}$  flux at more selected locations was fairly straight forward to employ, while the empirical correlation between  $^{222}\text{Rn}$  flux and gamma dose rate requires further improvement for producing the  $^{222}\text{Rn}$  flux map. Such a map can be used to validate atmospheric transport models.

A comparison of atmospheric  $^{222}\text{Rn}$  concentration measurements using two different types of detectors was conducted. We recommend the use of two-filter detectors for measuring variations in atmospheric  $^{222}\text{Rn}$  concentration. Our campaign showed that two-filter detectors minimize the effects of wet deposition and forest canopy on variations of atmospheric  $^{222}\text{Rn}$  concentration. Measurements obtained by a one-filter detector are still dependant on the disequilibrium factor between  $^{222}\text{Rn}$  and its short-lived progeny, which is more variable under rainy conditions and when air passes through a forest canopy. To determine the disequilibrium factor between  $^{222}\text{Rn}$  and its short-lived progeny at one site, the influence of precipitation and land cover should be taken into account while the quantified factor of influence could be adjustable.

Natural variations in  $^{222}\text{Rn}$  flux from soil surface and  $^{222}\text{Rn}$  concentration near surface (0.1 and 6.5 m above ground level) were observed during summer nights in the Carpathian Basin in Hungary (mid August to early September 2009). The inversion trapping of  $^{222}\text{Rn}$  during nighttime was observed in response to the evolution of the nocturnal stable boundary layer. An estimated 72 % of  $^{222}\text{Rn}$  emitted from soil was retained under 6.5 m above ground level during stable nights, which were characterized by light wind, clear sky and strong cooling. This stability could last the entire night period from sunset to sunrise of the following morning. Evidence

from the conservation of  $^{222}\text{Rn}$  emitted from the surface into a shallow boundary layer indicates the two-stratum structure with a shallow very stable boundary layer (vSBL) next to surface. The shallow vSBL is decoupled and isolated from the atmosphere above it. But, when strong intermittent turbulence happens, this structure can be interrupted. On 2 of 14 nights we observed intermittent interruption events, resulting from sudden increase of temperature and wind speed. In a large continental basin it seems to be rare that the stability of a nocturnal boundary layer is interrupted by large scale atmospheric motions during the night period. More detailed observations of  $^{222}\text{Rn}$  associated with more comprehensive meteorological monitoring are encouraged in future studies.

A first attempt to estimate the flux density of total bacterial cells was made by mass balance approach involving measured  $^{222}\text{Rn}$  concentrations and estimated  $^{222}\text{Rn}$  flux density. Air samples were collected at the High Altitude Research Station Jungfrauoch under fair and cloudy weather conditions over a 4-month period from late June to early October 2010. The station is characterized by the changing influence of boundary layer air and free troposphere. The free tropospheric background concentration of total bacterial cells was fairly constant with an average value of  $3.4 \cdot 10^4$  cells  $\text{m}^{-3}$ . The bacterial cell flux density between boundary layer and free troposphere was small, about 1 to 4 times  $10^2$  cells  $\text{m}^{-2} \text{s}^{-1}$ . Precipitation (rain and fog) may in some case have reduced the number concentration of total bacteria by wet deposition before the bacterial cells could have reached the station, while enrichment of  $^{222}\text{Rn}$  was not influenced. Under windy conditions, the concentration of total bacteria increases through an increased emission with winds and the exchange between boundary layer to free troposphere becomes larger, which may affect cloud processes. In this study we have not taken into account the influence of natural decay on variations of  $^{222}\text{Rn}$  concentration during atmospheric transport. To improve the quantification of bacterial flux density estimate, the sink of  $^{222}\text{Rn}$  should be considered in future studies. More air samples should be collected under different weather conditions to further analyze meteorological effects on atmospheric concentration and flux of total bacteria to cloud altitude. In the long-term, observations should explore diurnal and seasonal variations.

Our results indicate that the variability of meteorological conditions have a strong influence on the transport and exchange of aerosols and of greenhouse gases. Especially under certain meteorological conditions boundary layer air enriched with such components can reach high a altitude. The  $^{222}\text{Rn}$  tracer method appears to be most appropriately used to monitor the transport and exchange of atmospheric compounds and to help quantifying the impact of the responsible meteorological factors. These results can also provide fundamental input for evaluation and further development of atmospheric transport and climate models.

## Appendix

# Other Aspects

### A.1 Further improvement of the $^{222}\text{Rn}$ flux map

Preliminary European radon flux map has been made by Szegvary in 2007 (<http://www.unibas.ch/environment>), using the terrestrial gamma dose rate. This map shows high radon exhalation values in Spain compared with the rest of Europe. To verify predicted magnitude and trend of  $^{222}\text{Rn}$  flux in Spain and further accurate description of European  $^{222}\text{Rn}$  flux map, a radon flux campaign has been carried out in July, 2008 in some representatives regions of Spain. Cooperated with Huelva University and Technical University of Catalonia, different passive techniques for  $^{222}\text{Rn}$  flux measurements (electret, canister, AlphaGUARD) will be inter-compared. The chosen sites are all included into the REA (Red de Estaciones Automaticas) network of the CSN (Consejo de Seguridad Nacional) to simultaneously get the information of meteorological factors and gamma dose rate.

The results show us a good agreement between the different used methods. The magnitude of  $^{222}\text{Rn}$  flux we estimated fits well in Madrid, but too high elsewhere. The flux is increasing from Valencia to Madrid, which shows the same trend as we estimated. We add the measured points in Spain to the empirical relation between  $^{222}\text{Rn}$  flux and  $\gamma$ -dose rate (Fig. 16). It shows very little difference of the fitted linear slope before and after adding the Spanish points.

**Tab. 6.** Results of  $^{222}\text{Rn}$  flux measurement using AlphaGUARD.

Site	$^{222}\text{Rn}$ AVER [ $\text{Bq}/\text{m}^2/\text{h}$ ]	$^{222}\text{Rn}$ atom/ $\text{cm}^2/\text{s}$
Teruel	41.2	0.55
Los Pedreros	44.2	0.58
Quintanar de la Orden	56.2	0.74
Madrid	110.9	1.47

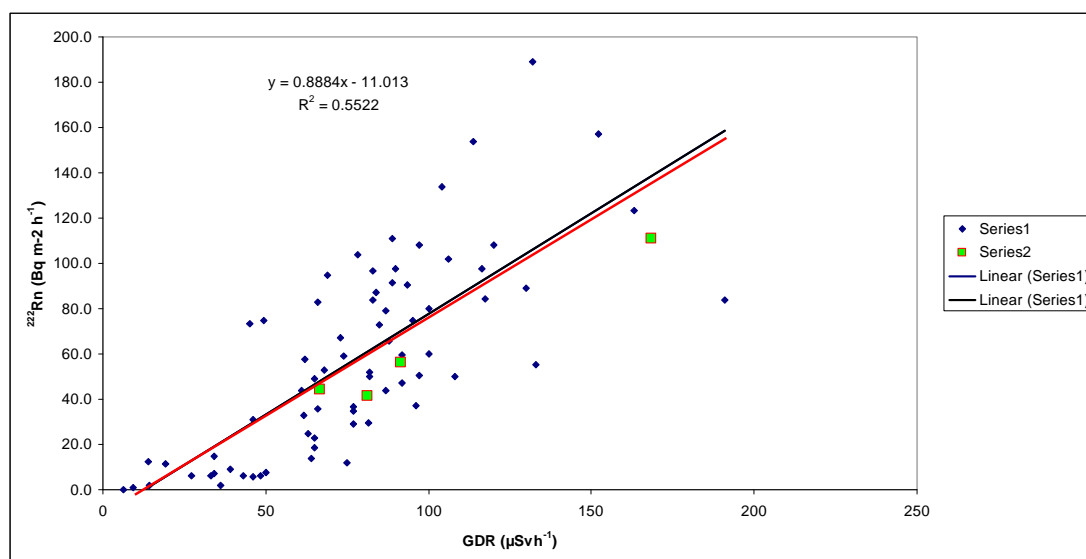


**Fig. 16.** Empirical relation between  $^{222}\text{Rn}$  flux and  $\gamma$ -dose rate (GDR). The green points show the values we measured in Spain. The blue line and red line represent the fitted linear slope before and after adding the Spanish points, respectively.

## A.2 Improve the verification of non- $\text{CO}_2$ greenhouse gas emissions by $^{222}\text{Rn}$ tracer method from Jungfraujoch

Since June 2008 the continuous measurements of atmospheric  $^{222}\text{Rn}$  activity concentration has been started at Jungfraujoch in Switzerland. Fig. 17 shows an Example of  $^{222}\text{Rn}$  (ANSTO) measurements and HFC-134a measurements (from EMPA). We could see that the  $^{222}\text{Rn}$  and HFC fit very well. With the help of back trajectory and footprint analyses, the flux of HFC-134a gas can be estimated. Table 7 shows the comparison of flux estimates for HFC-134a based on the current assumption of a spatially homogenous  $^{222}\text{Rn}$  flux of  $76 \text{ Bq m}^{-2} \text{ h}^{-1}$  and based on our improved  $^{222}\text{Rn}$  estimates. With our improved radon flux estimate, the HFC-134a gas emission can be more accurately determined. Measurement at Jungfraujoch will be finished at the end of February and then a one-year campaign will be carried out in Hungary.

**Tab. 7.** Comparison of flux estimates for HFC-134a based on the current assumption of a spatially homogenous  $^{222}\text{Rn}$  flux of  $76 \text{ Bq m}^{-2} \text{ h}^{-1}$  and based on our improved  $^{222}\text{Rn}$  estimates.

Date	$F_{\text{Rn}}$ ( $\text{Bq m}^{-2} \text{ h}^{-1}$ )	$\Delta C_{\text{HFC-134a}}$ (ppt)	$\Delta C_{\text{Rn}}$ ( $\text{Bq m}^{-3}$ )	$F_{\text{HFC-134a}}$ ( $\text{g km}^{-2} \text{ d}^{-1}$ )
26.July 2008	45	10	3	11
	76	10	3	18
02.Aug. 2008	35	9	1.3	18
	76	9	1.3	37

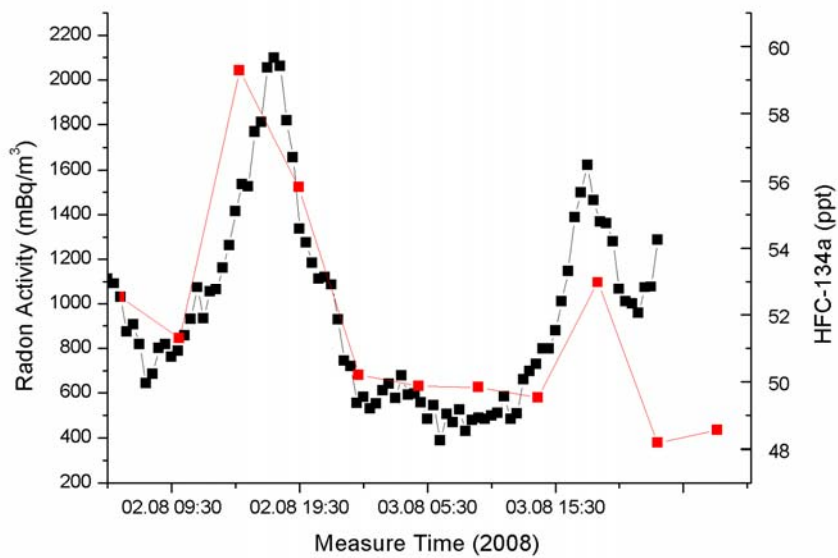
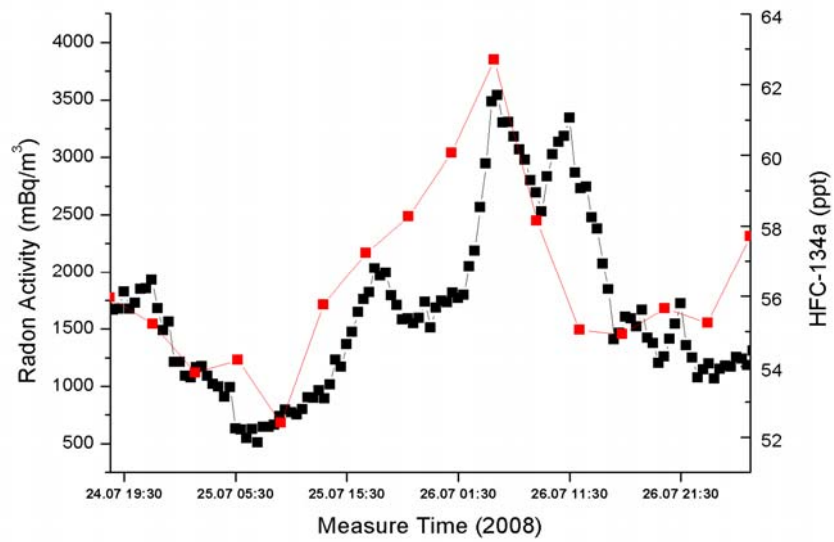


**Fig. 17.** Measurements of  $^{222}\text{Rn}$  and HFC at Jungfraujoch during late July to early August 2008 (HFC data from Stefan Reimann, Empa).





# Bibliography

Akata N., Kawabata H., Hasegawa H., Sato T., Chikuchi Y., Kondo K., Hisamatsu S., and Inaba J., Total deposition velocities and scavenging ratios of  $^7\text{Be}$  and  $^{210}\text{Pb}$  at Rokkasho, Japan. *J.Radioanal.Nucl.Chem.*, Vol. 277, No. 2 347-355, 2008.

Albrecht, B. A. (1989) Aerosols, cloud microphysics, and fractional cloudiness. *Sci.*, 245, 1227-1230.

Arnold, D., Vargas, A., Vermeulen, A. T., Verheggen, B., and Seibert, P. (2010) Analysis of radon origin by backward atmospheric transport modelling. *Atmos. Environ.*, 44, 494-502.

Banta, R.M., Mahrt, L., Vickers, D., Sun, J., Balsley, B. B., Pichugina, Y. L., Williams, E. J. (2007) The very stable boundary layer on nights with weak low-level jets. *J. Atmos. Sci.*, 64: 3068–3090.

Bauer, H., Kasper-Giebl, A., Löflund, M., Giebl, H., Hitzenberger, R., Zibuschka, F. and Puxbaum, H. (2002) The contribution of bacteria and fungal spores to the organic carbon content of cloud water, precipitation and aerosols. *Atmos. Res.*, 64, 109 – 119.

Beyrich, F. (1994) Sodar observations of the stable boundary layer height in relation to the nocturnal low-level jet. *Meteorol. Z.*, 3: 29-34.

Biraud, S., Ciais, P., Ramonet, M., Simmonds, P., Kazan, V., Monfray, P., O'Doherty, S., Spain, T. G., and Jennings, S. G. (2000) European greenhouse gas emissions estimated from continuous atmospheric measurement and radon-222 at Mace Head, Ireland. *J.Geophys.Res.-Atmos.*, 105, 1351-1366.

Bochicchio, F. (2008) The radon issue: Considerations on regulatory approaches and exposure valuations on the basis of recent epidemiological results. *Appl. Radiat. Isot.*, 66, 1561-1566.

Bowen, B. M., Baars, J. A., and Stone, G. L. (2000) Nocturnal wind direction shear and its potential impact on pollutant transport. *J. Appl. Meteorol.*, 39: 437–445.

Brunke, E. G., Labuschagne, C., Parker, B., van der Spuy, D., and Whittlestone, S. (2002) Cape point GAW station  $^{222}\text{Rn}$  detector: factors affecting sensitivity and accuracy. *Atmos. Environ.*, 36, 2257-2262.

Burrows, S. M., Elbert, W., Lawrence, M. G. and Pöschl, U. (2009a) Bacteria in the

global atmosphere – Part 1: Review and synthesis of literature data for different ecosystems. *Atmos. Chem. Phys.*, 9, 9263-9280.

Burrows, S. M., Elbert, W., Lawrence, M. G. and Pöschl, U. (2009b) Bacteria in the global atmosphere - Part II: modeling of emissions and transport between different ecosystem. *Atmos. Chem. Phys. Discuss.*, 9, 10829-10881.

Charlson, R. J., Schwartz, S. E., Hales, J. M., Cess, R. D., Coakley, J. A., Hansen, J. E., and Hofmann, D. J. (1992) Climate forcing by anthropogenic aerosols. *Sci.*, 255, 423-430.

Chi, M. C. and Li, C. S. (2007) Fluorochrome in monitoring atmospheric bioaerosol and correlations with meteorological factors and air pollution. *Aerosol Sci. Technol.*, 41, 672-678.

Christner, B. C., Morris, C. E., Foreman, C. M., Cai, R. and Sands, D. C. (2008) Ubiquity of biological ice nucleators in snowfall. *Sci.*, 319, 1214.

Coakley, J., Cess, R. D., and Yurevich, F. B. (1983) The effect of tropospheric aerosols on the earth's radiation budget: a parameterization for climate models. *J. Atmos. Sci.*, 40, 116-138.

Collaud Coen, M., Weingartner, E., Furger, M., Nyeki, S., Prévôt, A. S. H., Steinbacher, M., Baltensperger, U., 2011. Planetary boundary influence at the Jungfraujoch analyzed by aerosol cycles and synoptic weather types. *Atmos. Chem. Phys. Discuss.*, 11, 985-1024.

Collé, R., Unterweger, M. P., Hutchinson, J. M. R., Whittlestone, S., Polian, G., Ardouin, B., Kay, J. G., Friend, J. P., Blomquist, B. W., Nadler, W., Dang, T. T., Larsen, R. J., and Hutter, A. R. (1996) An international marine-atmospheric <sup>222</sup>Rn measurement intercomparison in Bermuda Part II: Results for the participating laboratories. *Journal of Research of the National Institute of Standards and Technology*, 101, 21-45.

Conen, F., Neftel, A., Schmid, M., and Lehmann, B. E. (2002) N<sub>2</sub>O/Rn-222 – soil flux calibration in the stable nocturnal surface layer. *Geophys. Res. Lett.*, doi: 10.1029/2001GL013429.

Conen, F. and Robertson, L. B., (2002) Latitudinal distribution of radon-222 flux from continents. *Tellus*, 54B, 127-133.

Constantinidou, H. A., Hirano, S. S., Baker, L. S. and Upper, C. D. (1990) Atmospheric dispersal of ice nucleation-active bacteria: The role of rain. *Phytopathology*, 80, 934-937.

- Countess, R. J. (1976) Rn-222 flux measurement with a charcoal canister. *Health. Phys.*, 31, 455-456.
- De Martino, S., and Sabbarese, C. (1997) A Method for Emanation Coefficient Measurement of  $^{222}\text{Rn}$  and  $^{220}\text{Rn}$  from Soils. *Phys. Chem. Earth*, 22, 19-23.
- DeMott, P. J., and Prenni, A. J. (2010) New Directions: Need for defining the numbers and sources of biological aerosols acting as ice nuclei. *Atmos. Environ.*, 44, 1944-1945.
- Dentner, F., Feichter, J., and Jeuken, A. (1999) Simulation of the transport of Rn-222 using on-line and off-line global models at different horizontal resolutions: a detailed comparison with measurements. *Tellus*, 51(B), 573-602.
- Di Giorgio, C., Krempff, A., Guiraud, H., Binder, P., Tiret, C., and Dumenil, G. (1995) Atmospheric pollution by airborne microorganisms in the city of Marseilles. *Atmos. Environ.*, 30, 155-160.
- Dörr, H., Kromer, B., Levin, I., Münnich, K. O., and Volpp, H. J. (1983) CO<sub>2</sub> and Radon-222 as tracers for atmospheric transport. *J. Geophys. Res.*, 88, 1309-1313.
- Draxler, R. R., and Rolph, G. D. (2003) Hybrid Single-Particle Lagrangian Integrated Trajectory (HYSPLIT) Model. <http://www.arl.noaa.gov/ready/hysplit4.html>.
- Dueñas, C., Liger, E., Cañete, S., Perez, M., and Bolivar, J. P. (2007) Exhalation of  $^{222}\text{Rn}$  from phosphogypsum piles located at Southwest of Spain. *J. Environ. Radioact.*, 95, 63-74.
- Fremman, H. D., and Hartley, J. N. (1986) Measurement technology for radon in the soil. *Indoor Radon*, SP-54, 167-181.
- Gäggeler, H. W., Jost, D. T., Baltensperger, U., and Schwikowski, M. (1995) Radon and thoron decay product and  $^{210}\text{Pb}$  measurements at Jungfrauoch, Switzerland. *Atmos. Environ.*, 29, 607-616.
- Gaudry, A., Kanakidou, M., Mihalopoulos, N., Bonsang, B., Bonsang, G., Monfray, P., Tymen, G., and Nguyen, B. C. (1992) Atmospheric trace compounds at a European costal site - Application to CO<sub>2</sub>, CH<sub>4</sub> and COS flux determinations. *Atmos. Environ.*, 26(A), 145-157.
- Grossi, C., Vargas, A., Camacho, A., Lopez-Coto, I., Bolivar, J. P., Xia, Y., and Conen, F. (2011) Inter-comparison of different direct and indirect methods to determine radon flux from soil. *Radiat. Meas.*, 46 (1), 112-118, doi:10.1016/j.radmeas.2010.07.021

Harrison, R. M., Jones, A. M., Biggins, P. D., Pomeroy, N., Cox, C. S., Kidd, S. P., Hobman, J. L., Brown, N. L., and Beswick, A. (2005) Climate factors influencing bacterial count in background air samples. *Int. J. Biometeorol.*, 49 (3), 167-178.

Haszpra, L. (1998) Atmospheric CO<sub>2</sub> record from in situ measurements at K-puszta, Hungary. In Trends: A Compendium of Data on Global Change. Carbon Dioxide Information Analysis Center, Oak Ridge National Laboratory, U.S. Department of Energy, Oak Ridge, Tennessee, U.S.A.

Haxel, O. (1953) Eine einfache Methode zur Messung des Gehalts der Luft an radioaktiven Substanzen. *Zeitschrift für angewandte Physik*, 5, 241-242 (in German).

Henne, S., Furger, M., Prévôt, A.S.H., 2005. Climatology of mountain venting-induced moisture layers in the lee of the Alps. *J. Appl. Meteorol.*, 44, 620-633.

Hirsch, A. I., Michalak, A. M., Bruhwiler, L. M., Peters, W., Dlugokencky, E. J., and Tans, P. P., Inverse modelling estimates of the global nitrous oxide surface flux from 1998-2001. *Global Biogeochem.*, 20 (GB1008), doi:10.1029/2004GB002443, 2006.

Hoose, C., Kristjansson, J. E., Chen, J. P., and Hazra, A. (2010) A classical-theory-based parameterization of heterogeneous ice nucleation by mineral dust, soot and biological particles in a global climate model. *J. Atmos. Sci.* 67, 2483-2503.

Hutter, A.R., and Knutson, E.O. (1998) An international inter-comparison of soil gas radon and radon exhalation measurements. *Health. Phys.*, 74 (1), 108-114.

Iida, T., Ikebe, Y., Suzuki, K., Ueno, Z., and Wang, Y. J. (1996) Continuous measurements of outdoor radon concentrations at various locations in East Asia. *Environ. Internat.*, 22, Supplement 1, S139-S147.

Israel, H. (1951) Radioactivity of the atmosphere. *Amer. Meteo. Soc.*, Boston, 155-161.

Jacob, D. J., and Prather, M. J. (1990) Radon-222 as a test of convective transport in a general circulation model. *Tellus*, 42B, 118-134.

Jacob, D. J., Prather, M. J., Rasch, P. J., Shia, R. L., Balkanski, Y. J., Beagley, S. R., Bergmann, D. J., Blackshear, W. T., Brown, M., Chiba, M., Chipperfield, M. P., Degrandpre, J., Dignon, J. E., Feichter, J., Genthon, C., Grose, W. L., Kasibhatla, P. S., Kohler, I., Kritz, M. A., Law, K., Penner, J. E., Ramonet, M., Reeves, C. E., Rotman, D. A., Stockwell, D. Z., Vanvelthoven, P. F. j., Verver, G., Wild, O., Yang, H., and

- Zimmermann, P. (1997) Evaluation and intercomparison of global atmospheric transport models using Rn-222 and other short-lived tracers. *J. Geophys. Res.*, 102, 5953-5970.
- Jaenicke, R., Matthias-Maser, S., and Gruber, S. (2007) Omnipresence of biological material in the atmosphere. *Environ. Chem.*, 4(4), 217-220.
- Jones, A. M., and Harrison, R. M. (2004) The effects of meteorological factors on atmospheric bioaerosol concentrations — a review. *Sci. Total Environ.*, 326 (1), 151-180.
- Kaplan, I., 1963. Nuclear physics II. Addison-Wesley, Japan.
- Keller, G., Folkerts, K. H., and Muth, H. (1982) Method for the determination of  $^{222}\text{Rn}$  (radon) and  $^{220}\text{Rn}$  (Thoron) – exhalation rates using alpha spectrometry. *Radiat. Prot. Dosim.*, 3 (2), 83-89.
- Keller, G., and Schutz, M. (1988) Radon exhalation from the soil. *Radiat. Prot. Dosim.*, 24 (4), 43-46.
- Keller, C. A., Huwald, H., Vollmer, M. K., Wenger, A., Hill, M., and Reimann, S. (2010) Fiber optic distributed temperature sensing for the determination of the nocturnal atmospheric boundary layer height. *Atmos. Meas. Tech. Discuss*, 3, 2723-2741. doi: 10.5194/amtd-3-2723-2010.
- Kepner Jr., R. L., and Pratt, J. R. (1994) Use of fluorochromes for direct enumeration of total bacteria in environmental samples: past and present. *Microbiol. Rev.*, 58, 603-615.
- Kotrappa, P., Dempsey, J. C., and Stieff, L. R. (1993) Recent advances in electret ion chamber technology for radiation measurements. *Radiat. Prot. Dosim.*, 47 (4), 461-464.
- Kotrappa, P., Stieff, L. R., and Volkovitsky, P. (2004) Radon monitor calibration using nist radon emanation standards: steady flow method. *Radiat. Prot. Dosim.*, 113 (1), 70-74.
- Kreuzer, M., Heinrich, J., Wölke, G., Schaffrath, R. A., Gerken, M., Wellmann, J., Keller, G., Kreienbrock, L., and Wichmann, H. E. (2003) Residential radon and risk of lung cancer in Eastern Germany. *Epidemiology*, 14, 559 – 568.
- Lee, H. N., and Larsen, R. J. (1997) Vertical diffusion in the lower atmosphere using aircraft measurements of  $^{222}\text{Rn}$ . *J. Appl. Meteo.*, 36, 1262-1270.

Lehmann, B. E., and Lehmann, M. (1999) Radon-220 calibration of near-surface turbulent gas transport. *Geophys. Res. Lett.*, 26, 607–610.

Lehmann, B. E., Neftel, A., and Tarakanov, S. V. (2001) Continuous on-line calibration of diffusive soil-atmosphere trace gas transport using vertical  $^{220}\text{Rn}$ - and  $^{222}\text{Rn}$ -activity profiles. *Radiochim. Acta.*, 89, 839–843.

Lehmann, B. E., Ihly, B., Salzmann, S., Conen, F., and Simon, E. (2004) An automatic static chamber for continuous Rn-220 and Rn-222 flux measurements from soil. *Radiat. Meas.*, 38, 43–50.

Lehmann, B. E., Ihly, B., Salzmann, S., Conen, F., and Simon, E. (2003) An automatic static chamber for continuous  $^{220}\text{Rn}$  and  $^{222}\text{Rn}$  flux measurements from soil. *Radiat. Meas.*, 38, 43-50.

Levin, I., Born, M., Cuntz, M., Langendoerfer, U., Mantsch, S., Naegler, T., Schmidt, M., Varlagin, A., Verclas, S., and Wagenbach, D. (2002) Observations of atmospheric variability and soil exhalation rate of radon-222 at a russian forest site. *Tellus*, 54(B), 462-475.

Li, Y. H., and Chang, J. S. (1996) A three-dimensional global episodic tracer transport model. 1. Evaluation of its processes by radon-222 simulations. *J. Geophys. Res.*, 101(25), 931-947.

Lighthart, B., and Shaffer, B. T. (1994) Bacterial flux from chaparral into the atmosphere in mid-summer at a high desert location. *Atmos. Environ.*, 28, 1267-1274.

Lindemann, J., Constantinidou, H., Barchet, W., and Upper, C. (1982) Plants as sources of airborne bacteria, including ice nucleation-active bacteria. *Appl. Environ. Microb.*, 44, 1059-1063.

Lindemann, J., and Upper, C. D. (1985) Aerial dispersal of epiphytic bacteria over bean plants. *Appl. Environ. Microbiol.*, 50, 1229-1232.

López-Coto, I. Mas, J. L. Bolivar, J. P., and Garcia-Tenorio, R. (2009) A short-time method to measure the radon potential of porous materials. *Appl. Radiat. Isot.*, 67, 133-138.

Lugauer, M., Baltensperger, U., Furger, M., Gäggeler, H. W., Jost, D. T., Nyeki, S., and Schwikowski, M. (2000) Influences of vertical transport and scavenging on aerosol particle surface area and radon decay product concentration at the Jungfrauoch (3454 m above sea level). *J. Geophys. Res.*, 105, 19869-19879.

Lupu, A., and Cuculeanu, V. (2001) Code for calculating the vertical distribution of

radon isotopes and their progeny in the atmosphere. *Comput. Phys. Comm.*, 141, 149-162.

Malhi, Y. (1995) The significance of the dual solutions for heat fluxes measured by the temperature fluctuation method in stable conditions. *Boundary-Layer Meteorol.*, 74, 389-396.

Mahrt, L. (1998) Stratified atmospheric boundary layers and breakdown of models. *Theor Comput. Fluid Dyn.*, 11, 263–279.

Möhler, O., DeMott, P. J., Vali, G., and Levin, Z. (2007) Microbiology and atmospheric processes: the role of biological particles in cloud physics. *Biogeosci.*, 4, 1059–1071.

Möhler, O., Georgakopoulos, D. C., Morris, C. E., Benz, S., Ebert, V., Hunsmann, S., Saathoff, H., Schnaiter, M., and Wagner, R. (2008) Heterogeneous ice nucleation activity of bacteria: New laboratory experiments at simulated cloud conditions. *Biogeosci.*, 5, 1425-1435.

Moraswska, L. (1989) Two ways of  $^{222}\text{Rn}$  determining the emanation coefficient. *Health. Phys.*, 57, 481-483.

Moraswska, L., and Phillips, C. R. (1980) Determination of the radon surface emanation rate from laboratory emanation data. *Sci. of The Total Environ.*, 106, 253-262.

Moriizumi, J., Nagamine, K., Iida, T., and Ikebe, Y. (1996) Estimation of areal flux of atmospheric methane in an urban area of Nagoya, Japan, inferred from atmospheric radon-222 data. *Atmos. Environ.*, 30, 1543–1549.

Moriizumi, J., Ohkura, T., Hirao, S., Nono, Y., Yamazawa, H., Kim, Y. S., Guo, Q. J., Mukai, H., Tohjima, Y., and Iida, T. (2008) Continuous Observation of Atmospheric Rn-222 Concentrations for Analytic Basis of Atmospheric Transport in East Asia, *J. Nucl. Sci. Technol.*, Supplement 6, 173-179.

Morris, C. E., Georgakopoulos, D., and Sands, D. (2005) Ice nucleation active bacteria and their potential role in precipitation. *J. Phys. IV France*, 121, 87–103.

Morris, C. E., Sands, D. C., Bardin, M., Jaenicke, R., Vogel, B., Leyronas, C., Ariya, P. A., and Psenner, R. (2011) Microbiology and atmospheric processes: research challenges concerning the impact of airborne micro-organisms on the atmosphere and climate. *Biogeosci.*, 8, 17-25.

Nazaroff, W., and Nero, A.V. (1988) Radon and its decay products in indoor air. John

Wiley & Sons, New York.

Obrist, D., Conen, F., Vogt, R., Siegwolf, R., and Alewell, C. (2006) Estimation of Hg-0 exchange between ecosystems and the atmosphere using Rn-222 and Hg-0 concentration changes in the stable nocturnal boundary layer. *Atmos. Environ.*, 40, 856-866.

Oyha, Y., Neff, D. E., and Meroney, R. N. (1997) Turbulence structure in a stratified boundary layer under stable conditions. *Boundary-Layer Meteorol.*, 83, 139–161.

Penner, J. E., Dickinson, R. E., and O'Neill, C. A. (1992) Effects of aerosol from biomass burning on the global radiation budget. *Sci.*, 256, 1432-1434.

Petroff, A., Mailliat, A., Amielh, M., and Anselmet, F. (2008) Aerosol dry deposition on vegetative canopies. Part 1: Review of present knowledge. *Atmos. Environ.*, 42, 3625-3653.

Porstendorfer, J., 1994. Properties and behaviour of radon and thoron and their decay products in air. *J. Aerosol. Sci.*, 25, 219-263.

Prospero, J. M., Blades, E., Mathison, G., and Naidu, R. (2005) Interhemispheric transport of viable fungi and bacteria from Africa to the Caribbean with soil dust. *Aerobiologia*, 21, 1-19.

Quindós Poncela, L. S., Fernández, P. L., Gómez Arozamena, J., Sainz, C., Fernandez, J. A., Suarez Mahou, E., Martin Matarranz, J. L., and Cascon, M. C. (2004) Natural gamma radiation map (MARNA) and indoor radon levels in Spain. *Environ. Internat.*, 29, 1091-1096.

Raes, F., Dingenen, R. V., Vignati, E., Wilson, J., Putaud, J. P., Seinfeld, J. H. and Adams, P. (2000) Formation and cycling of aerosols in the global troposphere. *Atmos. Environ.*, 34, 4215-4240.

Rash, P. J., Feichter, J., Law, K., Mahowald, N., Penner, J., Benkovitz, C., Genthon, C., Giannakopoulos, C., Kasibhatla, P., Koch, D., Levy, H., Maki, T., Prather, M., Roberts, D. L., Roelofs, G.-J., Stevenson, D., Stockwell, Z., Taguchi, S., Kritz, M., Chipperfield, M., Baldocchi, D., McMurry, P., Barrie, L., Balkanski, Y., Chatfield, R., Kjellstrom, E., Lawrence, M., Lee, H. N., Lelieveld, J., Noone, K. J., Seinfeld, J., Stenchikov, G., Schwartz, S., Walcek, C., and Williamson, D. (2000) A comparison of scavenging and deposition processes in global models: results from the WCRP Cambridge Workshop of 1995. *Tellus*, 52B, 1025-1056.

Ronca-Battista, M., and Gray, D. (1988) The influence of changing exposure conditions on measurement of radon concentration with charcoal absorption technique.



*Radiat. Prot. Dosim.*, 24, 361-365.

Sáez Vergara, J. C., Romero Gutiérrez, A. M., and Rodríguez Jiménez, R. (2002) Resumen de las medidas comparadas en las estaciones de REVIRA. Acuerdo Especifico CIEMAT-CSN 97/187 sobre Optimización de la calidad en la explotación de la red REVIRA, Madrid.

Salmond, J. A., and McKendry, I. G. (2005) A review of turbulence in the very stable nocturnal boundary layer and its implications for air quality. *Prog. in Phys. Geogr.*, 29 (2), 171–188.

Schmidt, M., Graul, R., Sartorius, H., and Levin, I. (1996) Carbon dioxide and methane in continental Europe: a climatology, and <sup>222</sup>Radon-based emission estimates. *Tellus*, 48(B), 457-473.

Schmidt, M. (1999) Messung und Bilanzierung anthropogener Treibhausgase in Deutschland, Ph.D. Thesis, Univ. of Heidelberg, Heidelberg, Germany (in German).

Schmidt, M., Glatzel-Mattheier, H., Sartorius, H., Worthy, D. E., and Levin, I. (2001) Western European N<sub>2</sub>O emissions: A top-down approach based on atmospheric observations. *J. Geophys. Res.*, 106, 5507-5516.

Schmidt, M., Graul, R., Sartorius, H., and Levin, I. (2003) The Schauinsland CO<sub>2</sub> record: 30 years of continental observations and their implications for the variability of the European CO<sub>2</sub> budget. *J. Geophys. Res.*, doi:10.1029/2002JD003085.

Seibert, P., and Skomorowski, P. (2008) Untersuchung der orographischen Besonderheiten der Probennahmestellen Schauinsland und Freiburg und deren Auswirkungen auf die Genauigkeit von adjungierten atmosphärischen Ausbreitungsrechnung („Einzugsgebiete“). *Schriftenreihe Reaktorsicherheit und Strahlenschutz*, BMU-2008-713.

Stockburger, H., and Sittkus, A. (1966) Unmittelbare Messung der natürlichen und künstlichen Radioaktivität der atmosphärischen Luft. *Zeitschrift für Naturforschung*, 21a, 1128-1132 (in German).

Stull, R. B. (1988) An introduction to boundary layer meteorology, Kluwer Academic Publishers, Dordrecht, 666 pp.

Sun, J., Lenschow, D. H., Burns, S. P., Banta, R. M., Newsom, R. K., Coulter, R., Frasier, S., Ince, T., Nappo, C., Balsley, B. B., Jensen, M., Mahrt, L., Miller, D., and Skelly, B. (2004) Atmospheric disturbances that generate intermittent turbulence in nocturnal boundary layers. *Boundary-Layer Meteorol.*, 110: 255–279.

Szegavary, T., Conen, F., and Ciais, P. (2009) European  $^{222}\text{Rn}$  inventory for applied atmospheric studies. *Atmos. Environ.*, doi:10.1016/j.atmosenv.2008.11.025.

Szegavary, T., Conen, F., Stöhlker, U., Dubois, G., Bossew, P., and de Vries, G. (2007) Mapping terrestrial  $\gamma$  dose rate in Europe based on routine monitoring data. *Radiat. Meas.*, 42, 1561-1572.

Szgevarya, T., Leuenberger, M. C., and Conen, F. (2007) Predicting terrestrial  $^{222}\text{Rn}$  flux using dose rate as a proxy. *Atmos. Chem. Phys.*, 7, 2789-2795.

Taguchi, S., Lida, T., and Moriizumi, J. (2002) Evaluation of the atmospheric transport model NIRE-CTM-96 by using measured radon-222 concentrations. *Tellus*, 54 (B), 250-268.

Turnbull, P. C. B., Lindeque, P. M., Le Roux, J., Bennett, A. M., and Parks, S. R. (1998) Airborne movement of anthrax spores from carcass sites in the Etosha National Park, Namibia. *J. Appl. Microbiol.*, 84, 667-676.

Twomey, S. (1977) The influence of pollution on the shortwave albedo of clouds. *J. Atmos. Sci.*, 34, 1149-1152.

UNSCEAR (2000) Sources and Effects of Ionizing radiation. Report to the General Assembly, with scientific annexes. United Nations. New York.

Vargas, A., and Ortega, X. (2006) Influence of environmental changes on integrating radon detectors: results of an intercomparison exercise. *Radiat. Prot. Dosim.*, 123 (4), 529-536.

Whittlestone, S., Robinson, E., and Ryan, S. (1992) Radon at the Mauna Loa Observatory; Transport from distant continents. *Atmos. Environ.*, 26A(2), 251- 260.

Whittlestone, S., and Zahorowski, W. (1998) Baseline radon detectors for shipboard use: Development and deployment in the First Aerosol Characterization Experiment (ACE 1). *J. Geophys. Res.*, 103 (D13), 16743–16751.

Wiedinmyer, C., Bowers, R.M., Fierer, N., Horanyi, E., Hannigan, M., Hallar, A.G., McCubbin, I., and Baustian, K. (2009) The contribution of biological particles to observed particulate organic carbon at a remote high altitude site. *Atmos. Environ.* 43, 4278-4282.

Wilson, S. R., Dick, A. L., Fraser, P. J., and Whittlestone, S. (1997) Nitrous oxide flux estimates from South-East Australia. *J. Atmos. Chem.*, 26, 169-188.

WMO/GAW (2004) 1<sup>st</sup> International Expert Meeting on Sources and Measurements of

Natural Radionuclides Applied to Climate and Air Quality Studies. WMO TD No. 1201.

Wyers, G. P., and Veltkamp, A. C. (1997) Dry deposition of  $^{214}\text{Pb}$  to conifers. *Atmos. Environ.*, 31(3), 345-350(6).

Volz-Thomas, A., Geiß, H., and Kalthoff, N. (1999) The Schauinsland 1999. Ozone Precursor Experiment (SLOPE96): Scientific background and summary of main results. *J. Geophys. Res.*, 105(D1), 1553-1561.

Xia, Y., Sartorius, H., Schlosser, C., Stöhlker, U., Conen, F., and Zahorowski, W. (2001) Comparison of one- and two-filter detectors for atmospheric  $^{222}\text{Rn}$  measurements under various meteorological conditions. *Atmos. Meas. Tech.*, 3, 723-731.

Xia, Y., Conen, F., Haszpra, L., Ferenczi, Z., and Zahorowski, W. (2011) Evidence for nearly complete decoupling of very stable nocturnal boundary layer overland. *Boundary-Layer Meteorol.*, 138 (1), 163-170.

Yamada, K., Iida, T., Ikebe, Y., Miyachi, H., Nagao, I., and Komura, K. (1998) Time series analysis of atmospheric  $^{222}\text{Rn}$  concentrations and meteorological factors in JAPAN. *Proceeding of the 7<sup>th</sup> Tohwa University International Symposium*.

Yamamoto, M., Kofugi, H., Shiraishi, K., and Igarashi, Y. (1998) An attempt to evaluate dry deposition velocity of airborne  $^{210}\text{Pb}$  in a forest ecosystem. *J. Radioanal. Nucl. Chem.*, 227, 81-87.

Yankofsky, S. A., Levin, Z., Bertold, T., and Sandlerman, N. (1981) Some basic characteristics of bacterial freezing nuclei. *J. Appl. Meteorol.*, 20, 1013-1019.

Zahorowski, W., Chambers, S. D., and Henderson-Sellers, A. (2004) Ground based  $^{222}\text{Rn}$  observations and their applications to atmospheric studies. *J. Environ. Radioact.*, 76, 3-33.



# Yu Xia

---

Address: Leimenstrasse 6, 4051 Basel

Date of Birth: 26. Nov. 1980

Citizenship: P. R. China

Email: yu.xia@unibas.ch

## EDUCATION

- 2008-2011: PhD candidate in Environment Science, Institute of Environmental Geosciences, University of Basel, Switzerland  
PhD thesis: *Exploring atmospheric exchange with natural tracers.*
- 2004-2007: Master in Physics, Heidelberg University, Germany.  
Master thesis: *Influence of fingering flow on water table and capillary fringe.*
- 1999-2003: Bachelor in Physics, Fudan University, P.R.China.  
Bachelor thesis: *Characteristics and source of cobalt bluepigment in blue-and-white porcelain from Tang Dynasty by using PIXE.*

## PUBLICATIONS

**Xia Y.**, Sartorius H., Schlosser C., Stöhlker U., Conen F., and Zahorowski W., Comparison of one- and two-filter detectors for atmospheric  $^{222}\text{Rn}$  measurements under various meteorological conditions. *Atmos. Meas. Tech.*, 3, 723-731, 2010.

**Xia Y.**, Conen F., Haszpra L., Ferenczi Z., and Zahorowski W., Evidence for nearly complete decoupling of very stable nocturnal boundary layer overland. *Boundary-layer Meteorol.*, in Press, Doi: 10.1007/s10546-010-9548-2, 2010.

Grossi C., Vargas A., Camacho A., Lopez-Coto I., Bolivar J. P., **Xia Y.**, and Conen, F., Inter-comparison of different direct and indirect methods to determine radon flux from soi. *Radia. Meas.*, in Press, Doi: 10.1016/j.radmeas.2010.07.021, 2010.

## CONFERENCES

- 05.2010: 3<sup>rd</sup> International Disaster and Risk Conference IDRC, Davos, Switzerland.

- 04.2010: **Xia Y.**, Conen F., Haszpra L., Zahorowski W., Evidence for nearly complete decoupling of very stable nocturnal boundary layer from atmosphere. 11<sup>th</sup> Swiss Global Change Day, Bern, Switzerland.
- 03.2009: **Xia Y.**, Conen F., Bacterial flux into the atmosphere. 10<sup>th</sup> Swiss Global Change Day, Bern, Switzerland.
- 09.2008: **Xia Y.**, Conen F., <sup>222</sup>Rn tracer method for non-CO<sub>2</sub> greenhouse gas emission. Poster Presentation. IGAC 10<sup>th</sup> International Conference, Annecy, France.
04. 2008: 9<sup>th</sup> Swiss Global Change Day, Bern, Switzerland.

## **EDUCATIONAL COURSE**

- 11.2008: GAWTEC XV on Greenhouse Gases Data quality assurance and control, the Global Atmosphere Watch Training & Education Centre, Germany.